Politecnico di Torino

Department of Energy (DENERG)

CRS4

HPC for energy and environment

Smart Energy Systems

Stefano Lampis

Internship report:” *Study and CFD modeling of the behaviour of liquid-state Lead-Bismuth eutectic, with particular reference to the main heat exchanger of the CIRCE experimental facility, located at ENEA, Brasimone (Italy).*”

Academic tutor:

Prof. Pietro Asinari

CRS4 tutor:

Dr. Vincent Moreau

3/05/2017 - 31/08/2017

Table of contents

Introduction:

The main aim of this report is to illustrate the activities pursued during the internship at CRS4, highlighting its most important objectives, and paying particular attention to the personal learning process experienced throughout this working period. Furthermore, the technical conclusions of the work will be adequately summarized and presented in the last paragraph.

The abovementioned internship took place between the first days of May and the end of August 2017, with a break of one month and a half during the period of June and early July, due to exam session duties (working time reduced to only one day per week) for a total of 300 working hours (12 CFU). All activities were constantly supervisioned by Dr. Vincent Moreau of CRS4 and Prof. Pietro Asinari of Politecnico di Torino, in quality of internship tutors, together with the help of Dr. Manuela Profir.

The CRS4 research center:

The CRS4 (Center for advanced studies, research and development in Sardinia), is currently one of the top-level research centers in Italy, constantly researching on very diverse fields, ranging from energy and visual computing to high performance computing and biosciences, (only to quote a few of them). This internship was guided by the HPC for energy and environment team (led by Dr. Ernesto Bonomi) and, more precisely, under the supervision of Dr. Vincent Moreau of the Smart Energy Systems group (program head: Dr. Luca Massidda). The HPC for energy and environment team is involved in a wide spectrum of research activities, all aiming to provide satisfying answers to complex and diverse energetic issues, by employing multi-disciplinary methods, especially based on the numerical modeling of physical phenomena. In particular, the attention of the SES group is focused on applied research into all energy resources and technologies for industry, households and services.

Objectives:

On a scientific level, this internship was centered on the development of an adequate level of experience with numerical CFD models, with particular attention to the use of commercial software (STAR-CCM+) and to the management of the whole computing architecture surrounding it (Linux OS, CPU clusters…). These technical purposes were constantly supported by the application of the university theoretical knowledge, which has been strengthened and expanded, becoming the basis of each working step.

The whole work dealt with the study of the thermo-fluid dynamic behaviour of liquid state Lead-Bismuth Eutectic (LBE) in the first loop of the experimental CIRCE facility, located at

ENEA Brasimone (Italy); particular attention has been paid to the generation of an accurate CFD model for the main heat exchanger (HX) of the abovementioned facility, in the attempt to simulate some experiments that have been pursued in the past and better understand the characteristics of the HX and its role in the “bigger picture” of the behaviour of the whole facility.

In fact, this model will be later used as the starting point for the development of a CFD model for the whole CIRCE primary loop, which will be the basis of the Master Thesis stage.

From the perspective of a student, the main objectives of an internship should not only be focused on technical and scientific problems, but should also offer a first look on the working environment, thus being an important occasion for personal growth.

Technical activity report:

All activities pursued during this internship were constantly recorded and monitored by using a very detailed working diary, updated day by day. This allowed, in this last phase of the stage, to better understand the dynamics of the learning process, reconstructing it step by step from the beginning.

1. Phase 1: Beginning of the stage. (3/05/2017 – 12/05/2017)

The first working week was entirely devoted to the general approach to those that would have been the main issues of the stage. At the very beginning, since the whole CRS4 computing architecture and HPCN (high performance computing network) is based on the Linux/Ubuntu OS, an introduction to the basic procedures has been compulsory. The management of files, directories, bash files and software by using Terminal commands has been particularly challenging, especially considering the total lack of previous personal experience with such systems. Also, the management of the Home personal space on the shared CRS4 storage space has been rather difficult at the beginning, considering the very small amount of memory allowed (4GB maximum). As will be later explained, this caused some issues with the very first. sim files (STAR-CCM+ simulations) that exceeded the allowed memory. At the same time, other aspects of the stage thematics have been discussed, namely:

1) CFD applied mathematics and numerical models theory
2) Thermo-fluid dynamic properties of LBE
3) General approach to experimental HLM facilities
4) Introduction to the CFD modeling commercial software (STAR-CCM+), and practice of its basic tutorials. Particular emphasis was posed on the modeling of incompressible liquid flows and heat transfer.

Furthermore, in this same first internship phase, a good amount of time has been spent finding and reading documents about the general properties of HLM experimental facilities, articles on the LBE thermo-fluid dynamic characteristics and, especially, official ENEA documents about the CIRCE facility. These official documents, together with a large number of accurate technical drawings of the facility, allowed for a better understanding of the characteristics of the single components of the installation. Anyway, although each official CIRCE document depicted a different testing scenario for the facility, there was a rather problematic lack of really coherent data on some characteristics of the implant, especially regarding the water properties flowing inside the main HX. Some of this data could be later found of hypotized, as will be explained later.

2. Phase 2: First approach to the CIRCE-ICE HX and approximated modeling of the double bayonet tube (13/05/2017 -26/05/2017)

The second phase of the internship started with a detailed analysis of the main CIRCE HX and of its internal components considering its working behaviour under steady-state conditions.

A very simple technical scheme of the primary loop is presented in the following Figure 1.

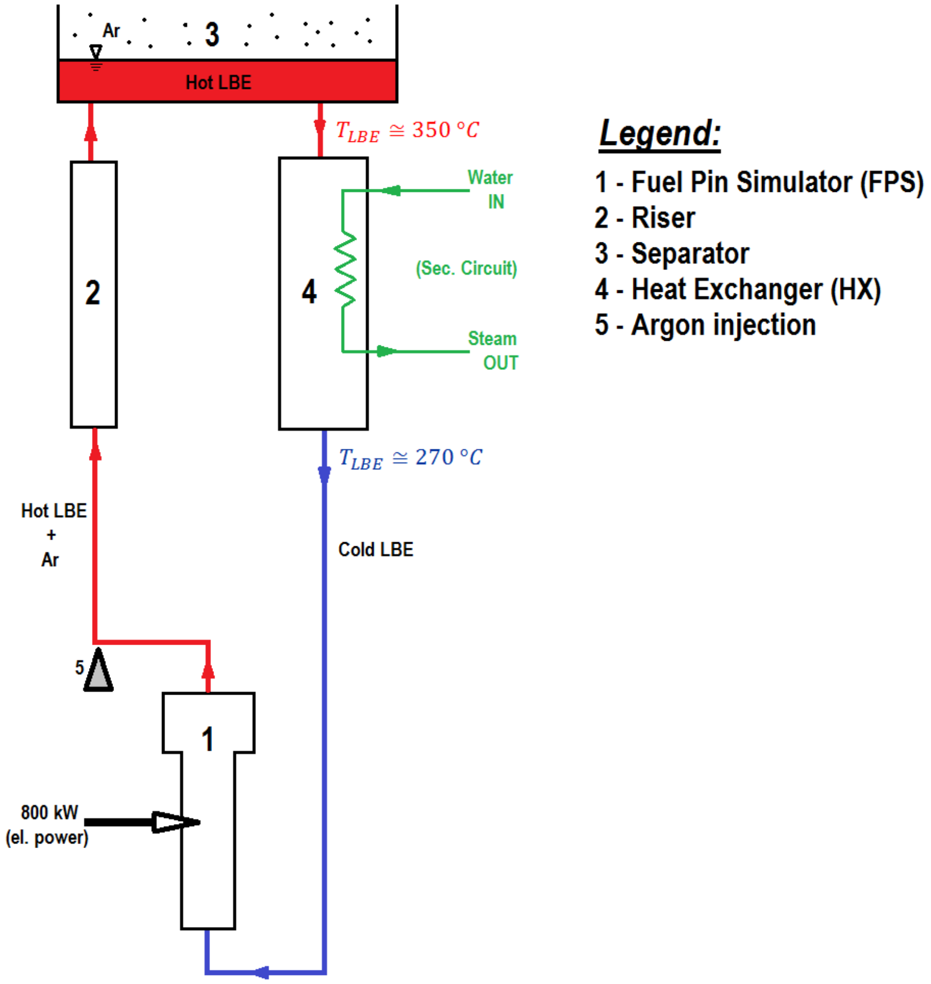

Figure 1: Technical scheme of the CIRCE-ICE experiment (LBE primary loop); A portion of the secondary circuit (representing the double bayonet tubes inside the HX (4) is depicted in green.

The HX (element 4 in Figure 1) plays the role of the heat sink inside the CIRCE-ICE loop, cooling down the LBE that had been previously heated up through the FPS (fuel pin simulator) at the bottom of the installation. To do so, the HX is designed as follows:

1) The HX inlet zone, communicating with the separator, allows the hot LBE (~350 degrees Celsius) coming from the riser to enter the HX.
2) The internal zone of the HX is composed of 91 identic double bayonet tubes, where the water of the secondary circuit flows, subtracting heat to the LBE and passing from a liquid sub-saturated condition (water inlet) to a wet steam condition (steam outlet).
3) The HX shell isolates the internal zone of the HX from the bulk zone of the facility.
4) The thermal characteristics of LBE flowing through the HX are constantly monitored using thermocouples, placed at the inlet and outlet zone of the component. All the energy balances present in the official documents are constructed using these simple sources of information.
5) The outlet zone of the HX is constituted of a grid, used to block the bottom part of the tubes and regularize the LBE flux and an ending shell skirt.

On this second part of the internship, the basic objective was to initialize the CFD modeling of the abovementioned HX, evaluating all the different aspects that could influence the model, and trying to find an adequate way to reach an acceptable solution.

After approaching the problem with various one-dimensional energy balance calculations on the primary (LBE) and secondary (cooling water) loops, the first step that was performed was the development of a very simple model of a single double bayonet tube inside the HX, by using the commercial software STAR-CCM+.

The basic idea behind this step was to model the water vaporization process inside the HX double bayonet tube, in order to understand how this could effectively influence the LBE behaviour in the primary loop in terms of heat subtraction.

Furthermore, this model could have been later used while modeling the whole HX, in order to impose a correct thermal boundary condition on the internal surface of the tubes.

After many attempts, anyway, it has been clear that the generation of this single-tube model would not have had much relevance towards the whole HX model, especially because of many numerical difficulties in running the solution; anyway, it allowed for a much deeper theoretical comprehension of the software numerical principles and the problems involved.

A basic scheme of the double bayonet tube can be visualized in the following Figure 2

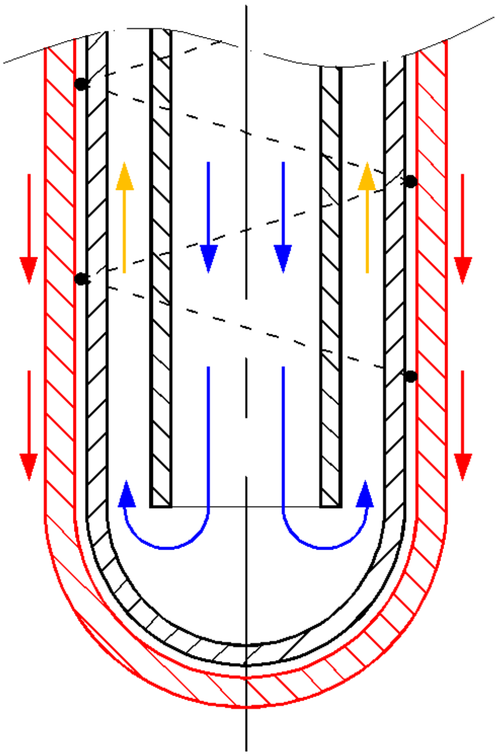

Figure 2,: Basic scheme of a double bayonet tube [2.].

2.1 The conductivity problem

As can be seen from the previous scheme (Figure 2) a ~1 mm layer of Helium and metallic powder is present in between the intermediate and the external steel tubes; the Helium layer has been designed in order to prevent mixing of LBE and water of the two different circuits in case of possible failures. In fact, the composition of the Helium inside the gap is constantly monitored, in order to detect any traces of water or LBE (signaling breaches in one of the intermediate or external tubes). Anyway, considering that such a thick helium layer would have caused an important reduction in the conductivity of the whole tubes assembly, a certain amount of metallic powder has been added. By doing this, the layer still prevents mixtures in case of failures, and the heat exchange efficiency is improved due to the conductivity increase (with respect to the helium-only case). The big modeling issue with this system is that the proportions of helium and metallic powder in the global mixture are completely unknown, and so it has been impossible to have a precise conductivity value for the whole tubes assembly from the official CIRCE literature.

Furthermore, in order to simplify the models, the intermediate and external tubes and the Helium+powder layer have been modeled, whenever needed, as a single "equivalent" external tube, with a thickness equal to the sum of the single layer thicknesses. From now on, this "equivalent" external tube will simply be referred to as the "external tube"

In order to estimate a correct conductivity for such part, two different extreme conditions have to be examined:

1) External tube made of 100% AISI 304 steel (conductivity of about k=16 W/mK), for its whole thickness (also comprehending the helium layer thickness)
2) Considering separate layers, with AISI 304 steel for the intermediate and external tubes and 100% Helium in the intermediate gap (no metallic powder)

In terms of conductivity, the real case, with the unknown amount of metallic powder inside the gap, will be an intermediate condition between the previous two.

With simple calculations, considering a simplified case of a plane wall with layers of the same thickness as the ones of the tube, the different values of conductivity for the two extreme cases have been approximately evaluated as:

1) 100% AISI steel – $k_{eq.} \cong 16\ W/mK$
2) Condition with 100% He inside the gap (no powder) – $k_{eq.} \cong\ 0.687\ W/mK$

It is highly noticeable how the presence of a 1 mm layer of Helium (thickness not negligible with respect to the total external tubes thickness) highly affects the conductivity of the whole assembly, which decreases by a factor above 20. The correct equivalent conductivity of the external tube should lie somewhere in between these two values and depends heavily on the microstructure of the metallic powder.

2.2 Creation of the STAR-CCM+ double bayonet tube model:

Since no CAD file could be found, the whole geometry of the double bayonet tube had to be created from scratch, using the data from the official CIRCE documents. Considering the axial symmetry, there was no need to create the whole geometry, but only a slice of a fourth of the tube (90 degrees) has been considered. The following picture (Figure 3) illustrates the final geometry, comprehending both the fluid (water) and solid (steel tubes) regions:

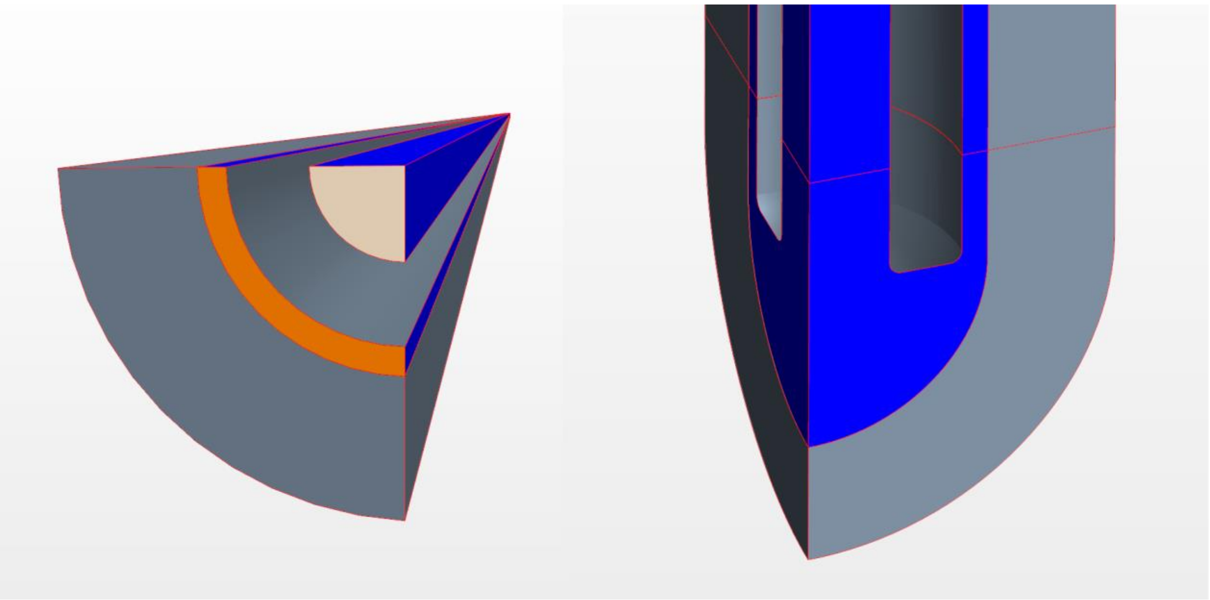

Figure 3:Geometry of the Double bayonet tube model. The water inlet (pink) and steam outlet (orange) sections are represented on the left. Right: bottom of the double bayonet tube.

The next step was centered on the creation of an adequate mesh for the abovementioned geometry.

The best way to generate the mesh for this component has been evaluated as:

1)Automated polyhedral mesh operation for the bottom part of the water fluid region

2)Directed mesh operation (using as source the surface mesh of the bottom fluid region)

for the whole height of the tube, with a double hyperbolic cell stretching function (in order to ensure cell growth continuity).

Furthermore, a prism layer mesher has been employed throughout the whole fluid region, in order to allow a more precise study of the boundary layer effects. For this first attempt, the global number of mesh cells was rather low (~10^5 cells) and the calculation could be run on 2 / 4 local CPUs.

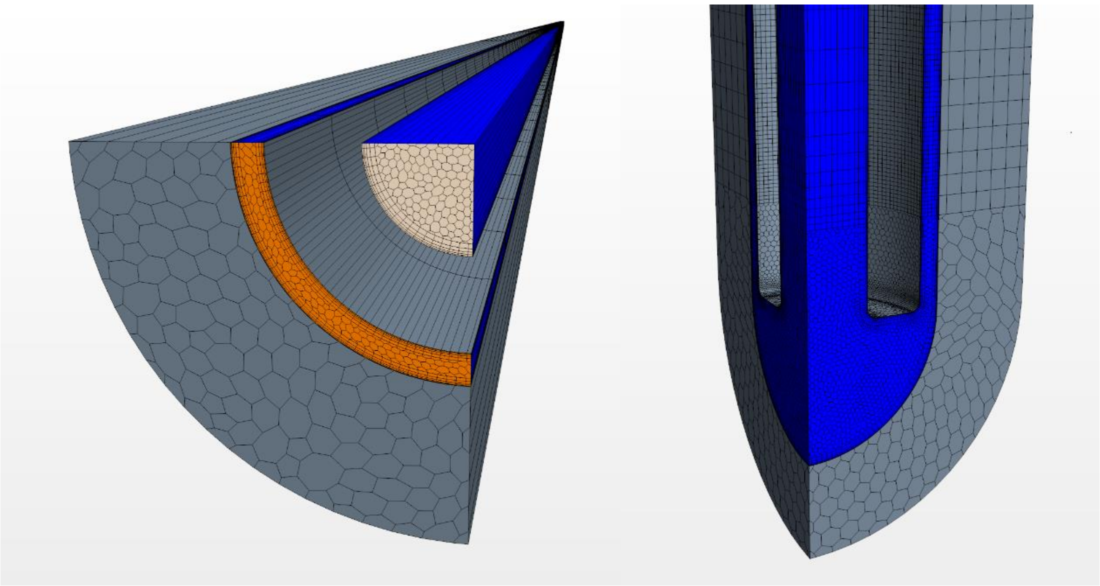

Figure 4: Definitive mesh for the double bayonet tube model.

2.2.1 First simulation – Segregated flow, constant density:

Once the mesh of the fluid region was ready, a first very simple segregated "cold" flow simulation has been run choosing the following models:

1) Liquid, with constant density: for this first attempt only water was considered inside the double bayonet tube. The evaporation process would have been implemented later, adding energy models and material properties dependences on temperature with a gradual process.

2) Segregated turbulent flow (RANS k-epsilon): the only equations solved in this first steps were continuity, momentum (X, Y, Z) and the turbulence kinetic energy and dissipation rate (as required by the RANS k-epsilon model).

The boundary conditions for the water fluid region were assigned as follows:

1) WATER MASS FLOW INLET: top of the tube, on the innermost circular surface. The imposed mass flow rate value has been obtained by considering the value of ~0.7 kg/s from the CIRCE official reference document [1.] (for all the 91 tubes), and then dividing it by 91 (single tube) and then by 4 (considering the one fourth symmetric slice analyzed).

2)WATER PRESSURE OUTLET: top of the tube, on the outer ring surface. The pressure value was set to 1 bar, as seen on a CIRCE official ENEA document.
3)SYMMETRY PLANES: because of the previously analyzed consideration on the axial symmetry, the “symmetry plane” condition had to be imposed on two walls.
3)NO-SLIP WALL CONDITION: on all the other walls except the symmetry planes, the shear stress condition of no-slip has been assigned.

The simulation has been run on 2 local CPUs, reaching convergence quite fast.

2.2.2 Modeling the evaporation:

The next step was obviously the implementation of a model for the water evaporation inside the external ring of the double bayonet tube, which required the solution of an energetic problem alongside the previously solved segregated fluid-dynamic one. In order to do so, different approaches have been tried, adding various models to the simulation and checking their validity step by step.

The energetic aspects of the model have been previously studied from the official documents and with theoretical considerations, in order to elaborate a satisfying way to simulate the heat transfer from the LBE (flowing downwards outside the external walls of the double bayonet tube) to the external fluid ring of the tube, where water flows upwards and vaporization occurs.

This translates into thinking about some adequate thermal boundary conditions to impose to the different surfaces of the fluid region. As a first attempt, such boundary conditions have been theorized as follows:

WATER INLET TEMPERATURE: considering the extremely varying values found in the official documents (15 to 50 degrees Celsius), an approximate intermediate condition of 25 degrees Celsius has been chosen.

EXTERNAL RING SURFACE (water vaporization region): Considering the total medium heat power removed at regime by the HX of ~650 kW (as seen in the CIRCE reference document), this value has been divided by 91, obtaining the medium total heat power removed by each double bayonet tube. This value has then been divided by the external cylindrical surface of the vaporizing water region, obtaining a heat flux of ~44.442 kW/m^2, and imposed as a constant boundary condition all over this surface.

All other surfaces were considered approximately adiabatic.

(Note that, up to now, the only modeled region has been the fluid one, later the model will comprehend also the external tubes, and the LBE flowing downwards outside them, and the boundary conditions will inevitably be assigned differently).

Once these boundary conditions were determined, the next step consisted in finding a way to model the water evaporation inside the double bayonet tube. Different approaches have been tried, namely:

1)Multiphase flow evaporation modeling:

this first attempt followed the guide of a STAR-CCM+ tutorial about the modeling of evaporating liquids using the VoF (volume of fluid) method, together with:

Segregated enthalpy model
Properties of water: IAPWS-IF97 model
Gravity

After having applied all the steps suggested by the tutorial and having run the simulation, it could be almost immediately evident that this VoF method was really too computationally expensive for the 2 local CPUs that were performing the simulation. In fact, not only the time requested for a single solver iteration was too high, but the residuals did not show any sign of convergence after quite some time.

It was clear at this point that this method was not affordable and had to be substituted with another one.

2) Model of vaporizing water with an “equivalent” liquid with strongly varying properties:

The basic idea behind the second approach to the evaporation problem consisted in modeling the water behaviour in the vaporization thermodynamic zone as a liquid with properties varying drastically with temperature. In fact, two different assumptions from basic thermodynamics could be made:

1) The water density at liquid state, in standard conditions can be evaluated around ~1000 kg/m^3, diminishing relatively slightly with temperature increasing at constant pressure.

When water heats up enough to reach and overcome the water saturated line, entering the liquid+vapour multiphase equilibrium zone, the density behaviour changes drastically because of the extremely low density of saturated steam that is being generated (~0.6 kg/m^3 at 1 bar).

This translates into a very steep decrease of density with steam quality increase in the liquid+vapour multiphase equilibrium zone, and ideally, with no pressure drop during vaporization, this process should occur at constant saturation temperature.

For numerical reasons, anyway, the pressure drop has been neglected, and the vaporization process has been spread over a certain temperature interval, in order to be able to assign a polynomial dependence of density on temperature that did not show, in any zone of the domain, a temperature derivative tending to infinite values.

That said, as a first approximation, the density dependence on temperature has been expressed by subdividing the temperature variation interval into three different zones, (pre-heat zone, vaporization zone, and overheated steam zone) and in each interval, the density decrease is modeled as linear with temperature (Figure 5):

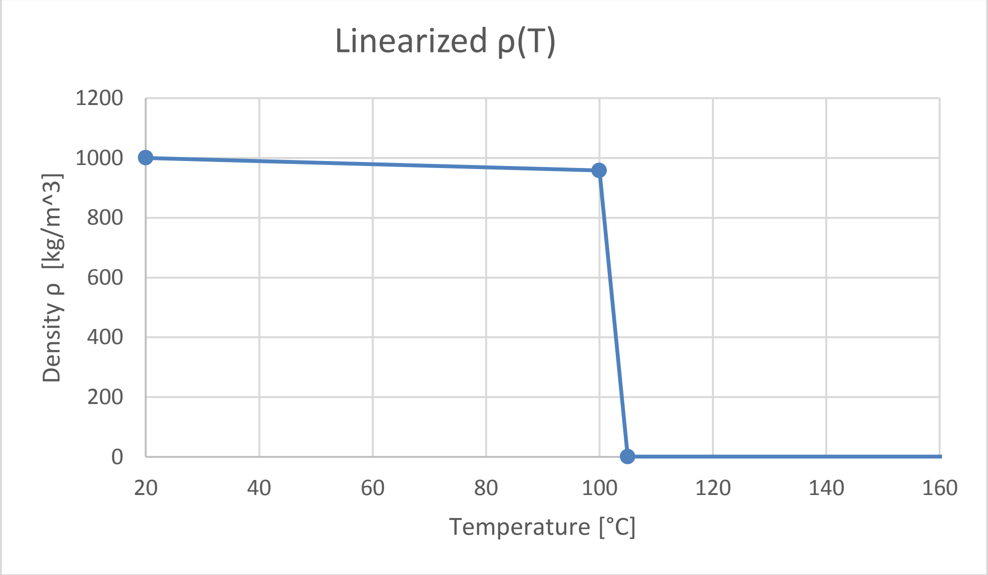

Figure 5: Density variation with temperature chosen to model vaporization.

2) If, as said before, the evaporation process takes place with no pressure drop, it is obviously isothermal (at saturation temperature). This means that the fluid, during vaporization, can be theoretically considered infinitely inert from a thermodynamic point of view, because it absorbs energy (heat power) without changing its temperature.

Considering that, in all this model, the only fluid is a “numerically equivalent” liquid with drastically changing properties, it can be said that:

$$dh \cong c_p dT$$

which would be obviously not correct if steam was physically considered. In fact, it is known that the previous relationship is not valid in liquid+vapour multiphase equilibrium.

In order to obtain the effect of letting the liquid absorb energy without changing temperature, the specific heat (which describes the thermal inertia of the fluid) should have the following dependence on temperature (Figure 6), where the upwards arrow symbolizes a Dirac function (on the vaporization temperature).

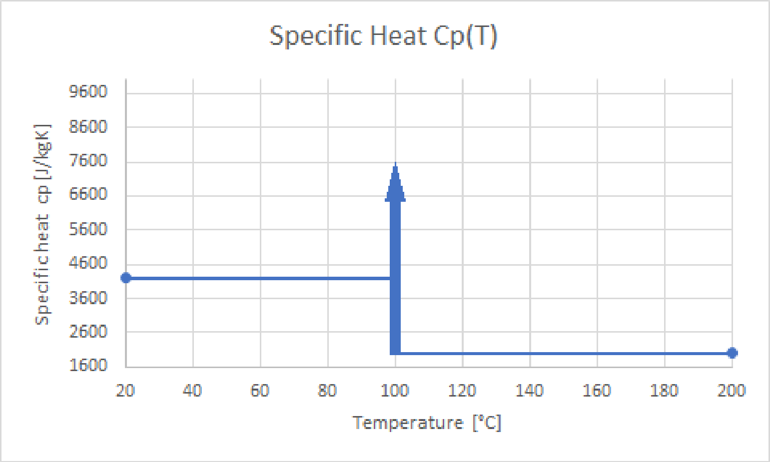

Figure 6: Theoretical expression of the specific heat variation with temperature: the arrow represents a Dirac, modeling an infinite thermal inertia of the fluid during vaporization.

For obvious numerical reasons, the vaporization interval has been spread just like it has been done for the density variation, and the Dirac has been approximated initially in the way depicted in (Figure 7) (notice that, from theory, the area under the $c_p(T)$ function has to match the specific enthalpy variation experienced by the liquid):

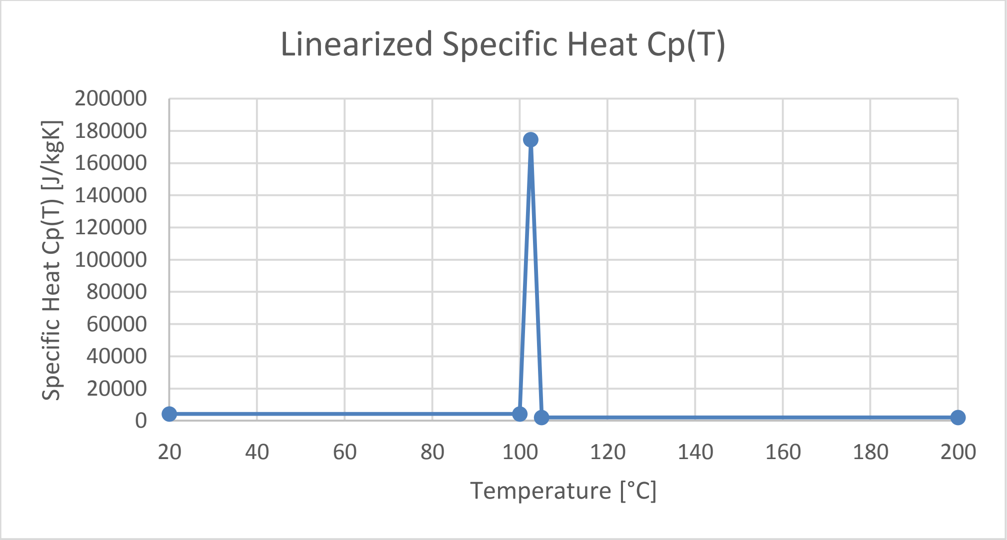

Figure 7: Actual linearization of the previous theoretical expression of the specific heat.

Furthermore, the models added to the physics in this case were:

- Segregated fluid enthalpy
- Gravity

As It would have been later noticed, the simple presence of the gravity model would cause complications due to the strong density variation with temperature, that would be reflected on the continuity and momentum equation due to buoyancy effects.

2.2.3 Running the simulation:

After having imposed these liquid properties and the previously explained boundary conditions, the simulation has been run, and the results were really not satisfying. In fact, the steep density and specific heat variations with temperature caused very important instabilities of the solvers, that could not reach convergence.

The first attempt at solving these issues consisted in varying the conjugated gradient solver parameters, assigning, for every equation, a stricter convergence tolerance and a higher number of maximum solver cycles, together with a strong reduction of the under-relaxation factors.

Consequently, the behaviour of the calculations surely improved, but the simulation was structurally unstable at its core, and the residuals kept diverging multiple times whenever the liquid met the vaporization conditions.

As it has been noticed after some theoretical analyses, the behaviour of the residuals was heavily influenced by the derivative discontinuities of the $\rho(T)$ and $c_p(T)$ during vaporization. Furthermore, some cells could probably not feel the specific heat "Dirac", because of a too short vaporization interval, thus feeling a much lower c_p (they passed from temperature values below the vaporization interval to others above it in only one iteration) and increasing their temperature way above realistic values (causing major calculation errors).

Consequently, the vaporization temperature interval needed to be increased in order to ensure much less steep variations of density, and the specific heat dependence on temperature had to be somehow changed in order to take into account the abovementioned effects.

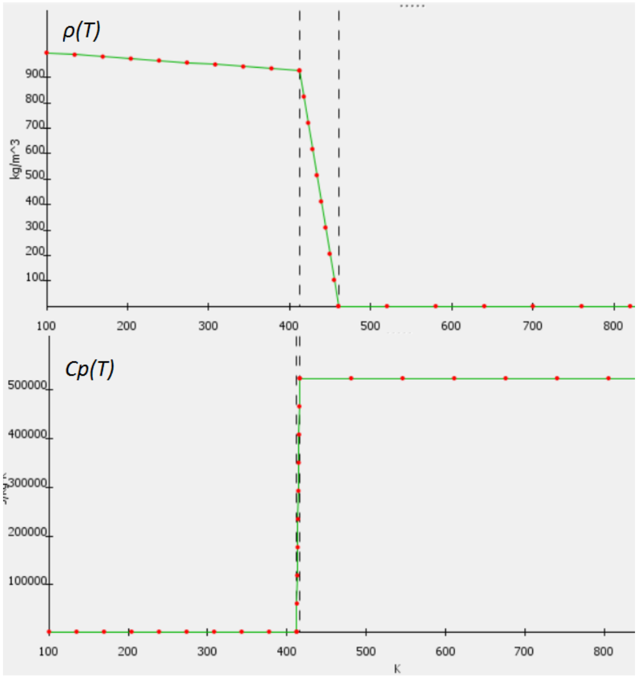

Figure 8:Definitive expressions for density and specific heat employed to model vaporization.

After many attempts, the best conditions that could ensure an acceptable convergence were the following ones (Figure 8):

Notice that these expressions of $\rho(T)$ and $c_p(T)$ were the first ones giving acceptable numerical results, but surely were not really satisfying from the perspective of adherence to physical reality. Furthermore, the vaporization interval considered for density was ranging from 412 K to 460 K (taking into account that water is pressurized, and vaporization occurs at a higher temperature than 373 K (i.e. 100°C)). This is a clear sign of the limits of the CFD modeling techniques chosen to describe a complex phenomenon such as vaporization.

2.2.4 Adding the external tube and the LBE flow

After having considered only the fluid region, the next natural step of the simulation consisted in adding the external tube, and applying the heat flux boundary condition to its outer surface (contacting with LBE).

The external tubes geometry had been previously created, so the only steps further needed were the creation of the mesh (depicted in Figure 4), the choice of the physics solid models and the setting of the boundary conditions. Initially, an excessive conductivity value of 16 W/mK has been used, effectively neglecting the influence of the Helium layer inside the tubes. This has been corrected later, and a more adequate conductivity of 1.1 W/mK, close to the harmonic mean of the two extreme cases, was chosen (the same one employed in the later, HX half model).

After running the simulation a first time with a condition of a constant heat flux (using the same value as before of 44.4 kW/m^2), gave apparently good results in terms of stability.

The external LBE fluid region was then added; to create this region it has been compulsory to consider the hexagonal matrix of the whole HX, and find its fundamental dimensions and characteristics. Approximately, each tube interacts with a hexagonal-based prismatic region of LBE surrounding it. In this case, since only one fourth of the tube had been modeled, it was necessary to create, at CAD geometry level, a 90° slice of the abovementioned prismatic region, which has then been imported into the simulation and meshed.

All the LBE temperature-varying characteristics [4.] were added when choosing the physical models, and the boundary conditions were set accordingly to the official CIRCE reference documents.

The obtained results (with a tubes conductivity of 1.1 W/mK) are summarized in the following Figure 9:

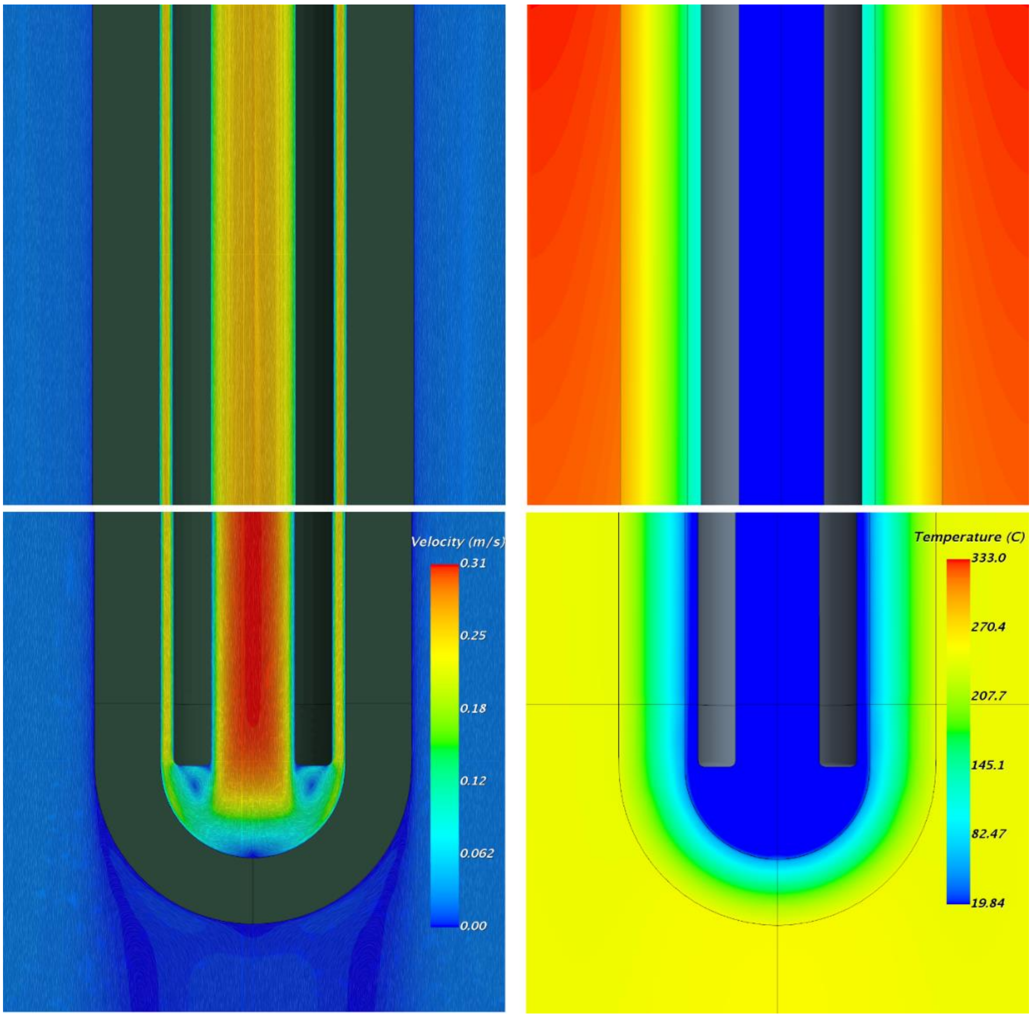

Figure 9: Double bayonet tube simulation. Left: velocity field at the top and bottom regions of the tube. Right: corresponding temperature field in the same fashion.

2.2.5 Conclusions:

After concluding the modeling for this single tube element of the HX, it has become clear that some very complex physical processes, like vaporization, require very computationally-demanding methods to be appropriately solved. With the choice of simplified temperature-varying properties models, it has been impossible to reach accurate and reliable results, and, in the end, this first model had no further use in the following parts of the stage work. At the same time, considering the high difficulty encountered, the technical numerical experience gained through this second phase of the work, together with a deeper comprehension of the HX mechanics, has had a huge impact on the most important work, in the third phase that will be further discussed.

3. Phase 3: Analysis and modeling of the whole CIRCE-ICE Heat Exchanger. (29/05/2017 – 31/08/2017).

After analyzing the single double bayonet tube model, the focus has been shifted towards the more interesting, bigger-scale problem of the whole CIRCE-ICE main Heat exchanger.

The objective of this phase of the internship was the creation of a reliable STAR-CCM+ model of the abovementioned HX, capable of appropriately simulating its working behaviour under steady state conditions, in order to investigate how this component can influence the general behaviour of the CIRCE primary loop. In fact, this model will be later used as the basis for the master thesis stage, where all the transient cases of the experiments regarding the whole facility will be studied.

3.1 General characteristics of the CIRCE-ICE HX.

In the global picture of the CIRCE primary loop, the HX plays the very important role of the heat sink of the circuit, and has a thermal duty of ~800kW, in order to subtract from the LBE the heat power that was previously supplied by the FPS.

The scheme reported in Figure 1 shows the main characteristics of the CIRCE primary loop, highlighting the average temperatures of the LBE throughout the circuit (it is important to notice that these values are indicative, and do not change too much from one case to another, thus being a good example of the general expected thermal behaviour for LBE throughout the circuit).

It is important to notice that the HX is installed in the higher part of the facility, in order to promote the natural circulation of LBE through the loop, due to the density increase caused by the heat subtraction.

From a geometrical point of view, the HX can be subdivided into three different regions:

1)The Separator region

2)The Intermediate region

3)The Outlet region

3.1.1 The separator region:

Figure 10: Picture of the real separator zone of the CIRCE facility. The 91 double bayonet tubes of the HX are depicted, together with the riser outlet and its three thermocouples. [1.]

As can be seen from Figure 1, after being heated up in the FPS, the LBE flows upwards through the riser thanks to the Argon-pump system, and inside the HX passing through the separator (a volume with both the purposes of connecting riser and HX, and allowing the Argon to exit the liquid LBE).

In this region, the liquid LBE makes its first contact with the 91 double bayonet tubes that run down through the whole body of the HX, and starts exchanging heat power with the vaporizing water flowing inside them.

Some other key details must be highlighted when describing the separator; in fact, this particular zone of the facility is one of the most difficult to model, for different reasons:

1) The multiphase condition (LBE+Ar) of the flow coming from the riser would require extremely computationally-expensive methods (like the VoF) to be modeled, and thus needs to be simplified, becoming a constant source of uncertainties and errors.

2) The top part of the separator is not sealed, and the LBE actually presents a free surface there (separating LBE and Argon exiting the mixture). This means that many complex

projection effects will take place, some that not even an accurate VoF model would be capable of describing with accurate precision.

3) It is almost certainly known that some LBE leakage from the separator to the bulk may take place in this region. The modeling of such leakage would be rather complex and of no particular relevance for the modeling of the single HX, while it may have a significant influence on the behaviour of the whole facility, and especially on the bulk temperature field. Hence, this effect has been considered negligible in this phase, while further research will be pursued in the next master thesis stage.

Furthermore, the CIRCE separator has a rather complex geometry, as shown in the picture above.

As will be accurately described later, a precise and realistic modeling of this geometry would have been too expensive from a computational perspective, since the whole model would have become totally devoid of symmetries; the geometry of the separator has thus been simplified as symmetrical, trying anyway to respect the most important dimensions of the element.

3.1.2 The intermediate region (HX "column")

This is the main body of the CIRCE heat exchanger, isolated from the external bulk zone of the facility by a low-conductivity shell.

In this intermediate region, the LBE flows down through the hexagonal matrix pattern formed by the 91 double bayonet tubes, exchanging heat power with them and lowering its temperature.

The pressure losses along this region are almost totally referable to the noticeable piezometric difference between the inlet and the outlet (from the official CIRCE drawings, the whole LBE-immersed length of the tubes is ~3.45 m), while the pressure losses due to viscous friction are relatively negligible.

In order to keep under control the temperature of the LBE entering the HX, three thermocouples are placed on a section of the HX located 30 mm under the separator bottom, disposed at 120 degrees in order to extract a medium temperature value representative of the whole flow.

3.1.3 The outlet region

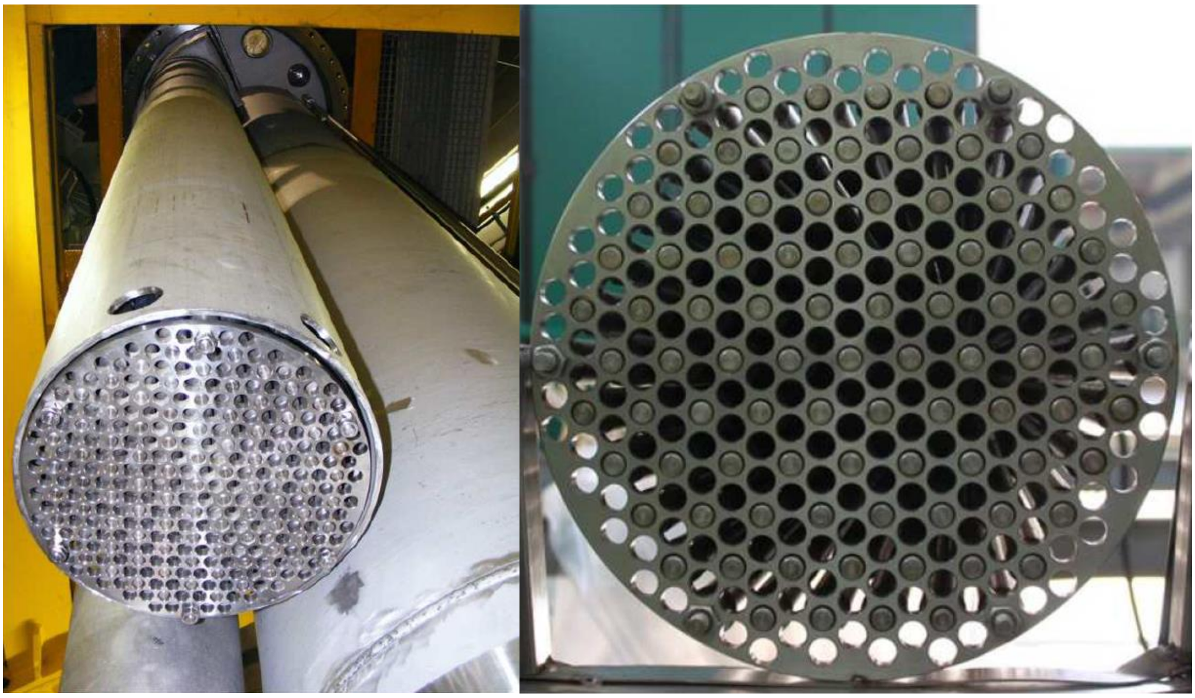

Figure 11:Pictures of the real outlet region of the CIRCE HX. In the top picture, the global structure of the HX can be seen, while in the bottom one a detail of the grid is presented. The HX skirt is not represented in these images. [2.]

The downmost, ending region of the HX is designed in order to regularize the flow exiting the HX, guiding it back down to the FPS lower zone and avoiding the upflow in the undesired upper regions of the LBE bulk (that would affect drastically the temperature field in such region).In the attempt to do this, the HX shell has been designed with an additional ending “skirt”, with a length of ~30 cm (not visible in Figure 11). This skirt allows the flow to develop downwards, avoiding the abovementioned undesired upward refluxes.

Furthermore, in order both to regularize the exiting flow and to block the double bayonet tubes in their downmost part, a grid has been placed in the section connecting the HX original shell and the added ending skirt

At the bottom of this skirt, in a section 100 mm above its ending, six thermocouples of different lengths (53 mm and 115 mm) have been placed in a regular 120 degrees pattern.

Together with the previously mentioned thermocouples in the intermediate region, these ones are used to calculate, with appropriate energy balances, the total heat power subtracted by the whole HX and to estimate the conditions of the steam exiting the double bayonet tubes.

3.2 HX Modeling in STAR-CCM+

The modeling of this HX required various steps of growing complexity, ranging from the first very simple models, where only an intermediate portion of the HX was considered, to the last model, where all the three previous regions were considered, reaching the maximum level of detail.

3.2.1 The first HX model: HX slice

The basic idea behind this first approach to the HX model, has been the analysis of a very simple 30 degrees slice of LBE, taken from the previously described intermediate HX portion.

3.2.1.1 Geometry and mesh generation:

The first step towards the creation of this model has been, as usual, the generation of the geometry, and since no official CAD file was found, the model had to be created from scratch, searching for all the data from the official CIRCE documents. After some research, some valid and detailed official drawings of the HX were found, and are reported in Figure 12.

Since the 91 tubes inside the cylindrical HX vessel are disposed in a hexagonal matrix pattern, a 30 degrees slice of the HX was considered a very good geometry to start with, because the whole HX geometry could have been later obtained from it just by using replication and/or mirroring patterns at CAD level.

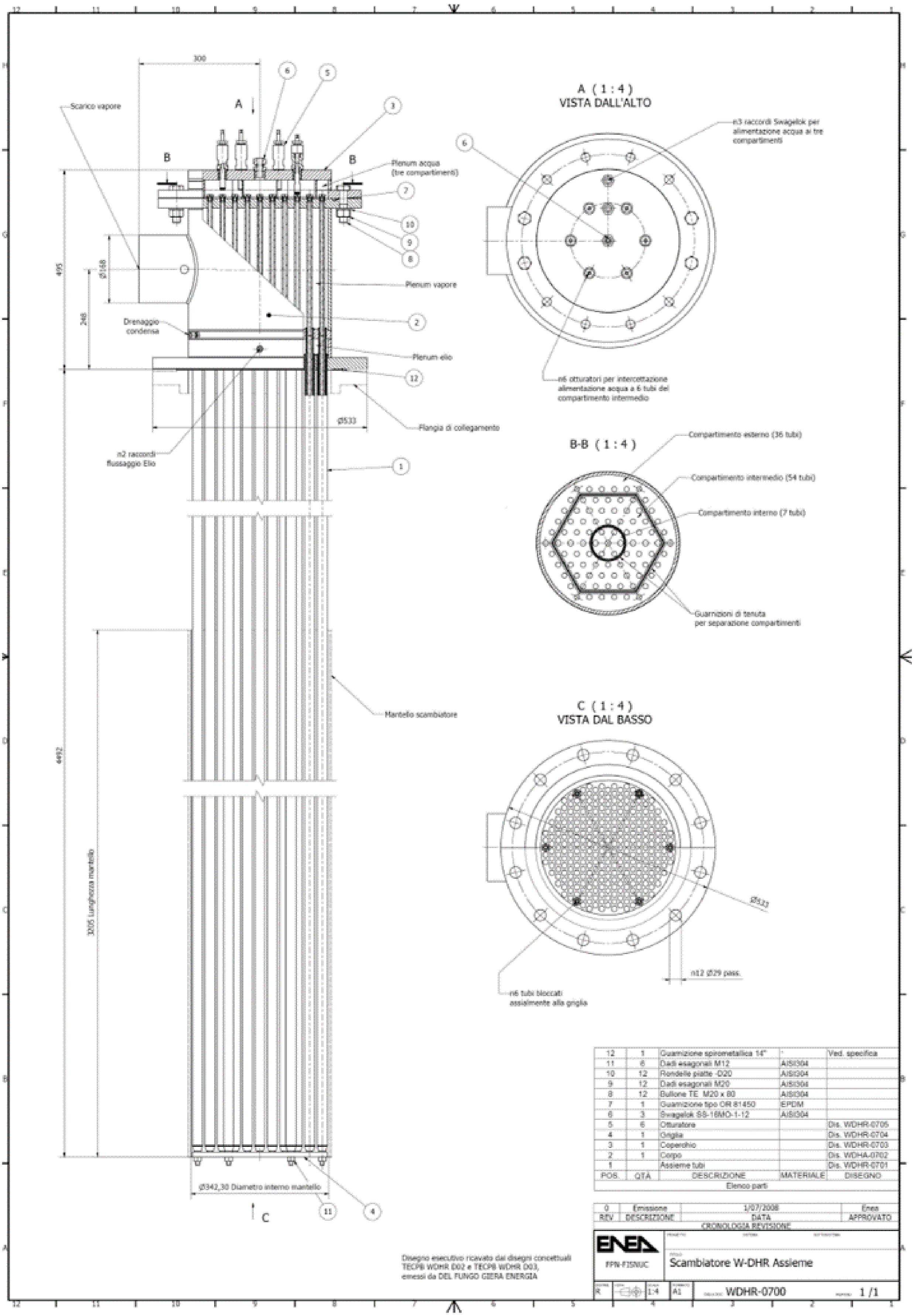

POS.	QTÀ	DESCRIZIONE	MATERIALE	DISEGNO
12	1	Guarnizione spirometallica 14"	-	Ved. specifica
11	6	Dadi esagonali M12	AISI304	
10	12	Rondelle piatte -D20	AISI304	
9	12	Dadi esagonali M20	AISI304	
8	12	Bullone TE M20 x 80	AISI304	
7	1	Guarnizione tipo OR 81450	EPDM	
6	3	Swagelok SS-16MO-1-12	AISI304	
5	6	Otturatore		Dis. WDHR-0705
4	1	Griglia		Dis. WDHR-0704
3	1	Coperchio		Dis. WDHR-0703
2	1	Corpo		Dis. WDHA-0702
1		Assieme tubi		Dis. WDHR-0701

Elenco parti

REV	DESCRIZIONE	DATA	APPROVATO
0	Emissione	1/07/2008	Enea

CRONOLOGIA REVISIONE

Figure 12:Official technical description of the HX geometry. [2.].

The geometry was then created using the information from the drawing above, and furthermore, almost every design parameter was exposed, in order to allow later major variations of the geometry directly from the simulation level of STAR-CCM+. For instance, the vertical length of the HX slice could be changed, and this allowed to gradually reach, with various steps, the condition of 3.45m vertical length (whole LBE-immersed double bayonet tube length).

In order to start with a simple condition, the first considered HX slice had a very small vertical length of 0.5 m, and its representation is shown in Figure 13(left) (please notice that only the LBE fluid region is displayed here, the solid part of the tubes would have been added later). As can be noticed, the top region of the slice was divided from the bottom part, for meshing purposes.

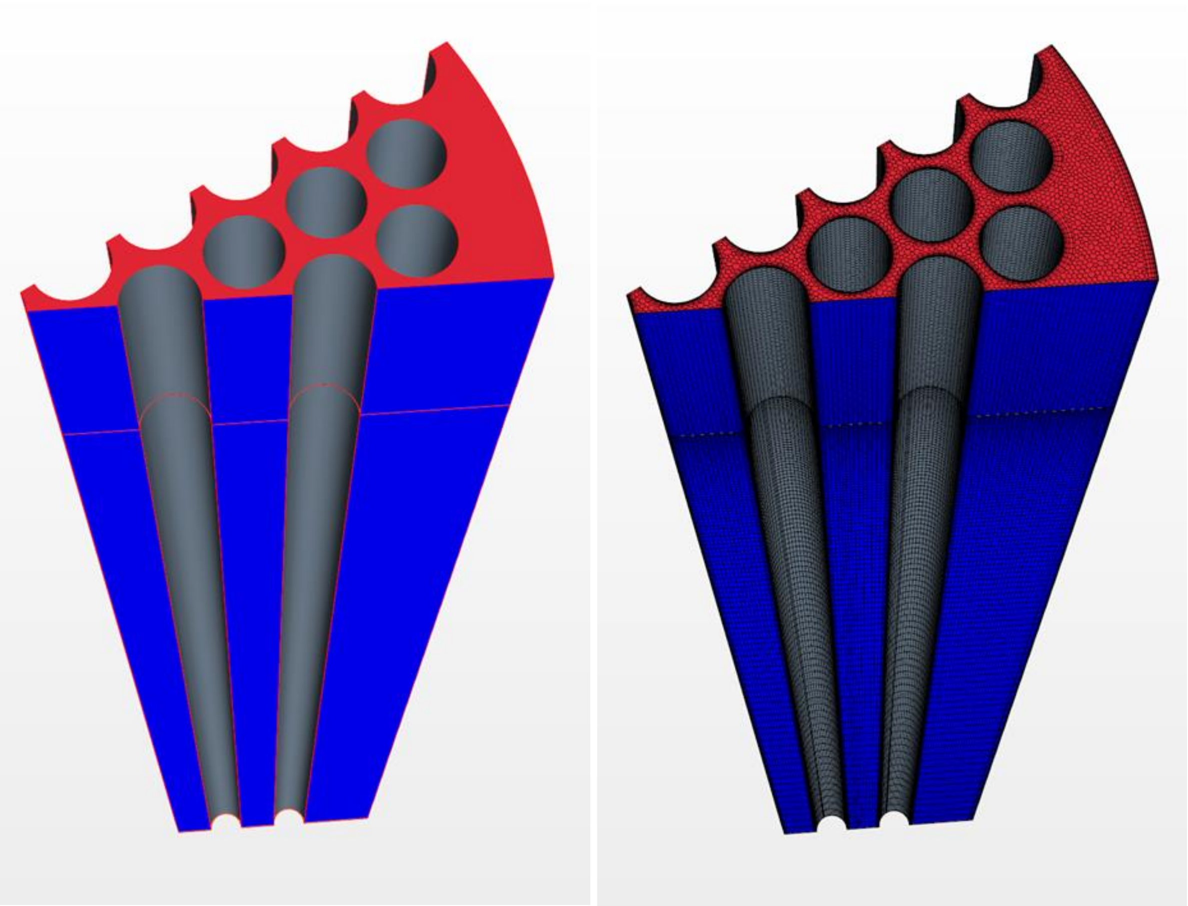

Figure 13: Geometry and mesh for the first HX slice model

In fact, the mesh for this element has been created considering two separate regions (Figure 13, right):

1)HX Slice "short" top region (INLET): automated polyhedral mesh operation, with adequate custom controlled surface refinement near the surfaces contacting with the tubes.

2) HX Slice “long” bottom region: this part has been meshed using a directed mesh operation, using as a source the contacting surface mesh of the HX top slice. In both parts, a prism layer mesher has been employed, in order to ensure a correct solution of the boundary layer effects.

3.2.1.2 Selecting models and boundary conditions:

In order to start with a very simple condition, the very first case that has been studied for the abovementioned geometry was the segregated “cold” flow condition, with no thermal aspect considered (yet).

Hence, the chosen physical models for this initial step were:

1)Segregated flow

2)Constant density

3)Turbulent flow, modeled with standard RANS k-epsilon

The boundary conditions on the surfaces of the CFD domain (liquid LBE) were imposed as follows:

LBE MASS FLOW INLET (top surface of the domain) : the LBE mass flow rate value for this inlet boundary has been computed considering the value of ~56 kg/s, found in the official CIRCE reference documents, and dividing it by 12 (considering that only a 30 degrees slice of the whole HX was considered in this case).

LBE PRESSURE OUTLET (bottom surface of the domain): considering that almost the whole pressure drop that the LBE experiences by flowing through the HX can be referred to piezometric effects (because of the strong height variation of 3.45 m together with the very high LBE density of ~10^4 kg/m^3), the pressure at the outlet of the domain has been fixed to 1 bar, and the pressure values throughout the domain are expressed as pressure differences relatively to this value.

ALL OTHER WALLS: NO SLIP SHEAR STRESS CONDITION

3.2.1.3 Running the simulation:

Considering the not too high number of volume mesh cells, the simulation could still be run on 2 local CPUs, and the solvers showed good stability, reaching convergence with no particular problems.

3.2.1.4 Adding the thermal models

After reaching convergence with the segregated "cold" model, the next step was the implementation of the thermal models in the simulation. This implies that the real LBE properties had to be considered from this point on (density, dynamic viscosity and specific heat expressed as temperature-dipendent functions), together with the solution of the segregated enthalpy equation, and the presence of gravity.

Although the considered geometry was still very different from the actual HX geometry, it felt as a good idea to start implementing the thermal models in order to have a first glimpse at how they behaved together with the other previously selected models ("cold" segregated flow).

In fact, some different aspects have to be considered at this stage:

1) the LBE has a very low Prandtl number, due to the very high value of its thermal conductivity compared to its dynamic viscosity. This essentially means that this fluid tends to be much more sensible to the rate of thermal diffusion near boundary walls than it is to the rate of momentum diffusion (and thus, always shows a thermal boundary layer thicker than the viscous one).

2) as it has been previously said, the LBE density has been modeled as a temperature dependent function, and is thus a sort of "bridge" between the equations of enthalpy momentum and continuity.

3) The gravity is now present in the momentum equation.

These elements, if considered together, explain how the velocity field is extremely affected by the temperature field and, in general, by the heat transfer phenomena; hence, buoyancy effects are heavily present and need to be kept under strict control.

Hence, the added models in this phase were:

1) Segregated fluid enthalpy

2) Polynomial density (and temperature varying properties in general).

The expressions for density, specific heat and dynamic viscosity variations with temperature were extracted from [4.], and are reported in the following Table 1):

Property	SI unit	Correlation	Temp. range (K)	Estimated error
Melting point	K	$T_M = 398$	n/a	1
Latent heat of melting	kJ/kg	$L = 38.6$	n/a	0.3
Density	kg/m^3	$\rho = 11065 - 1.293T$	$T_M - 1300$	0.8%
Heat capacity at constant pressure	J/kg.K	$c_p = 164.8 - 3.94\times10^{-2}T + 1.25\times10^{-5}T^2 - 4.56\times10^{5}T^{-2}$	$T_M - 1100$	7%
Dynamic viscosity	Pa.s	$\mu = 4.94\times10^{-4}\exp(754.1/T)$	$T_M - 1200$	8%
Thermal conductivity	W/m.K	$k = 3.284 + 1.617\times10^{-2}T - 2.305\times10^{-6}T^2$	$T_M - 1200$	15%

Table 1: LBE temperature-depending properties, expressed according to [4.]

3.2.1.5 Imposing the thermal boundary conditions

Since the geometry was, at this stage, still very different from the real one, and referring to only a portion of the intermediate region of the HX, it was not yet compulsory to have an extreme level of precision on the imposed boundary conditions, that have thus been determined in an approximate way. Essentially, the main aim of this phase has been to verify the coherence of the CFD solution (thermal field, velocity field and an approximated energy balance) with the imposed conditions, in order to have more confidence with the models when passing to geometries of growing complexity.

The imposed boundary conditions were:

1) LBE INLET TEMPERATURE – CONSTANT TEMPERATURE: 600 K (~327 °C, intermediate value).

This value has been chosen considering that the temperature of LBE at the inlet of the HX is, from the CIRCE reference document, of about 348 °C, and also remembering that the modeled region is, up to now, a small portion of the whole intermediate part of the HX, far from the inlet. In this sense, it appeared as a good approximation to consider as the domain inlet a section where the temperature had already decreased from its maximum value.

2) TUBES-CONTACTING SURFACE - CONSTANT TEMPERATURE: 373 K (~100 °C)

Remembering that, up to now, the solid double bayonet tubes were not added to the model, the only way to simulate the heat exchange at the surfaces where LBE is actually contacting with the tubes was to impose there an adequate thermal boundary condition.

For this first and very unrealistic attempt, a fixed temperature condition of ~100 °C, intermediate between the water inlet temperature of 10/50 °C and the vaporization temperature of ~120 degrees (vaporization takes place at higher saturation pressure than 1 atm, as will be later described) was considered acceptable, and capable of giving information about the stability and coherence of the model.Another option could have consisted in imposing a constant heat flux boundary condition, but the effect of it on the LBE flow would have been too strong and evaluated as “innatural”.

It has to be kept in mind, anyway, that the real heat exchange regime at the surfaces where LBE contacts with the tubes is determined essentially by the behaviour of the water of the secondary circuit, which flows inside them and vaporizes. Hence, in the most realistic models, the thermal boundary condition imposed must respect the water physical behaviour, and in the later, more complex models this has been done with particular attention.

3) HX EXTERNAL WALL (SHELL): ADIABATIC

3.2.1.6 Running the simulation:

The simulation has then been run on 2 local CPUs, and reached convergence with good stability. The results are shown in the following Figure 14:

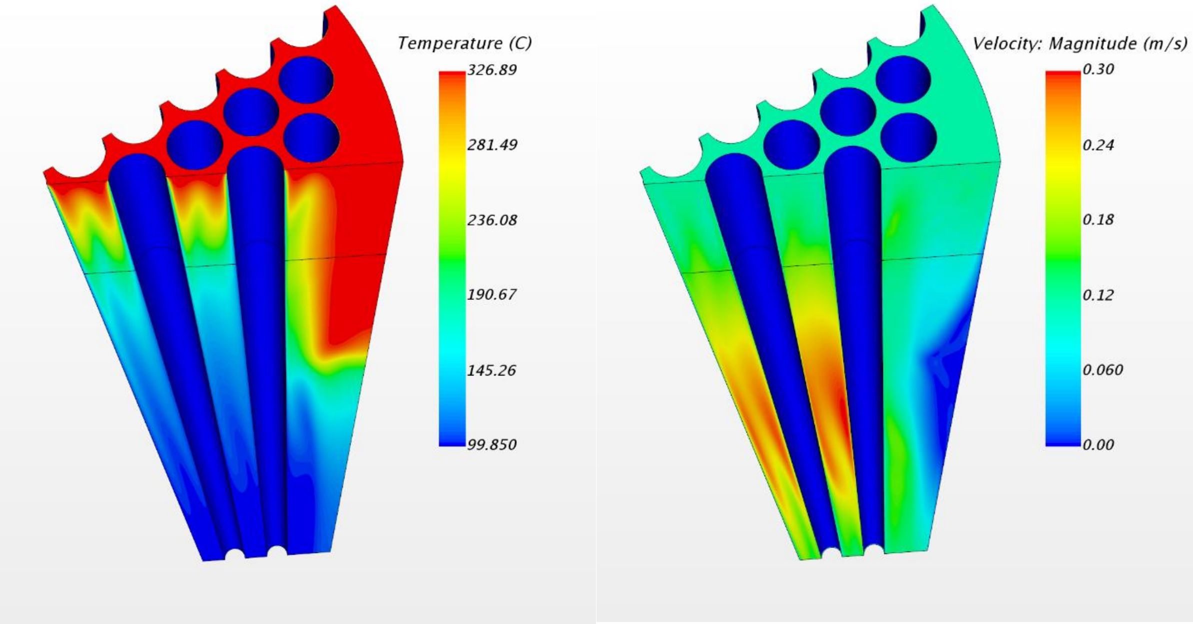

Figure 14: Velocity and temperature field for the first complete simulation of the HX slice (0,5 m length)

3.2.1.7 Increasing the vertical length of the analyzed HX slice

In order to better understand how the solution would have behaved considering a longer portion of the HX intermediate region, the geometry of the HX slice model has been progressively changed, by making use of the exposed parameters that had been created when generating it from scratch. So, the HX slice length has been increased multiple times, computing the solution at every length with the same boundary conditions that had been set for the initial model. The steps have been:

1) HX slice length= 0.5 m (initial model)

2) HX slice length = 0.7 m

3) HX slice length = 1 m

4) HX slice length = 2

Notice that, at each step, the top inlet region of the slice (the one meshed with the polyhedral mesher) has been kept at a constant length, while the lower, longer part (the one meshed with the directed mesher) has been elongated, and the number of directed mesh layers have been increased in order not to have excessive cell dimensions.At the last step (2 m length), the number of cells of the volume mesh for the whole model was of about 10^6, and the only 2 CPUs of the local machine were starting to fatigue and perform slower than before. In order to reach convergence faster, the calculations were then distributed on all 4 local CPUs, and their speed marginally improved. Anyway, with meshes of this magnitude, the need for the CPU clusters was already felt.It is important to notice how highly the velocity field is affected by the temperature field. The following Figure 15 shows this effect with particular detail (with reference to the HX slice length of 0.5 m, but the same effect has been observed for any chosen HX slice length).

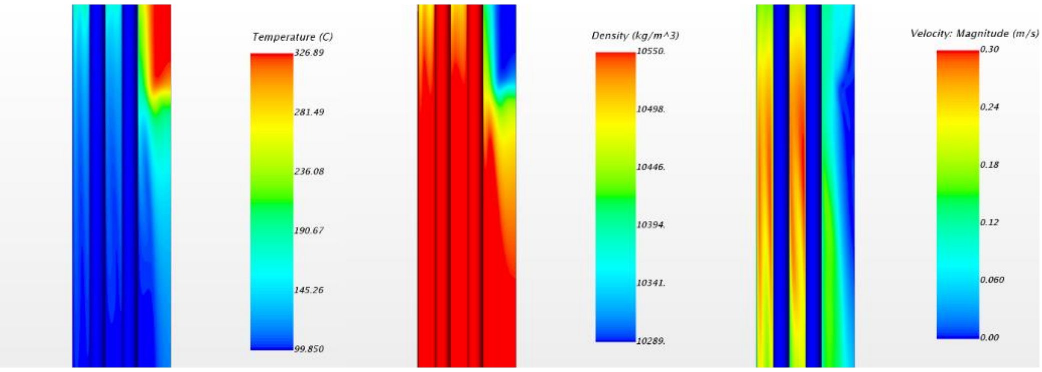

Figure 15: Temperature, density and velocity magnitude fields for the HX slice model (0.5 m length). Similar results have been obtained for all the different lengths of the slice.

This effect is clearly due to the influence of the heat transfer near the tubes: in fact, the hot LBE flow exchanges heat with the water/steam mixture inside the tubes, lowering its temperature. This leads to a strong increase in LBE density in the region near the tubes surface, where the thermal boundary layer has a dominant effect. Since the model is also considering the effects of gravity, the effect of this local increase in density is an acceleration of the flow near the tubes (coldest region); Due to continuity, this local acceleration "calls" fluid from the upward region, causing what can be perceived as a sort of "pulling fluid" phenomenon towards the tubes. This, always for continuity issues, generates a local high-vorticity zone, with very low velocity magnitudes, and a considerable amount of LBE flowing upwards near the external wall of the HX and re-uniting with the zone where the "pulling" thermal phenomenon starts.

All these natural convection issues are strictly linked to the previously explained properties of LBE, and particularly to its low Prandtl number, which testifies how relatively strongly the fluid perceives the thermal influence of the cold double bayonet tubes.

3.2.1.8 Adding an outlet region (simulation of the outflow into the LBE bulk)

The HX slice region that has been considered up to now was meant to represent a generic portion of the whole intermediate region of the HX, rather far from its inlet and outlet regions, and thus presenting a very regular flow.

Yet, as explained in the introductory paragraph, the CIRCE HX has a rather complex geometry at both the inlet and outlet sections, and the real LBE flow is highly influenced by it. It is thus necessary to design more accurately both the outlet and inlet regions when aiming to reach adequate levels of modeling precision.

Hence, in order to better understand the behaviour of the LBE flow at the bottom of the HX, a lower LBE outlet region has been added. This region has been designed to somehow simulate the bulk region of the CIRCE main vessel, thus allowing for a more natural and realistic outflow condition for the LBE.

This has been done also for two other main reasons:

1) Considering what has been previously said about the effects of the heat exchange on the velocity field near the outlet of the HX, it would be more appropriate to let the flow develop naturally through that region and into the bulk, in order to better understand its real behaviour.

2) In a more realistic model of the HX, the presence of the grid at the bottom of the HX (where the ending “skirt” contacts with the shell) should be taken into account. This has been done by employing a porous baffle interface, with appropriately calculated resistance values, without actually creating the grid geometry.

So, this outlet LBE region comprehends the LBE inside the HX skirt, the baffle interface simulating the grid, and a portion of the bulk region of the CIRCE main vessel. Furthermore, the last one has been designed with an ending “nozzle-like” shape at the bottom, meant to guide the flow towards the outlet of the whole CFD domain. The ending part of the double bayonet tubes has been approximately considered plane, at section where the baffle interface representing the grid was located; this is an absolutely acceptable geometric simplification.

All the geometric parameters of this region were exposed, in order to manage them more easily directly at simulation level (not entering the CAD environment).

The chosen mesh for this bottom part of the CFD domain has been generated employing a polyhedral mesher, with a more accurate refinement of the cells along the central part of the region, connecting vertically the HX skirt to the ending nozzle, in order to monitor more accurately the flow characteristics there. A prism layer mesher has also been employed for a better description of the boundary layers.

The results are shown in Figure 16.

The characteristics of the baffle interface representing the grid were calculated with reference to [5.] .

The resulting value for the porous resistance coefficient of the interface is kt= 5.1; as it would have been later noticed, this value causes quite a high regularizing effect on the flow exiting the HX shell and entering the skirt, even if the estimated grid pressure loss accounts to “only” ~350 Pa .

At this point, a brief test simulation has been run in order to check the flow behaviour in the new region and verify the appropriateness of the mesh. The boundary conditions used for this test mesh where identical to the previous model for both the inlet (imposed mass flow rate), the tubes-contacting surfaces (imposed temperature) and all other surfaces except for the outlet.

In fact, the previous outlet was located at the section where the baffle interface is now present, while the new outlet is located at the very bottom of the CFD domain, at the end of the “nozzle”. The imposed outlet boundary condition is still a fixed value of 1 bar of pressure, with the same hypotheses explained for the previous outlet.

The test simulation behaved well and, as explained in the next paragraph, some other steps towards the gradual improvement of the model could be made.

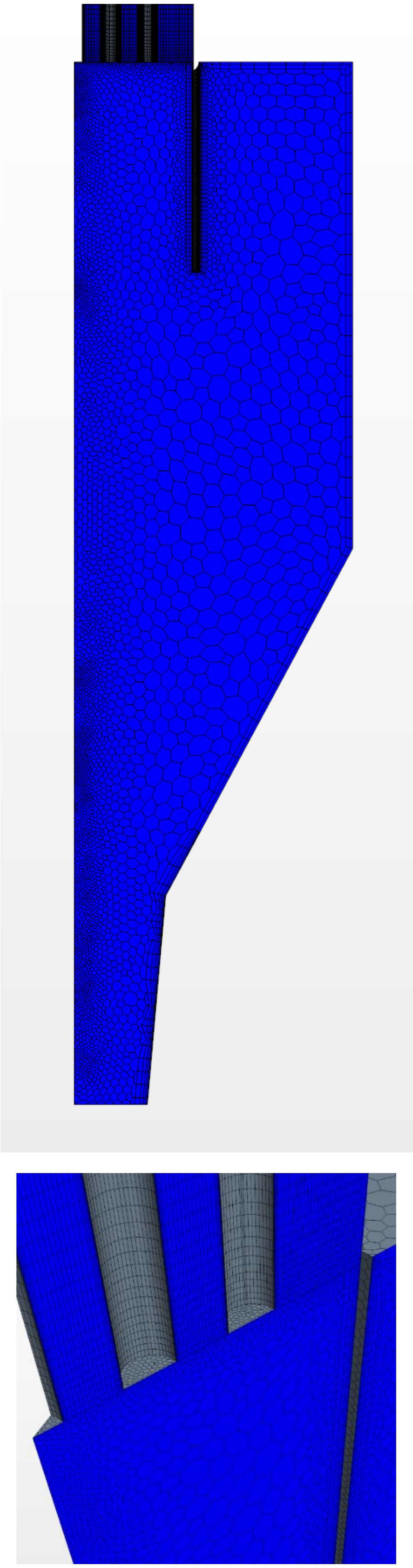

Figure 16:Mesh for the outlet region, and detail of the baffle interface area

3.2.1.9 Refining the model: creating the geometry of the external part of the double bayonet tubes

Until now, the thermal boundary condition employed to simulate the heat exchange between LBE and water of the secondary circuit has been an imposed constant temperature of 373 K at the LBE contact surfaces with the tubes. This condition is particularly severe and unrealistic, for a different number of reasons:

1) The water vaporizes inside the tubes, which means that a correct boundary condition should be the imposition of a temperature profile on their internal surface rather than the external one.

2) The water evaporating inside the tubes varies its temperature, essentially because the evaporation does not take place immediately at the bottom (the water here is still in a sub-saturated liquid condition) and furthermore, the pressure drops of ~1.5 bar between the water inlet and the steam outlet of the double bayonet tube.

This means that, in general, the temperature on the internal surface of the tubes is certainly not constant, and varies with the Z coordinate (height of the tube). As can be understood, in the most realistic models, a reliable temperature profile at the internal surface of the tubes had necessarily to be evaluated and imposed as a boundary condition, in order both to reach acceptable outlet conditions for the LBE and to satisfy the energy balances required by the water vaporization process. This level of precision on the temperature profile would have been reached only later, in the more refined HX half model, and is described in paragraph 3.2.3 (and following)

For now, creating the geometry of the tubes and assigning a constant temperature on their internal surface was considered a good step forward.

In order to proceed, the CAD geometry for all the HX tubes has been created and imported into the simulation, defining a new solid region of the model. These tubes are comprehensive of both the AISI 304 steel internal and external tubes and the intermediate Helium+powder layer.The biggest problem at this point has been the search for a good way to mesh the whole geometry:

1) The upper part of the tubes has been meshed using the same automated mesh operation employed for the upper LBE inlet part (in order to have a coherent mesh between the LBE and solid tubes).

2) The very bottom part of the tubes has been "sliced" at CAD level in order to allow the use of a polyhedral mesher for the very small ending region.

3)The intermediate part of the tubes (connecting their upper region to their bottom) has been meshed by means of a directed mesher, starting from the existing surface mesh of the upper region of the tubes. Furthermore, since a large number of different surfaces were created at CAD level, the software encountered many difficulties (at simulation level) in recognizing automatically most of the interfaces, especially the solid/fluid ones. To solve this, all interfaces were manually created by coupling the appropriate surfaces. After trying different approaches, the correct interfaces were established, and the mesh could be generated in the appropriate desired way. Figure 17 shows the geometry and mesh of the whole domain, comprehending the solid tubes.

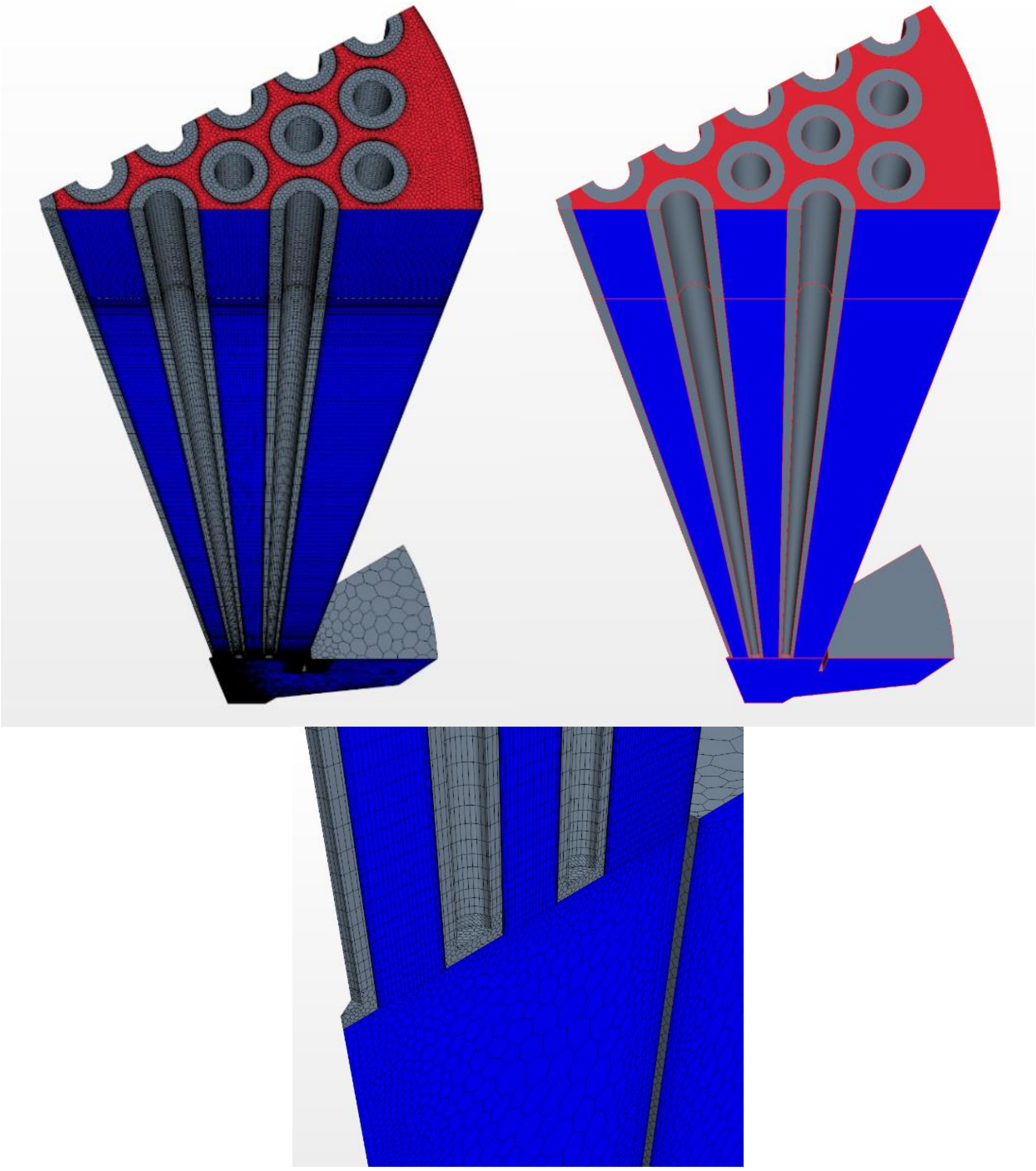

Figure 17:representation of the geometry and mesh for the solid tubes region (only the external part of the double bayonet tubes). A detail of the mesh near the baffle interface is also depicted (bottom)

3.2.1.10 Comment on the tubes physics and boundary conditions

The chosen boundary condition for this first attempt at modeling the tubes still consisted in imposing a fixed temperature of 100 °C, but this time on the internal surface of the tubes. The heat exchange phenomena would thus depend heavily on the tubes physical properties.

The physics continuum chosen to describe the tubes (solid region) was based on the "segregated solid energy" model. Some issues were encountered when choosing the properties of the material, especially with regards to the conductivity of the tubes since, as explained in paragraph 2.1, this value is really not an easy one to determine with good accuracy.

The conductivity was evaluated as follows:

First approach: when the tubes were added for the first time into the model, all the considerations described in paragraph 2.1 had still not been figured out, and the importance of the 1mm Helium+metallic powder layer inside the tubes had been largely underestimated. Hence, for this first approach, the tubes conductivity was set to the one of the AISI 304 steel (no helium layer) of 16 W/mK.

After running the simulation, the results were obviously totally different from the expected ones Figure 18, since the LBE temperature at the outlet reached really low values (around 127 °C, reaching the thermal equilibrium with the temperature inside the tubes) and the total heat power removed, measured with an energy balance between the LBE inlet and baffle interface (outlet) was somewhat around 1600 kW. The expected values for LBE temperature at the outlet and heat power removed by the HX are, from the official CIRCE documents:

LBE outlet temperature: around 270 °C

Heat power removed by HX: ranging from 650 to 800 kW.

It was clear that conductivity played the biggest role in this, and after some theoretical considerations, it could be understood that the importance of the 1mm Helium+powder layer could not be neglected.

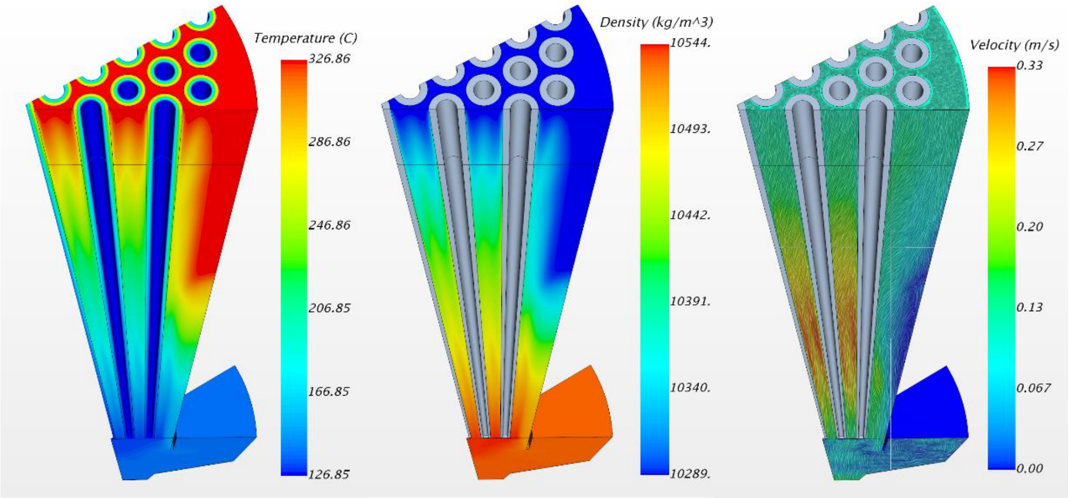

Figure 18: Results of the HX slice model (2 m length), obtained with a tubes conductivity equal to 16 W/mK, expressed as temperature, density and velocity fields.

Second approach: Henceforth, knowing the importance of the Helium+powder layer, the new conductivity was estimated firstly as equal to 0.687 W/mK, value assumed in case of no presence of metallic powder inside the Helium gap (hence this was a low guess on the real conductivity). The simulation has been run again, and the results were much closer to the desired ones (Figure 19)

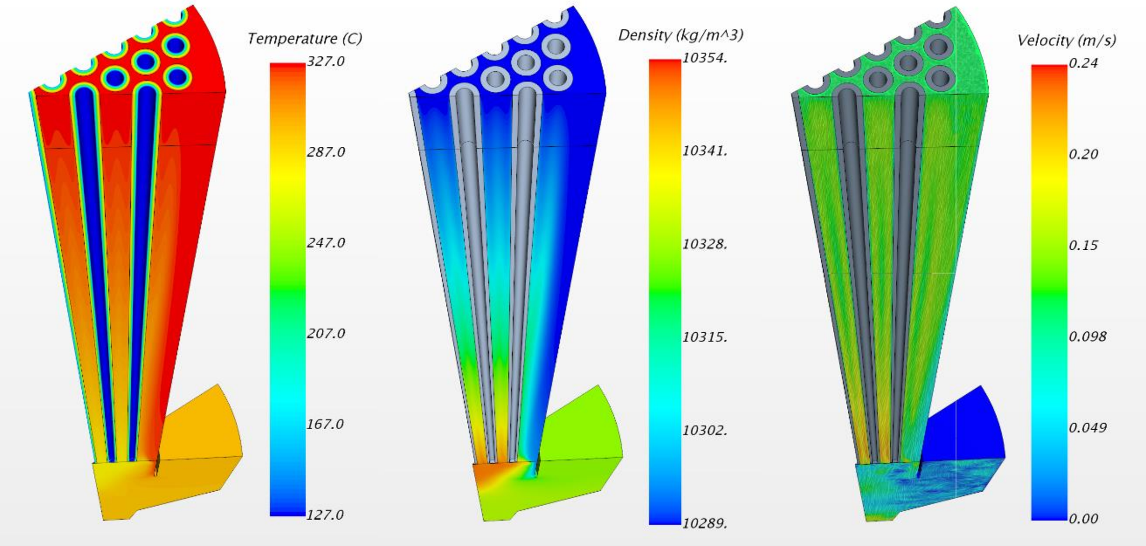

Figure 19:Results of the HX slice model (2 m length), obtained with a tubes conductivity equal to 0.687 W/mK, expressed as temperature, density and velocity fields. The outlet temperature now reaches a more realistic value.

Comparing the two cases it appears evident how conductivity plays an important role in the whole energetic problem. The real conductivity of the Helium+powder layer should be greater than the value of 0.687 W/mK, but not too much. Different values will be tried later on.

3.2.1.11 Considering the whole HX length and adding a lateral inlet region

The next steps consisted essentially in:

1)Modifying the considered HX length in order to reach the value of the full immersed tube length (3.45 m).

2)The 3D CAD geometry has been modified by adding a new lateral inlet region, whose purpose is to simulate approximately the LBE inlet from the separator, even if the real geometry of the CIRCE facility is very different (this has been only a first attempt at the modeling of the HX in its wholeness).

3.2.1.12 Generating the mesh

The meshing process required particular attention, since both the addition of a new part and the increase in the HX length cause a drastic growth in the total number of cells of the CFD model (a first mesh attempt reports ~1.8x10^6 cells).

The process has been completed by meshing the new lateral inlet part by means of the same operation employed for the upper LBE part (where the previous vertical inlet was located) and the upper part of the tubes. This allowed for a coherent mesh throughout the whole upper region of the HX. Subsequently, in order to allow the LBE flow to develop enough along the inlet before entering the HX tubes region, a Surface/Volume extruder has been used to expand the length of the lateral inlet zone.

In the end, by applying some surface and volume custom controls in order to refine (or coarse) the mesh where needed, the computational cost of the simulation could be slightly reduced (reaching a total number of cells of ~1.6x10^6).

Figure 20 depicts the geometry and mesh for this last HX slice model.

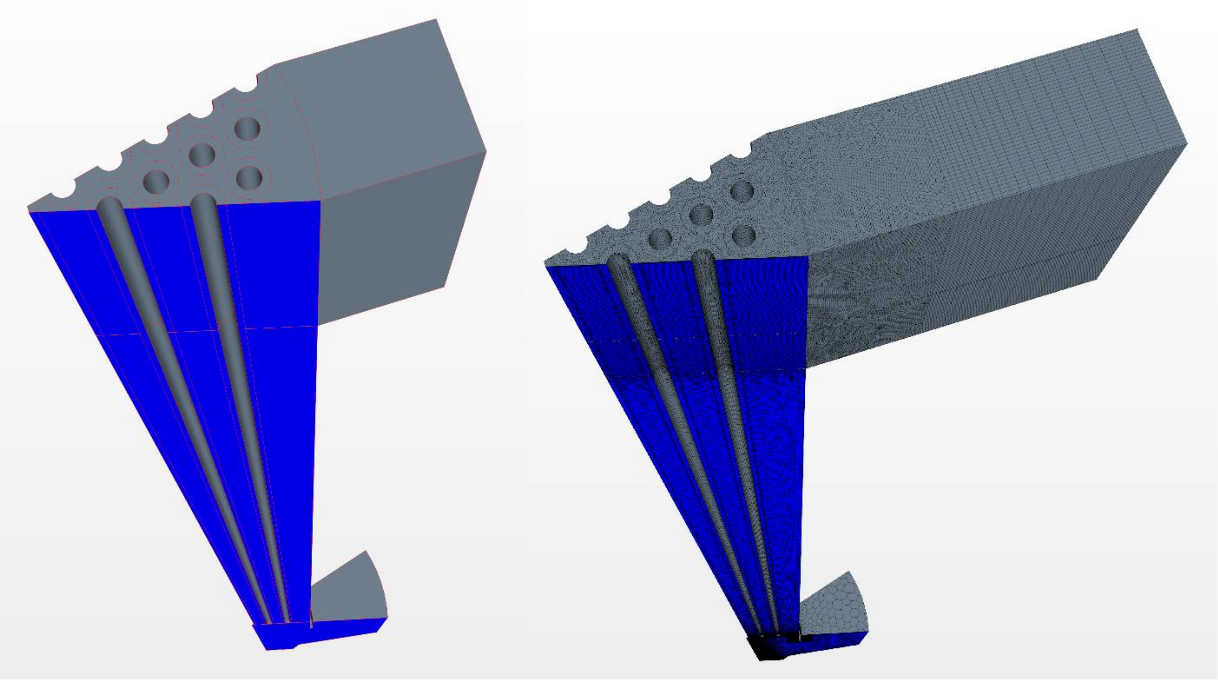

Figure 20:: Geometry and mesh for the HX slice model (3.45 m length, whole immersed tube), also comprehending the outlet and inlet regions.

3.2.1.13 The boundary conditions

The previous vertical inlet of the CFD domain has been replaced by the new lateral one, keeping the same LBE inlet mass flow rate condition of 4.75 kg/s (one twelfth of the 57 kg/s total).

Notice that the boundary representing the free LBE surface in the inlet region has been modeled as a Slip condition Wall (the modeling of a realistic free surface would require the usage of very computationally-demanding models, as explained in paragraph 3.1.1).

The temperature boundary conditions were changed in two regions:

1)LBE INLET TEMPERATURE – Since the whole length of the HX is now considered, this value has been changed to the nominal value of 348 °C found in the CIRCE reference document [1.]

2)TEMPERATURE INSIDE THE TUBES – This value was changed to 400 K

All the other boundary conditions were not changed with respect to the previous models.

3.2.1.14 Running the simulation

The simulation has been run, and showed good signs of convergence. The results were coherent to the ones depicted in Figure 19.

Other attempts have been made by incrementing the tubes conductivity in order to consider the presence of the metallic powder inside the helium gap (keeping it realistically relatively near to 0.687 W/mK), and it could be noticed that, with a conductivity of 1.1 W/mK the results were quite near the desired ones (Figure 21). This value will anyway need to be checked and eventually changed when the more realistic model of the whole half of the HX will be taken into account (together with the correct boundary conditions for temperature inside the tubes).

This is the maximum level of approximation that could be obtained with such a simple geometry. In order to be able to better analyze the whole HX behaviour, further progress towards a more realistic geometry must be done.

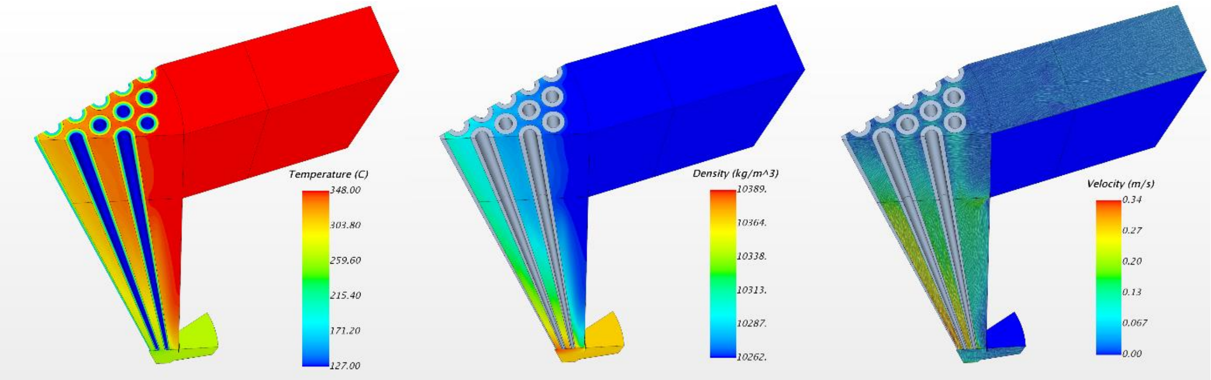

Figure 21:Results of the last HX slice model, with k_eq.=1.1 W/mK, in terms of temperature, density and velocity fields.

3.2.2 A more realistic approach: The HX half model

The next step involves the evaluation of the behaviour of the HX considering the real CIRCE configuration, where the LBE flows from the Riser into the separator and then into the HX. In order to do this, the geometry of the CFD model had to be reconstructed as faithfully as possible starting from the previous model (HX slice) and updating it in order to consider an entire half of the HX.

Within this model, many different analyses regarding energy balances, temperature fields and more have been pursued, and will be exposed in the conclusions, together with their comparison to the real CIRCE official data.

3.2.2.1 Creation of geometry and mesh for the HX half

The geometry for the half HX simulation has been obtained by rearranging the modular geometry of the HX slice model by means of circular patterns and mirroring techniques. This procedure allowed for the generation of the HX half semi-cylindrical tubes region. The contacting separator region has been approximated to a very simple rectangular prism (Figure 22): in fact, the original separator (Figure 10) has a very complex and irregular shape that would not have allowed the use of any symmetry, meaning that the whole HX column would have to be modeled.

In the separator region, the LBE inlet of the CFD domain is located at the bottom, and corresponds to the outlet of the riser. Particular attention has been paid in respecting the most important dimensions of the original separator when approximating its geometry: the outlet diameter of the riser is equal to the real one, and the distances between the riser, the tubes and the walls of the separator have been in chosen accordingly to the real geometry. This means that essentially, the riser has only been “bent” to a rectangular prism, but the most important dimensions have remained as similar as possible to the original.

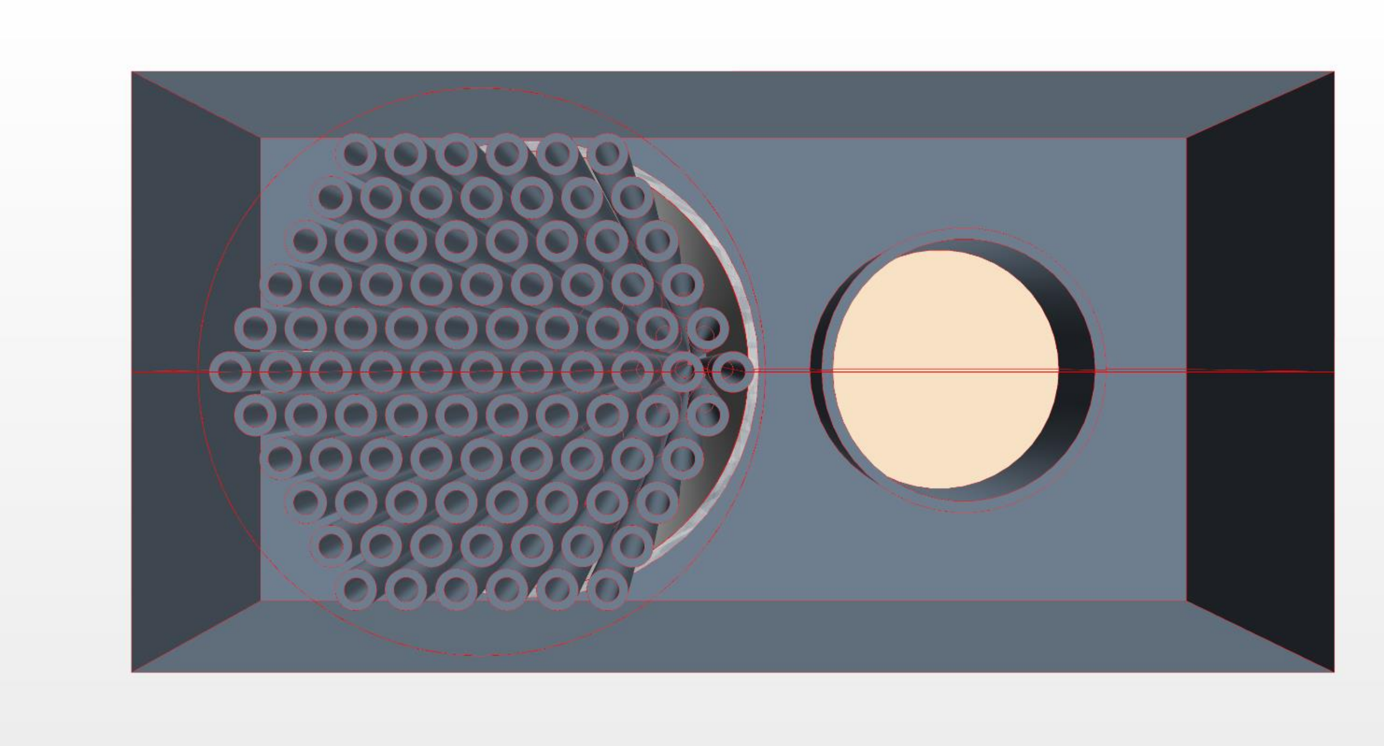

Figure 22:Representation of the whole geometry of the HX separator region, comprehending both the modelled (top) region and the mirrored one (bottom). The horizontal red line represents the trace of the symmetry plane.

By applying this simplification only half of the HX could be considered and an acceptable solution has been obtained, without the need of doubling the computational costs.

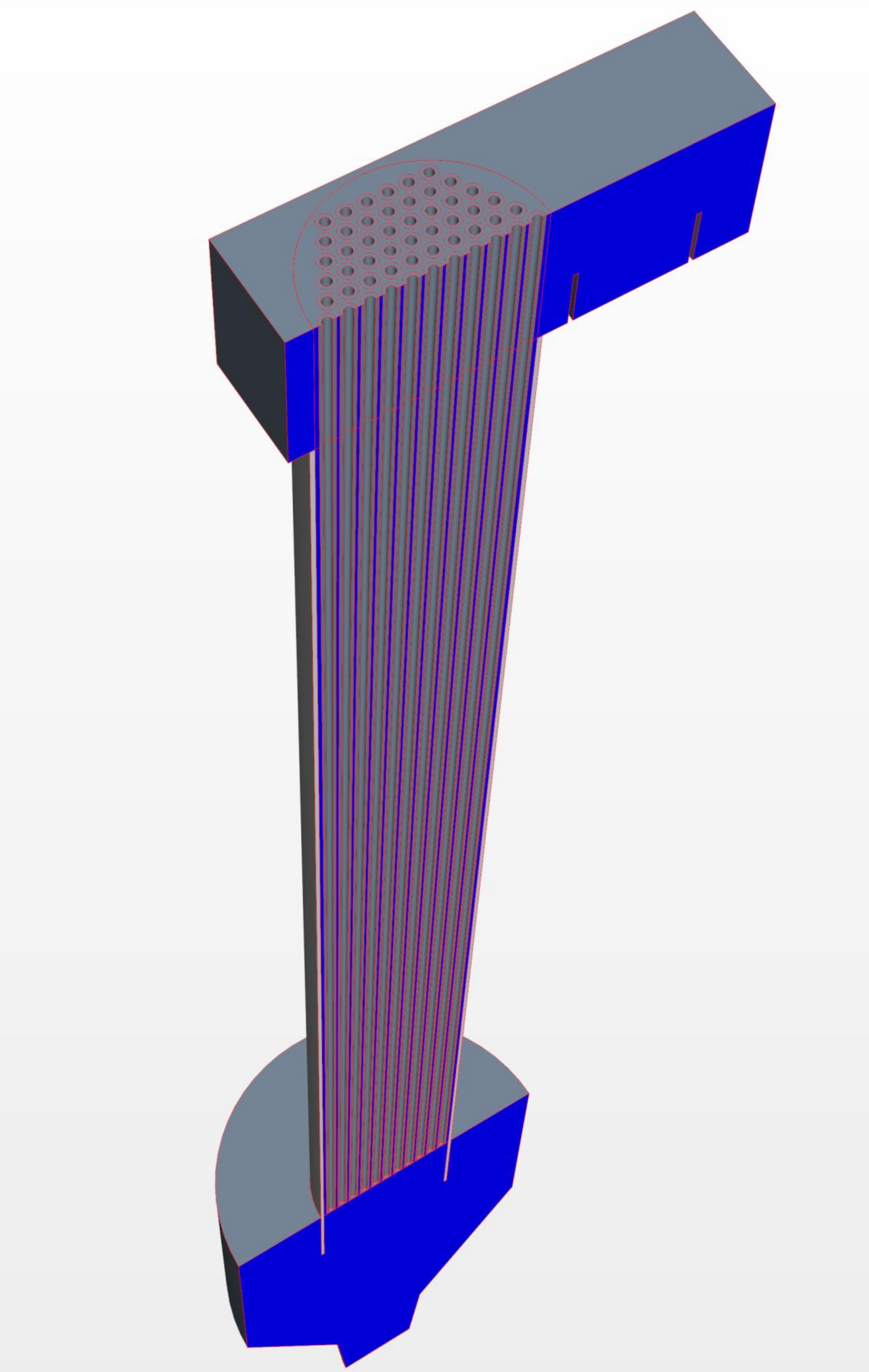

Figure 23:Geometry of the HX half model (comprehending only half of the whole HX)

3.2.2.2 Management of the tubes – The Rings/Matrix tubes map

One of the first problems that emerged after completing the creation of the HX half geometry was the management of the really high number of double bayonet tubes that had been generated (91 in the whole real HX, half in this model).

It was clear almost immediately that a good management system had to be thought of, otherwise later, at simulation level, many issues regarding interfaces, boundary conditions etc. could have been encountered.

The whole tubes system has thus been reorganized, directly at CAD level, in a sort of “matrix” form, by renaming each tube (still only a “body” in this environment) considering its position within the whole tubes hexagonal pattern.

In a scheme that is illustrated in Figure 24, the generic single tube was referred to as “ *TUBE i / j“,* where “i” stands for its position within the 6 “rows” of the hexagonal pattern , while “j” stands for its position within the “columns” of the i-th row.

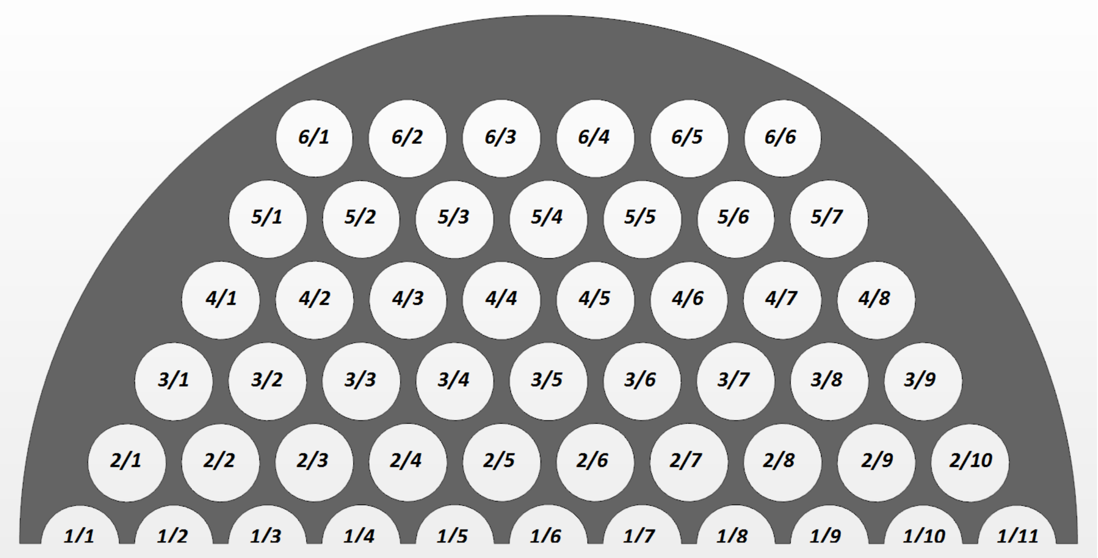

Figure 24: Scheme of the "matrix" map system for the HX tubes.

This allowed, later, to have a more accurate and faster control whenever referencing to a particular tube in the model was needed.

The whole geometry has then been imported into the CFD simulation environment, where the regions of the CFD domain have been defined as follows:

1) LBE REGION: This fluid region comprehends all the LBE flowing inside the CFD domain, and is thus composed of the LBE flowing through the separator, the HX vertical column and the outlet region.

2) FIVE TUBE RINGS: The tubes have been gathered into five different concentric "tube rings" regions (Figure 25). This configuration has been chosen in order to be able, when needed, to assign different boundary conditions to the tubes in various zones of the HX. Doing this would have been hypothetically possible even without this “rings” rearrangement, but in this way the management procedures became much clearer and easier.

   Hence, from this point on, each tube could be precisely identified both in the whole hexagonal structure and in the tube rings system.

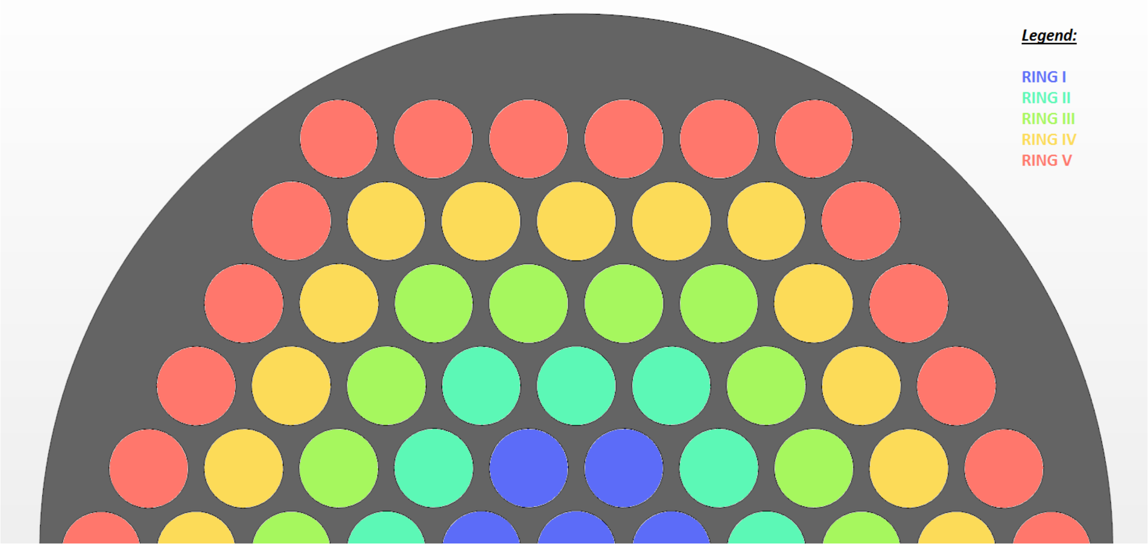

Figure 25: Scheme of the five tube "rings".

3.2.2.3 Creating the mesh for the HX half model

This phase was obviously more challenging than the meshing process for the previous models: in fact, within the different regions of this geometry, a wide amount of rather different dimensions could be encountered, ranging from the very small interstitial LBE region between the tubes (order of 10^(-3) m) to the large region of the LBE bulk outlet (order of 1 m).

Also, considering that an entire half of the HX was modeled at that point, particular attention had to be paid to avoid an excessive mesh refinement in the tubes region, since the 3.45 m height of the HX column could have caused the generation of a really heavy mesh, thus increasing the computational cost and slowing down the calculations too much during the running phase.

After trying different approaches, the final mesh was generated as follows:

1) TOP REGION (top part of the LBE tubes region, LBE separator region, and solid tubes top region, Figure 26):
    - Polyhedral mesh
    - Default base size of 5 mm
    - 2 prism layers (only in LBE fluid regions, disabled elsewhere), for a total thickness of 33% of base size
    - Volumetric custom control: 200% size of cells in the separator region (not comprehending the zone around the tubes).

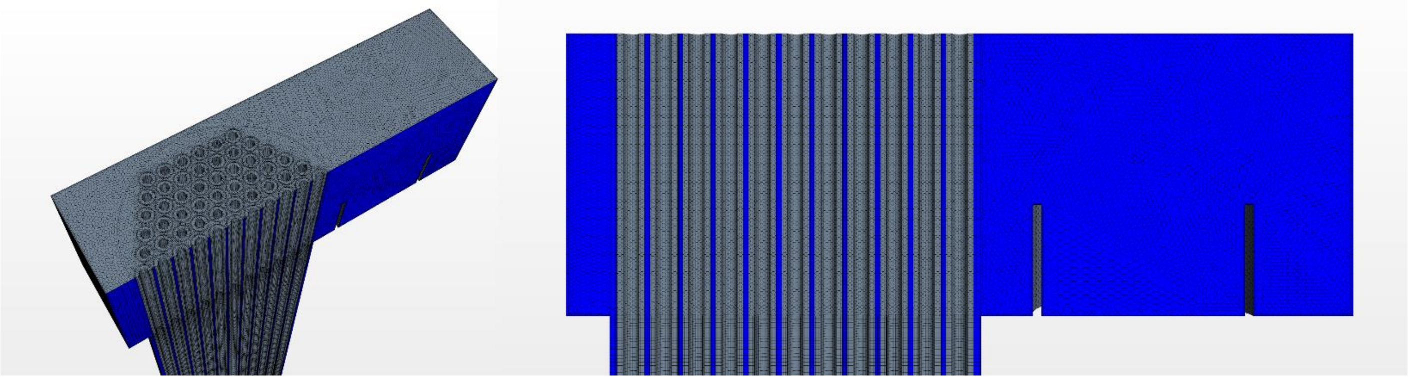

Figure 26:Mesh for the top region of the HX model.

The last step allowed for a less refined mesh throughout the separator region, while the top part of the tubes and the semi-circular LBE region surrounding them kept the small base size of 5 mm.

2) LBE AND TUBES INTERMEDIATE REGION (HX “COLUMN”, Figure 27):

   These regions were meshed using two different directed mesh operations, one for the LBE region around the tubes, and another for the vertical length of the tubes.

   Both directed meshers made use of the respective contacting surface mesh from the top region. The chosen number of directed mesh layers was 270, for both the operations.

Furthermore, some technical issues have been encountered while meshing these regions. In fact, the directed mesher returned the same error different times, referring to problems in the validity of the CAD geometry of the parts. The solution to this problem has been reached by re-tessellating each part (at the Part level, before even defining the mesh operations) with a finer tessellation. The directed mesher could then work fine and generate the requested meshes.

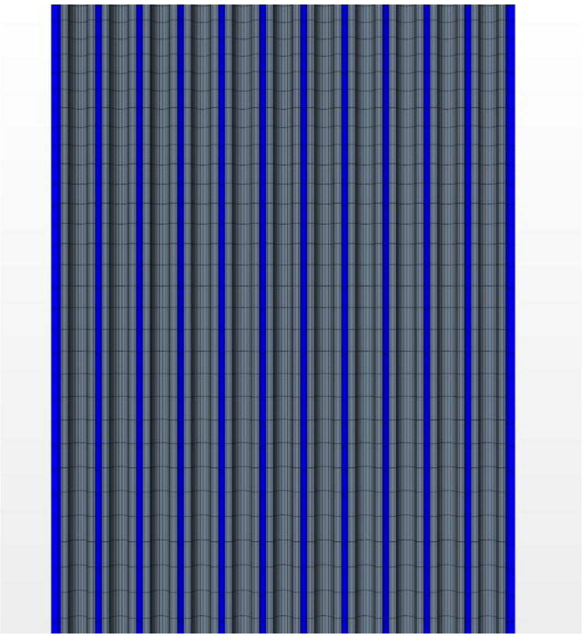

Figure 27:Mesh for the HX intermediate region (HX column).

3) OUTLET LBE REGION (Figure 28: This region was meshed using a polyhedral mesher and a prism layer mesher for the boundary layers. The central part of the mesh of this region has been refined as it had previously been done also for the HX slice model (cells with 80% of the base size).

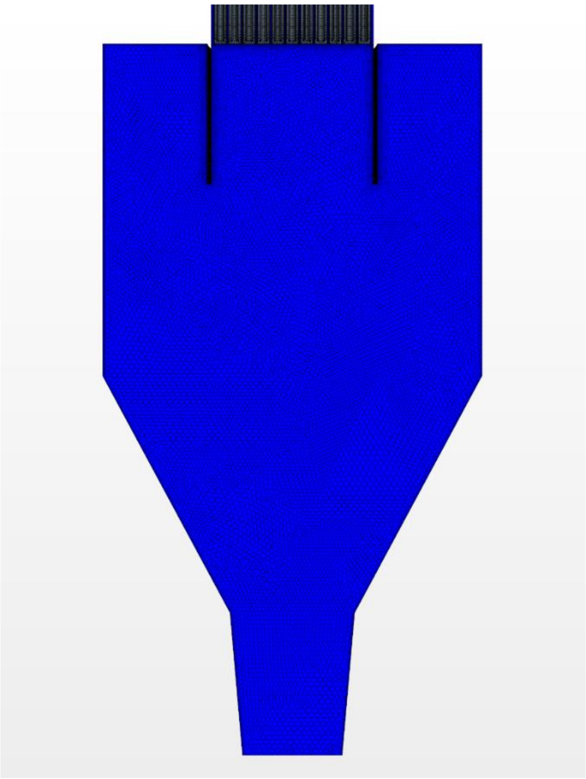

Figure 28:Mesh for the outlet region of the HX

The global number of cells for the whole volume mesh accounted to almost 4.34x10^6. In a later occasion, this mesh needed a further refinement in the outlet region, for LBE flowing inside the HX skirt; in that case, the number of cells rose up to 4.7x10^6.

Considering the very high number of cells for both the cases, it was obviously impossible to rely only on the 4 CPUs of the local machine, and thus, every calculation from now on has been run in parallel on the CRS4 Eolo clusters, choosing the adequate number of CPUs from time to time.

3.2.2.4 *First HX half simulation: the "cold" segregated flow approach – (LBE fluid region ONLY)*

As usual, the problem has been approached with gradual steps, the first one being the evaluation of the general behaviour of the flow within approximated segregated "cold" flow conditions.

Hence, the selected models for LBE for this first step were:

- CONSTANT LBE DENSITY (hypothetical value of 10^4 kg/s)
- SEGREGATED TURBULENT FLOW MODEL, with standard RANS k-epsilon model

This means that the only equations solved were continuity, momentum along the three axes, turbulence kinetic energy and dissipation rate. The thermal aspects will be taken into account after, when adding the solution of the segregated enthalpy equation.

Remembering that all real properties of LBE show a noticeable dependence on temperature, described in the previous models with polynomials and exponential functions, it must be taken into account that this first step of the simulation is very far from being a realistic representation of the actual flow inside the HX.

3.2.2.5 *The segregated "cold" flow boundary conditions*

The boundary conditions for this model were set as follows:

1) LBE MASS FLOW INLET: the LBE mass flow rate inlet boundary condition was imposed on the semi-circular outlet section of the riser (connecting to the separator, in the upper region of the geometry). The imposed value of 28 kg/s was computed considering half of the total mass flow rate flowing in the CIRCE primary circuit ([1.][3.]), of 56 ÷ 57 kg/s, thanks to the symmetry.

2) SLIP CONDITION WALL: this condition, as previously mentioned, was set on the top LBE surface of the upper region (separator and top of the LBE HX column); This has been done to simulate in an extremely approximate way the LBE free surface in the separator. A no slip shear stress condition would have been totally disrespectful of the physics of such free surface.
3) PRESSURE OUTLET: condition of 1 bar (relative, see the considerations in paragraph 3.2.1.2) imposed at the outlet of the nozzle of the bulk region.
4) NO SLIP CONDITION: on all other walls, except the intermediate symmetry plane.

3.2.2.6 Running the simulation and analysis of the first results

The simulation has been run in parallel on the Eolo clusters employing 80 CPUs, and converged well after ~1750 iterations.

The most important things to be noticed are:

1) the geometry of the separator causes some vorticity in the region “behind” the HX tubes (opposite side of the separator compared to the riser outlet, Figure 29); the inflow of LBE into the HX column from this zone of the separator is important, and leads to a partially asymmetric flow through the intermediate and bottom part of the HX.

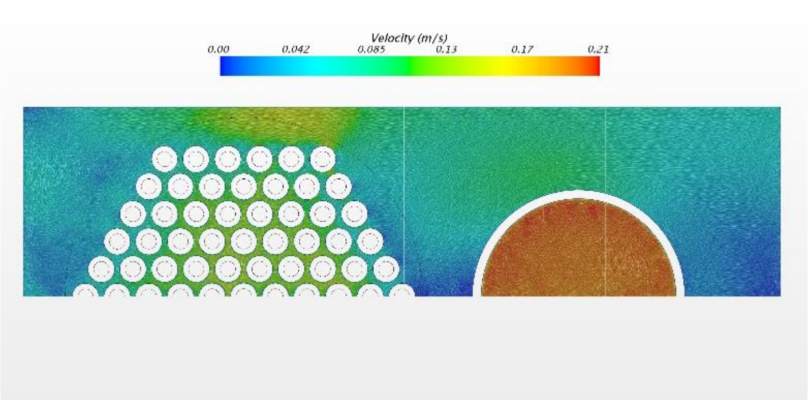

Figure 29: Section of the separator region (perpendicular to Z direction).

2) considering a plane section cutting the whole CFD domain with an angle of 30 degrees with respect to the symmetry plane, it is interesting to notice that the "pulling" effect due to natural convection observed in the previous models is not present, since this was still a "cold" model, and no heat exchange took place. This is a further proof that the "pulling towards the tubes" LBE effect illustrated in

paragraph 3.2.1.7, is totally linked to the heat exchange phenomena, not yet considered here.

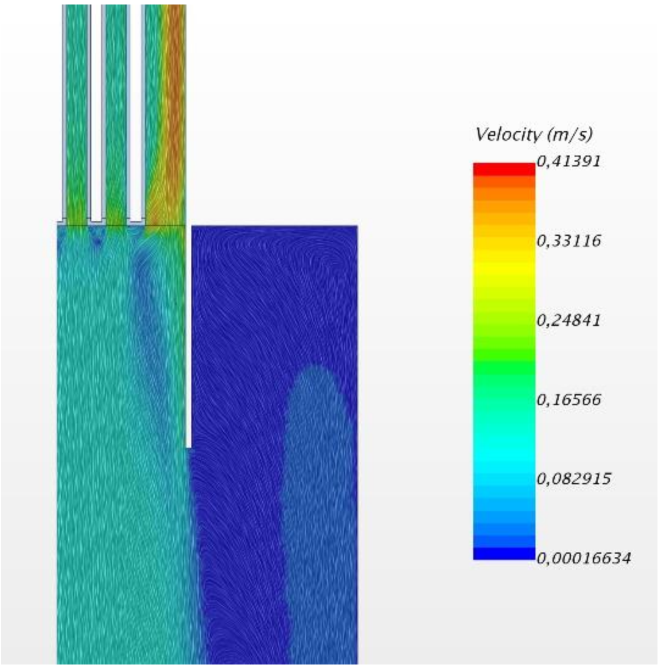

Figure 30: Section of the HX inclined of 30 degrees with respect to the symmetry plane.

3.2.2.7 *Implementing the thermal model and running a first complete simulation (LBE and tubes)*

After running the segregated “cold” flow model and obtaining results that validated the mesh quality and the general coherence of the fluid-dynamic problem, the thermal energetic model could be implemented. Precisely, the added models have been:

1) LBE Polynomial density, and temperature varying properties in general, with reference to Table 1.

2)Segregated fluid enthalpy (LBE region)

3)Segregated solid energy (solid tubes)

Henceforth then, also the tubes physics is modeled in the simulation. Their physical properties have been chosen accordingly to the best results obtained from the previous HX slice simulation. With this philosophy, the equivalent conductivity value that allowed to reach the most accurate results in that case had been 1.1 W/mK, and this has been the first value that has been chosen for this new model.

3.2.2.8 The boundary conditions

The previously illustrated boundary conditions for the segregated flow approach (paragraph 3.2.2.5) have been kept unaltered, while the boundary conditions for the thermal models still had to be imposed. This has been done as follows:

1)LBE INLET TEMPERATURE: 348 °C, with reference to the official CIRCE document [1.].

2)INTERNAL SURFACE OF ALL THE TUBES: 400 K (~127 °C) fixed temperature condition, constant along the whole tubes length; this is not a realistic boundary condition, since it does not respect the physics of the water of the secondary circuit, and will later be improved.

3) ALL OTHER WALLS (EXCEPT SYMMETRY PLANE SURFACES): Adiabatic.

Also, some reports have been updated in order to more accurately monitor the value of the LBE temperature at the outlet, and the heat power subtracted by the whole HX (calculated with an energy balance between the LBE inlet section and the baffle interface section).

3.2.2.9 Running the simulation and analyzing the results

This simulation has then been run in parallel on 120 CPUs on the Eolo clusters, and converged after ~5000 iterations.

Some very basic reports have been run, especially:

1) **SURF. AVERAGED OUTLET TEMPERATURE (at the outlet section (nozzle) of the whole CFD domain):** in the real Circe facility, the average temperature of LBE exiting the HX should be around 270 °C, while here the average temperature reported was around 304 °C.

2) **HEAT POWER REMOVED BY THE WHOLE HX:** the value reported by the energy balance was around 720 kW, which is reasonable if compared to the operative range of CIRCE (650/800 kW), but still needs to be adjusted.

Please notice that these very first reports were still not accurate, and have been gradually improved, and re-built while the simulation improved through time. A reliable precision on the energy balances has been obtained only almost at the end of the whole internship period, as only experience allowed to better understand how to calculate them appropriately in different (but coherent) ways.

Anyway, the purpose of starting to calculate these values from now (very approximate case) lied in verifying at least their order of magnitude, in order to avoid macroscopic errors in the simulation.

The next step towards a more realistic model, has been the determination of a more accurate set of boundary conditions to be assigned on the internal surfaces of the double bayonet tubes, as explained in the following paragraphs.

3.2.3 Improving the thermal boundary conditions on the internal surfaces of the tubes – Simulating evaporation.

Many errors and imprecisions in the model are due to the imprecise thermal boundary conditions imposed inside the tubes; in fact, a fixed temperature of 400 K, constant along the whole tubes length is not realistic since it does not respect the thermodynamic process experienced by the vaporizing water of the secondary circuit. Hence, the new objective was the theoretical determination of the right temperature profile that does actually respect it.

The next theoretical analyses on the water behaviour have been aided by the considerations made throughout the modeling of the single double bayonet tube (chapter 2); furthermore, the following method has been used until the end of the work, with satisfying results especially in the last model.

3.2.3.1 *Important note* on the *uncertainty for water parameters*

Much difficulty was encountered while trying to find reliable data about the water transformation along the secondary circuit in the official CIRCE documents; in fact, a lot of uncertainty was found on:

1) water inlet temperature to the HX tubes: in the official CIRCE reference document [1.], this value was evaluated with a large uncertainty, ranging from 15 to 50 °C. In another official document [3.], a time-averaged value of~10 °C was reported..

2) pressure drop between inlet and outlet of the double bayonet tube: also this value was rather ambiguous in both documents, in fact in the official CIRCE reference document [1.], the inlet pressure for water is evaluated around 2 bar, while in the other official document [3.], much more precise values could be found. Here the whole pressure drop along the circuit is evaluated as ~1.5 bar, and the steam conditions at the outlet are 1 bar of pressure (equivalent to a saturation temperature of 100 °C) and a steam quality of~45%; from these values the inlet pressure of water could be evaluated to be around 2.5 bar (pressure at the outlet + 1.5 bar of pressure losses along the circuit).

It is important to spend some time precising such uncertainties because they highly influence the temperature profile of the water on the internal surface of the double bayonet tubes, and thus heavily affect the heat exchange phenomena in the whole HX.

In the following paragraph, the water properties are assumed with reference to [3.], i.e. the most accurate of the two documents, namely:

- WATER INLET PRESSURE: 2.5 bar
- WATER INLET TEMPERATURE: 10 °C
- STEAM OUTLET PRESSURE: 1 bar
- STEAM QUALITY: 45%
- WATER MASS FLOW RATE (whole HX): 0.57 kg/s

3.2.3.2 Analysis of the evaporation process in the single double bayonet tube

Let us consider the simple scheme of the water thermodynamic evolution inside the double bayonet tube reported in Figure 31.

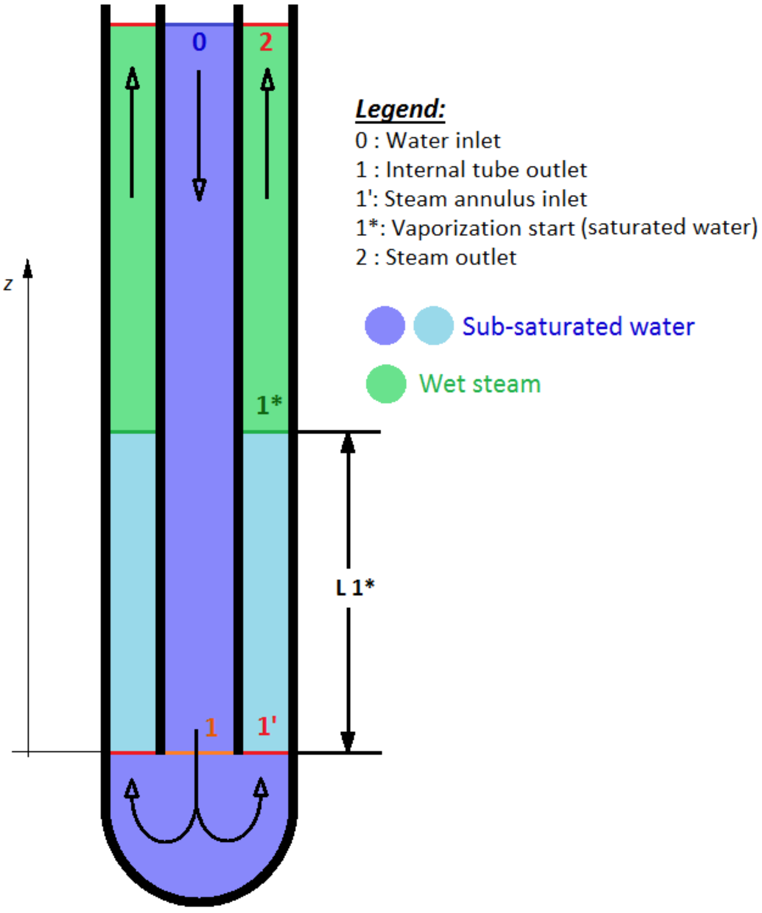

Figure 31:Scheme of the water transformations along the double bayonet tube.

With reference to the previous paragraph, the water entering the tube (at section 0) is at 2.5 bar of pressure and at a temperature of 10 °C. This water then flows down the internal tube of the double bayonet, arriving at its bottom (section 1). Then the water enters the external side of the double bayonet (1'), receiving heat from the LBE flowing downwards outside the external tube, and thus increasing its temperature. When the water reaches the section 1* (saturated liquid condition) vaporization starts, and the liquid+steam multiphase mixture flows up reaching the outlet section (2), with a steam quality of 45%, a pressure of 1 bar and a temperature of 100 °C. The water mass flow rate is 0.57 kg/s for the whole HX, hence, considering the total of 91 tubes, the mass flow rate inside a single tube is equal to 6.3x10^-3 kg/s.

In the following Table 2, the geometric characteristics of the double bayonet tubes are reported:

TUBES GEOMETRY	Inner tubes O.D [m]	0,0127
	Outer tubes O.D[m]	0,0254
	Intermediate tubes O.D [m]	0,01905
	L = Tube length [m]	3,45
	D (Inner tubes I.D.) [m]	0,0067
	Thickness Inner tubes [m]	0,003
	Thickness Outer tubes [m]	0,00211
	Thickness Intermediate tubes [m]	0,00211
	Surface of Inner tubes section [m^2]	0,000035255
	Surface of Steam side annulus [m^2]	0,000046054
	K (Dint / Dext steam side annulus)	0,8564
	Dh (Annulus hydraulic diameter) [m]	0,00213

Table 2: Geometric characteristics of the double bayonet tubes.

Remembering some important input data, namely:

Inlet pressure of water (0) [bar]	2,5
outlet pressure of steam (2) [bar]	1
Water viscosity (cost.) [Pa*s]	0,00100207
Water density (cost.) [kg/m^3]	1000
Water mass flow rate through HX single tube[kg/s]	0,0063

Table 3: Input parameters for the water inside the double bayonet tubes

N.B.: approximately, density and viscosity of water have been modeled as constant.

From these values, the following parameters can be calculated:

Velocity (0-1) [m/s]	0,18	Velocity (1'-1*) [m/s]	0,14
Reynolds (0-1)	1.187,91	Reynolds (1'-1*)	289,103

Table 4:Average velocity and Reynolds number values calculated in the different regions of the double bayonet tube.

As can be seen from Table 4, both the Reynolds numbers in the regions 0-1 and 1’-1* refer to a laminar flow regime (remember that no steam is present in these regions, since evaporation starts at 1*).

The first consideration to be done involves the pressure drop of the water flow between sections 0 and 1, which has been estimated with the usual relationship:

$$\Delta P = f\frac{L}{D}\left(\frac{1}{2}\rho u^2\right) \quad (1)$$

where f is the friction factor, interpolated from the Moody chart (knowing the average Reynolds number of the flow in the 0-1 region), L is the length of the tube (3.45 m) and D its internal diameter, u and ρ respectively the water velocity and density.

The pressure drop along the annulus of the steam side, for the zone 1'-1* (water starting to be heated up by LBE) has been evaluated using the Hagen Poiseuille generalized method for Laminar incompressible flow, according to [6.], namely:

$$\left(\frac{\Delta P}{L}\right) = \frac{64\varphi(K)}{Re} \cdot \frac{\frac{1}{2}\rho u^2}{D_h} \qquad (2)$$

Where $\varphi(K)$ depends on the internal and external diameters of the annulus (factor K , see reference [6.] for further details), D_h is its hydraulic diameter, upon which the Reynolds number Re_{1-1^*} of the section is calculated, u and ρ respectively the water velocity and density.

It is yet a problem to determine where vaporization actually starts, and especially at which height (L_1^*) this happens inside the double bayonet tube. The pressure drop has been evaluated per unit length $\left(\frac{\Delta P_{1-1^*}}{L_{1^*}}\right)$, in order to later hypotize the height of the 1* section L_{1^*} (evaporation start) and find the related pressure drop.

N.B: The pressure drop related to the bottom of the tube (1’-1*) has been considered negligible.

The results for the 0-1 section are illustrated in Table 5:

(L/D) (0-1)	514,93
friction factor 0-1 (laminar) (f=64/Re)	0,05
DeltaP/L (0-1') [bar/m]	0,0013
DeltaP (water side 0-1') [bar]	0,004

Table 5: Pressure drops along the 0-1 section of the double bayonet tube.

While, for the section 1’-1*:

Phi(K)	1,4994
DeltaP/L (1'-1*) [bar/m]	0,014

Table 6: Evaluation of the pressure drop per unit length along the annulus region 1’-1*.

This means that, hypothesizing the length L_{1^*}, the value of the pressure drop along every section of the tube can be calculated (obviously, the value of the pressure drop between 1* and 2 is then calculated by difference from then total of 2.5 bar). For example, with a L_{1^*} equal to 1 m (random value), the obtained values are (Table 7):

L 1* (hypothesis) [m]	1
DeltaP (0-1') [bar]	0,004
DeltaP/L (1'-1*) [bar/m]	0,014
DeltaP (1'-1*) [bar]	0,014
DeltaP (1*-2) [bar]	1,484317127
P 1* (saturation pressure) [bar]	2,4812

Table 7:Pressure drops along the different regions of the double bayonet tubes, and calculation of the saturation pressure P_{1^*} .

The calculation highlights that the pressure drop along the internal tube (0-1) of the double bayonet, which is not influenced by the value of L_{1^*} is quite low (~4 mbar); knowing that the total pressure drop (from sections 0 to 2) is 1.5 bar, it is quite clear that, for any value of L_{1^*} almost all the pressure drop is concentrated on the external side (steam side) of the double bayonet, hence between sections 1’ to 2.

The saturation pressure P_{1^*} is thus very close to the value of 2.5 bar, as can be seen from the table above.

3.2.3.3 Analysis of the thermodynamic process

A $P-h$ diagram helps a lot in identifying the different physical transitions experienced by water in this process. Figure 32 represents the water transformations along the double bayonet tube; every step will then be discussed.

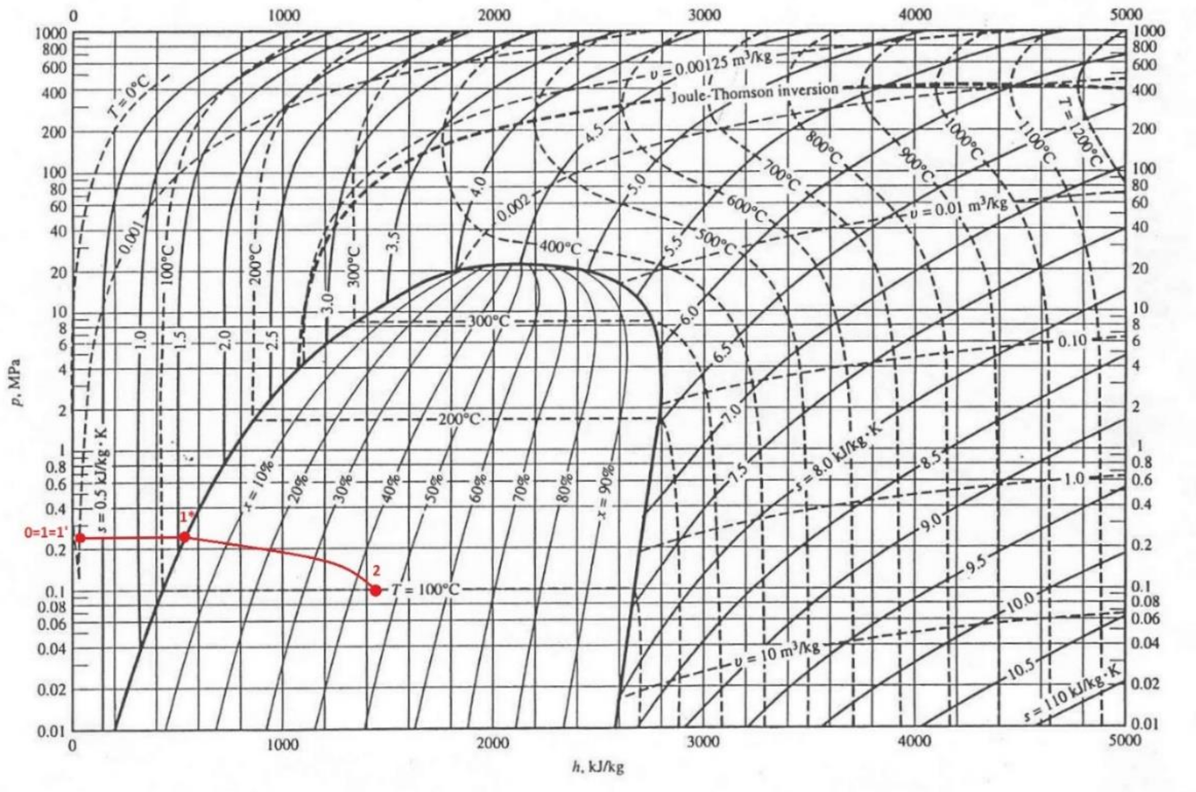

Figure 32:: Pressure-enthalpy diagram depicting (in red) the thermodynamic evolution experienced by water along the double bayonet tube.

3.2.3.4 Water transformation 0-1

It can easily be seen with a simple energy balance that, with the hypothesis of adiabatic internal walls of the double bayonet (considering that they are accurately insulated from the annulus of the steam side), and considering the very small contribution of the potential energy variation, the transformation 0-1 is almost isenthalpic. In fact, from the generic 1st principle of thermodynamics for open systems (with clear meaning of the symbols):

$$\frac{dE_t}{dt} = \sum_j \dot{Q}_J - \dot{W} + \dot{Q}_{el.\backslash chem.} + \sum_{in} \dot{m}_{in} \left(h + \frac{u^2}{2} + gz\right)_{in} - \sum_{out} \dot{m}_{out} \left(h + \frac{u^2}{2} + gz\right)_{out} \quad (3)$$

Applying on the control volume between sections 0 and 1, and considering:

- Adiabatic walls $\sum_j \dot{Q}_j = 0$
- Stationary case $\frac{dE_t}{dt} = 0$
- No mechanical work and electrical or chemical energy fluxes $\dot{W}, \dot{Q}_{el.\backslash chem.} = 0$
- Same velocity u on sections 0 and 1
- Same mass flow rate $\dot{m}_{in} = \dot{m}_{out}$, due to continuity

The previous equation becomes:

$$(h + gz)_{in} = (h + gz)_{out} \tag{4}$$

Since the potential energy contribution Δgz is very small, the process is, as previously said, almost completely isoenthalpic.

$$h_{in} \cong h_{out} \tag{5}$$

Furthermore, considering the very small pressure drop experienced by water between sections 0 and 1, this means that the points 0, 1 (and also 1', remembering that the pressure drops at the bottom 1-1' were neglected) are almost on the same spot on the $P - h$ diagram.

3.2.3.5 *Water transformation 1-1*: pre-heating*

Neglecting the very little pressure drop at the bottom of the tube, the transformation 1-1* refers to the water entering the steam side annulus. In this region, water starts to be heated up by the heat flux due to the hot LBE flowing outside; hence its enthalpy rises, and reaches saturation conditions at the section 1*.

As previously said, the height L_{1^*} at which the saturation conditions are met, is not known in the frist place. Furthermore, the pressure drop between 1-1* depends on L_{1^*}, as expressed by eqn. (2).

Anyway, considering the results exposed in Table 7, the pressure drop between sections 1-1*, is very low, even for very high values of L_{1^*} , especially if compared to the total pressure loss of 1.5 bar between sections 0 and 2.

The heating process in the region 1-1* can thus be considered almost isobaric.

3.2.3.6 *Water transformation 1*-2: vaporization*

In this region, water starts vaporizing, and the pressure drops increase greatly. It is known that, with no pressure losses, vaporization occurs at constant saturation temperature, but this is not the case, since the reported pressure losses along this region are not negligible (almost 100% of the 1.5 bar pressure drop happens between 1* and 2), and temperature thus has to decrease. Also, the thermodynamic “path” of the transformation is surely nonlinear, and considering that the density of the mixture tends to drop really strongly with the increase in steam quality, then its average velocity in the higher sections of the annulus will be higher (in order to respect basic continuity), thus causing an increase in the pressure drop per unit length along the Z direction. Consequently, also the rate of temperature decrease along the Z direction will change at the higher sections of the annulus, and the temperature will decrease more steeply; in the next paragraph this will be explained with better detail.

3.2.3.7 The effect on the temperature profile: determining the boundary conditions for the HX half model.

Of this whole analysis, the only thing that actually influences the HX half model is the behaviour of the temperature of the water from section 1’ (=1) to section 2, i.e. the temperature along the annulus of the double bayonet tube. From this, in fact, it is possible to determine the temperature profile along the length of the tube which needs to be assigned to their internal surface in order to reach a new level of reliability of the model. This means that this temperature profile must be evaluated starting directly from the previous P-h diagram. Its qualitative form, for a single generic tube is graphically shown in the following plot (

Figure 33), as a function of the Z coordinate:

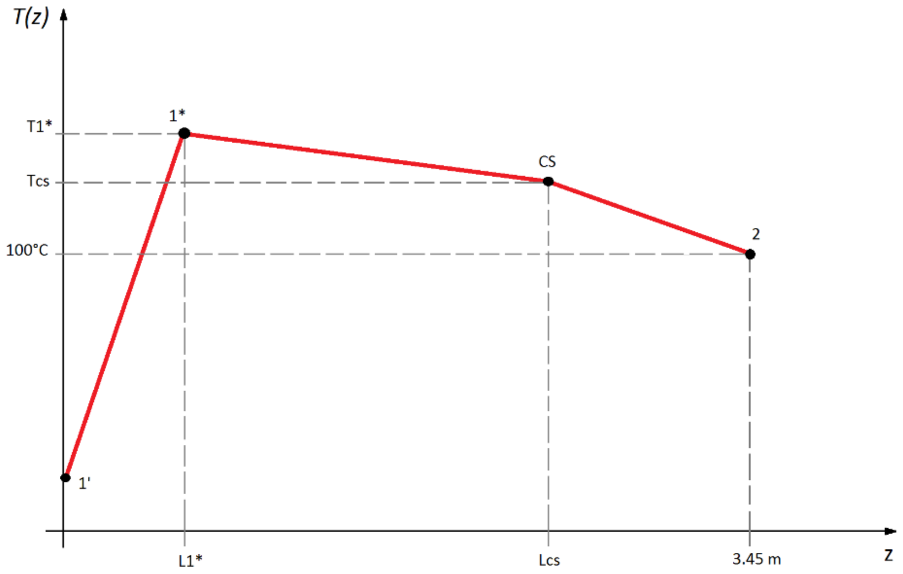

Figure 33:Qualitative expression of the temperature profile T(z) to be imposed on the internal surface of the tubes of the HX half model

1) The 0-1 region (inner tube) is obviously not considered in the plot, which only monitors the temperature on the internal surface of the external tube.

2) Three regions with different steepness values can be identified:
   - Pre-heat region (1’-1*)
   - Liquid+steam multiphase equilibrium (1*-2)
   - Inside region 1*-2, the zone between CS-2 shows a more pronounced decrease in temperature; this has been done with reference to the effect due to growing pressure losses discussed in the previous paragraph (3.2.3.6). In fact, as can be seen in the P-h diagram (Figure 32), an increase in the rate of pressure losses implies also a steeper temperature decrease.

3) With reference to the elements discussed in paragraph 3.2.3.2 and exposed in Table 7, and considering the very small value of the pressure losses per unit length along the 1’-1* region, i.e.:

$$\left(\frac{\Delta P_{1-1^*}}{L_{1^*}}\right) \cong 0.014\ bar/m$$

   It is thus clear that even for very large variations of the L_{1^*} (within the range of the whole tube length of 3.45 m), the pressure at the 1* section remains almost constant, and very close to the value of 2.5 bar (water inlet 0). This implies that also the saturation temperature at which vaporization starts, namely T_{1^*} in the $T(z)$ plot, remains almost constant for any chosen vaporization height L_{1^*}.

   This translates into the fact that the point 1* in the $T(z)$ plot has only an “horizontal” degree of freedom (changing L_{1^*} does not affect T_{1^*}, with good approximation).

   Considering these elements, and the data from the previous $p - h$ diagram, the T_{1^*} has been fixed to the value of 127 °C (i.e. the saturation temperature at 2.5 bar), with good approximation independently from L_{1^*}.

4) The point 2 has fixed coordinates, since it represents the outlet section of the double bayonet tube (z=3.45 m) and its temperature is an input parameter of the problem (1 bar saturated pressure, implying $\sim$ 100 °C).

3.2.3.8 Importing the temperature profiles calculated in Excel into the STAR-CCM+ software.

Once these elements were understood, a first attempt to generate a temperature profile consisted in considering the same $L_{1^*} = 0.5\,m$ for all the tubes. This was oviously a first guess, disconnected from any physical consideration, (that would have been introduced slightly later) but allowed to design the informatic architecture to import the temperature profiles calculated on Excel into the STAR-CCM+ software.This has been done by calculating the pressure losses and temperatures at each section of the double bayonet tube by means of the same Excel spreadsheet used before, this time considering the abovementioned $L_{1^*} = 0.5\,m$.

The following Table 8 shows the chosen value of 0.5 m for all the 5 “tube rings” regions:

L(1*) BASE VALUE [m]	**0,5**
Perturb. on L(1*) Base Value (RING I) [%]	**+0 %**
Perturb. on L(1*) Base Value (RING II) [%]	**+0 %**
Perturb. on L(1*) Base Value (RING III) [%]	**+0 %**
Perturb. on L(1*) Base Value (RING IV) [%]	**+0 %**
Perturb. on L(1*) Base Value (RING V) [%]	**+0 %**

TUBES REGIONS	L 1*	Pressure P1* [bar]
Ring I	0,50	2,488
Ring II	0,50	2,488
Ring III	0,50	2,488
Ring IV	0,50	2,488
Ring V	0,50	2,488

Table 8: Lengths L_{1^*} for the different ring regions of tubes. These values are expressed by employing a base value (here equal to 0.5 m), and then choosing the perturbation value (in percentage) for each ring. The consequent values of saturation pressure P_{1^*} are also calculated, with reference to paragraph 3.2.3.2.

Once this was done, the linear equations of the temperature profile T(z) were computed for the three different intervals (1-1* , 1*-L_cs , L_cs-2). Then, the whole 3.45 m length of the generic tube was divided into 100 parts, and the linear equations were interpolated onto this subdivision, creating a table of the kind of Table 9 for each “tubes ring” region:

TABLE XYZ for temperature along Z (RING I)				
Points	Data	X	Y	Z
1,00	283,24	0,00	0,00	0,00
2,00	284,01	0,00	0,00	0,01
3,00	284,87	0,00	0,00	0,02
4,00	285,73	0,00	0,00	0,03
…	**…**	**…**	**…**	**…**
342,00	373,83	0,00	0,00	3,41
343,00	373,66	0,00	0,00	3,42
344,00	373,49	0,00	0,00	3,43
345,00	373,15	0,00	0,00	3,45

Table 9: General template of the. osv tables used to import the temperature profile T(z) into STARCCM+

Hence, five tables of this kind were created. In this case the L_{1^*} was equal for every tubes ring region, but the spreadsheet has been organized in order to let the user choose different L_{1^*} for each region, as will be explained later.Within the table, the Data column refers to the temperature, in Kelvin degrees, to be assigned at each “point” of the abovementioned height subdivision, while X, Y, and Z refer to the coordinates (notice that, obviously, only Z is growing, from 0 to 3.45 m, comprehending the whole height of the tube). These tables have then been saved as five separate. osv table files (RING-I.osv, RING-II.osv… etc.), and then imported into STAR-CCM+ as X,Y,Z tables. Here, the simulation was modified in order to read these data and assign each table as a boundary condition for the internal surfaces of the tubes belonging to each respective ring region. In this way, whenever a change in the temperature profiles was needed, it was sufficient to calculate all the data on Excel, update the .osv tables, and letting STAR-CCM+ reload the files; in this way, the boundary conditions would update automatically

3.2.3.9 The logic behind the choice of the correct temperature profiles inside the tubes:

Knowing the general behaviour of the water temperature field inside the double bayonet tubes, it is now essential to choose a $T(z)$ temperature profile that adequately matches the energetic requirements for water itself to vaporize and undergo the transformations explained in the previous paragraphs.

To do this, the total heat power that the water flow inside a single tube needs to receive in order to pass from conditions 1’ (=1) to conditions 1* can be estimated with a very simple energy balance, applying eqn. (3) to the control volume delimited by sections 1’ and 1*.

Considering a water mass flow rate of 0.0063 kg/s (see Table 3), and knowing the values of the water specific enthalpy in 1’ and 1* (saturation enthalpy) from tables, such power has been evaluated as:

SECTION	**Pressure [bar]**	**Temperature [C]**	**State**	**h [kJ/kg] (approx.)**	**H.PWR 1'-1* (single tube) [kW]**
0	2,5	10,00	L	42,2647	3,08
1'	~ 2,5 (slightly less)	10,00	L	42,2647	
1*	~ 2,5 (slightly less)	127,00	L SAT.	533,997	
2	1	100	L+V (x=45%)	1434,60	

Table 10: Energy balance employed to calculate the total heat power needed for water to pass from conditions 1' to conditions 1* (saturation).

Within the STAR-CCM+ software, a large number of different reports were created at this point, with three main aims:

1) Monitoring the heat power removed by each single tube, throughout its whole 3.45 m length, both in absolute value and as a percentage of the power removed by the “medium tube” (see paragraph 4.2 for an accurate description). For this values also an interesting map has been realized, that will be shown later, while discussing the results of the simulation.

2) Monitoring the heat power removed by each whole tube rings region.

3) Monitoring the heat power removed by each single tube only throughout the pre-heating length (from the bottom to the chosen vaporization height L_{1^*}.

N.B.: All these calculations were performed with a surface integral of the heat flux, of the kind:

$$\dot{Q} = \int_S \vec{q} \cdot \vec{n}\, dS \qquad (6)$$

Were $\vec{q} \cdot \vec{n}$ represents the component of the heat flux normal to the internal surface of the tubes, and S is the surface itself. This form is totally fine for points 1) and 2).

A bit more complex has been the evaluation of the point 3), since the integral had to be performed only on the lower portion of the internal surface of the tubes (vaporization heigth L_{1*}). In order to do this, a new scalar "support" function has been created, defined as:

$$Supp.(z) = \begin{cases} 1 & if\ z \in [0, L_{1^*}] \\ 0 & if\ z \in [L_{1^*}, 3.45] \end{cases} \qquad (7)$$

This function is hence equal to 1 only where the z coordinate is not greater than the chosen L_{1^*} for the present tube, and is equal to 0 anywhere else. The integral could then be computed in the form:

$$\dot{Q}_{1'-1^*} = \int_S [Supp.(z) \cdot \vec{q}] \cdot \vec{n}\, dS \qquad (8)$$

And this actually returns the heat power subtracted only throughout the 1-1* region.

This last one is the value that has been kept under control in order to find the right temperature profile for each tube of the model. In fact, if the temperature profile is correct and coherent with the water evaporation process, the integral of eqn. (8) should approximately return the value of 3.08 kW) for each tube, i.e. the heat power removed as calculated with the energy balance presented in Table 10.

N.B: Furthermore, approximating, the value of the integral (8) calculated for each single tube has then been used to compute the averaged value of the Heat power removed between 1-1* within each one of the 5 "ring regions" of tubes; this allowed to have 5 reports that kept under constant control the average value of integral (8) for the tubes in each different "ring".

So, the basic idea of the "algorithm" to find the correct profiles is expressed in the following diagram (Figure 34):

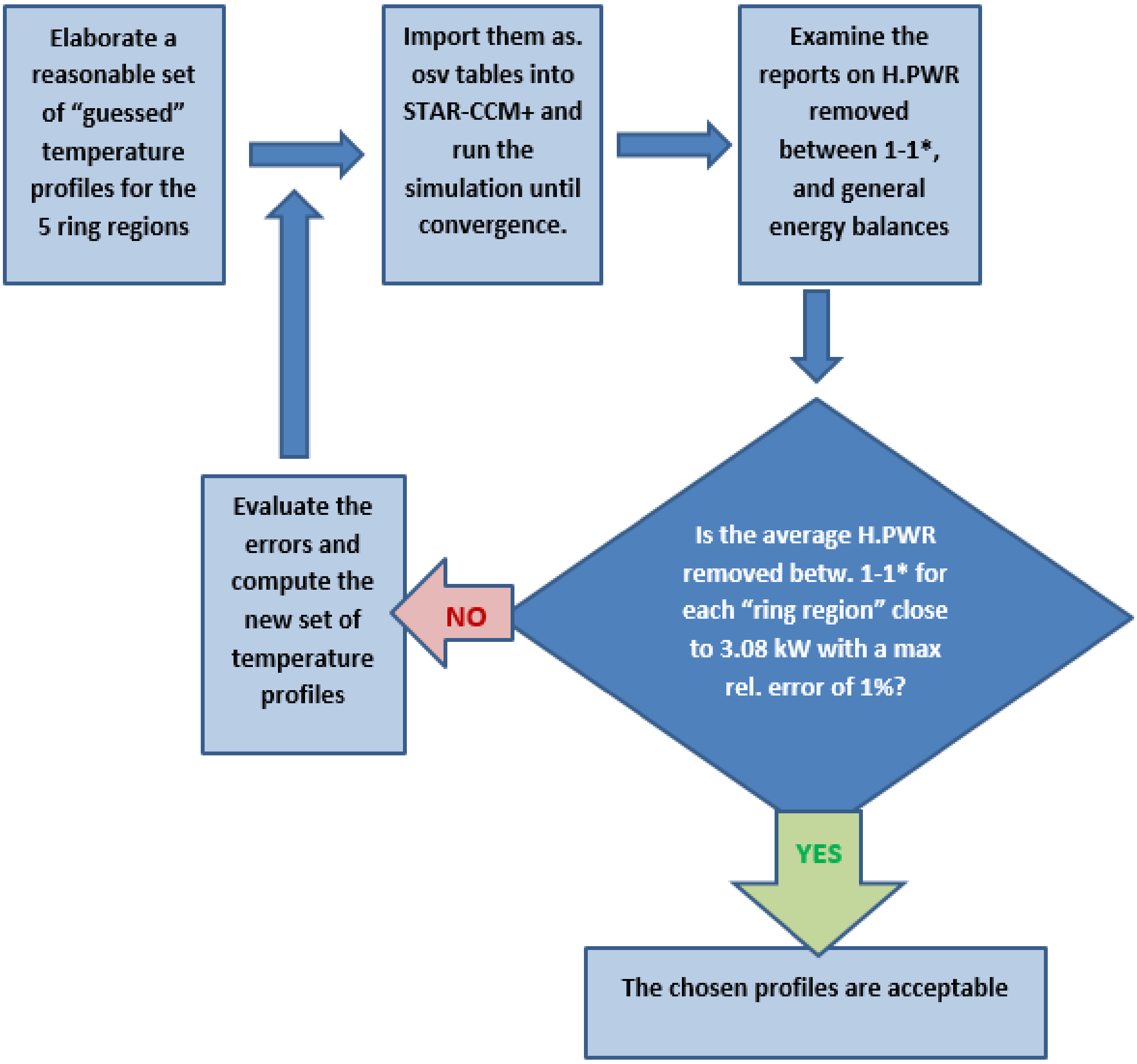

Figure 34: Diagram explaining the algorithm behind the choice of the definitive temperature profiles inside the tubes.

In the following paragraphs, the details of how this has been done for the HX half model will be discussed.

3.2.3.10 Running the HX half simulation:

Once the water evaporation process had been adequately studied and considered in the STAR-CCM+ model, the next step consisted in finding the abovementioned correct temperature profiles and running the simulation until satisfying results could be reached.

Setting a new coherent boundary condition for the LBE inlet temperature in the HX half model:

Since all the previous considerations for water have been made accordingly to one of the official CIRCE documents ([3.]), (because it reported much more detailed data on the evaporation process than document [1.]) it was necessary, for coherence reasons, to also update the other parameters of the model accordingly to document [3.]. This did not influence the general validity of the model, since both documents refer to different experiments operated in the same CIRCE-ICE primary loop.

In fact, the LBE boundary conditions were previously set accordingly to document [1.]. Essentially, the only parameter that needs to be changed is the inlet temperature of LBE, which varies from the value of 348 °C (as in [1.]), to the value of 355 °C (as in [3.]).

This change has a noticeable effect on the energy balances, and must not be underestimated.

All the other boundary conditions are kept unaltered, except for the temperature boundary condition inside the tubes, whose value of constant 400K for the whole length was substituted with the first attempt of a temperature profile, having a L_{1^*} of 0.5 m, and an evaporation temperature of 127 °C, as referred to in paragraph 3.2.3.8.

The conductivity of the tubes, accordingly to what has been done for the HX slice model, has been kept equal to 1.1 W/mK.

3.2.3.11 Finding the correct temperature profiles inside the tubes of the five ring regions

The simulation has then been run multiple times on the Eolo CPU clusters (varying the number of CPUs from time to time).

Accordingly to what has been said in paragraph 3.2.3.9, and with particular attention to the explained algorithm, the temperature profile boundary condition inside the tubes has been varied multiple times. The following plot in Figure 35 shows the behaviour of the five reports (one for each tubes ring region) on the heat power removed in the 1-1* region of the tubes, depending on the chosen temperature profile.

Every global variation of all the reports refers to a restart of the simulation due to a change in the temperature profile boundary condition.

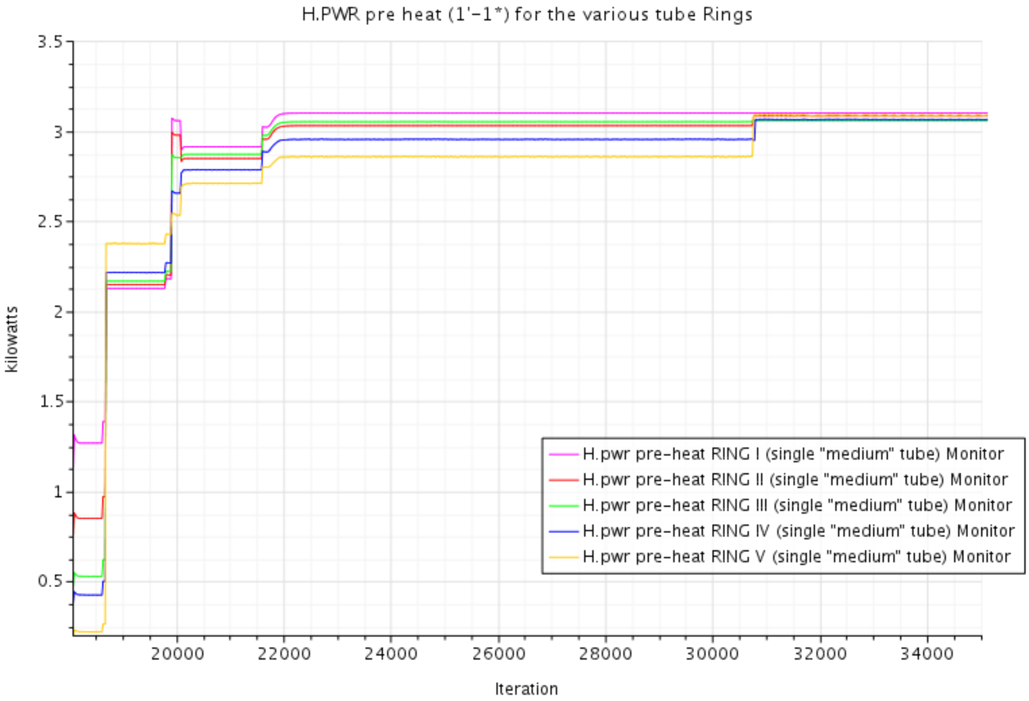

Figure 35:Reports on the heat power removed through the bottom part of each tube (1'-1*). Each report refers to the average value of all the tubes belonging to each ring region.

It can easily be seen that the heat power is very sensible to the variation of the temperature profiles. Also, after many attempts it could be understood that the percentage variation in the heat power removed between 1-1* is, with a good approximation and in a short interval, linear with the percentage variation on the L_{1^*} chosen for each tube ring region.

Knowing this, it was possible to determine the definitive characteristics of the temperature profile in each tube ring (calculated as % perturbation on a 1.2 m base value, in order to reach the correct value of 3.08 kW, and then reported in absolute value):

L(1*) BASE VALUE [m]	**1,2**
Perturb. on L(1*) Base Value (RING I) [%]	**+13 %**
Perturb. on L(1*) Base Value (RING II) [%]	**+12,6 %**
Perturb. on L(1*) Base Value (RING III) [%]	**+11 %**
Perturb. on L(1*) Base Value (RING IV) [%]	**+8 %**
Perturb. on L(1*) Base Value (RING V) [%]	**+2 %**

TUBES REGIONS	L 1*	Pressure P1* [bar]
Ring I	1,36	2,476
Ring II	1,35	2,476
Ring III	1,33	2,476
Ring IV	1,30	2,477
Ring V	1,22	2,478

Table 11: Definitive values of L_{1^*} for the various tubes ring regions

Hence, also absolute variations of a few centimeters on the L_{1^*} have a noticeable impact on the heat transport phenomena.

After reaching the correct value of heat power removed between 1-1* $\cong$ 3.08 kW for each tube region by imposing these profiles, the solution has been re-initialized and run again, in order to compute it from the beginning with the correct thermal boundary conditions inside the tubes, and avoid possible errors due to code “memory” of the previous solutions.

The following pictures (Figure 36 and Figure 37) show the graphic visualization of the correct profiles, alongside the behaviour of the 5 reports on the heat power removed between 1-1* during this new run of this simulation:

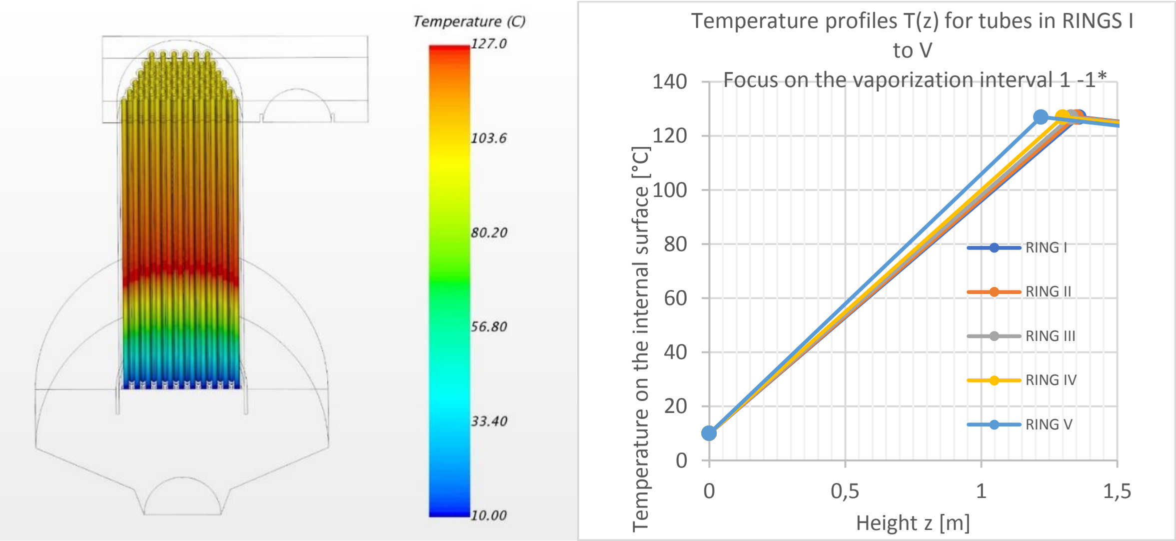

Figure 36:Definitive temperature profiles T(z) inside the tubes chosen for the HX half model. The plot illustrates the T(z) focusing on the first interval (1’-1*).

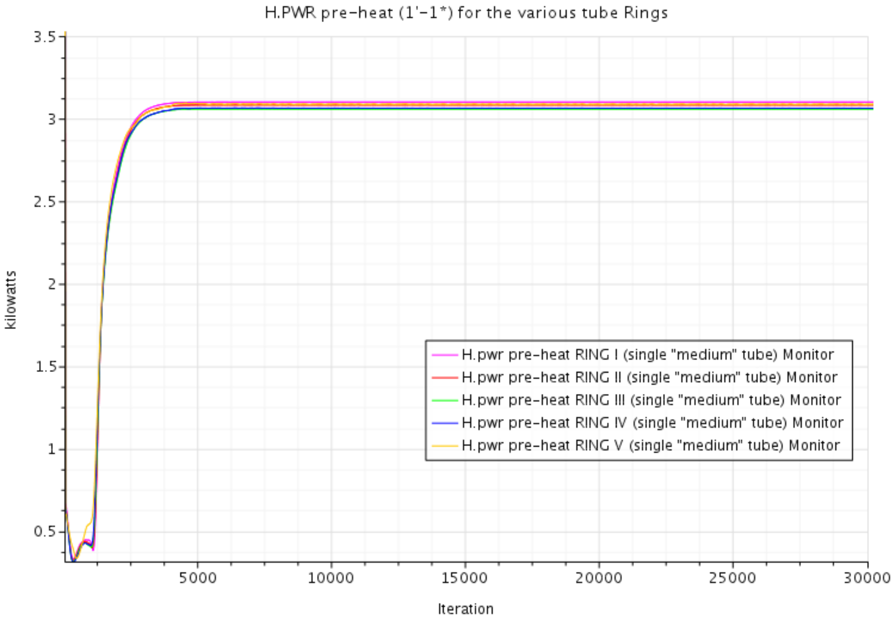

Figure 37:H.PWR removed in the pre-heat region of the tubes (1'-1*) after restarting the simulation.

It can be seen how the reports converge in a very stable way around the desired value, with a maximum relative error below 1%. From now on, this temperature profiles are considered correct, and will not be changed anymore.

4. Energetic analyses on the HX half model.

The next step of the work involved a more accurate analysis of some important energetic factors involving different HX regions, namely:

1) Analysis of the behaviour of different sections of the HX.
2) Evaluation of the behaviour of the different tubes in comparison to the “medium” theoretical tube behaviour.
3) Evaluation of the total heat power removed by the HX, by employing different methods, and comparison to the actual values measured at the CIRCE facility (simulation of the real thermocouples).

All these analyses were done by employing many reports that have been gradually created and upgraded during the internship period, and are reported here together only for order purposes. It is thus important to notice that they have not been created altogether, but along time, when the need for their generation was felt.

4.1 Analysis of the behaviour of different sections of the HX.

In order to better understand how well the HX performs throughout its geometry, the first approach that has been pursued consisted in creating a large number of sections perpendicular to the Z coordinate, at different heights of the HX. These sections were generated with no fixed geometrical rules, but were meant only to keep under control the various zones of the HX, and thus their “vertical density” tends to increase in zones where a much more accurate control was needed (e.g. the area of the HX column before and after the baffle interface grid, the separator zone and the upper part of the outlet region).

All these sections were then merged together in a single scene, illustrating the way temperature evolves while the LBE flow passes from the upper regions (separator) to the bottom ones of the HX. Figure 38 shows the temperature field in the abovementioned sections, from the separator (top left) to the coldest outlet region (bottom right).

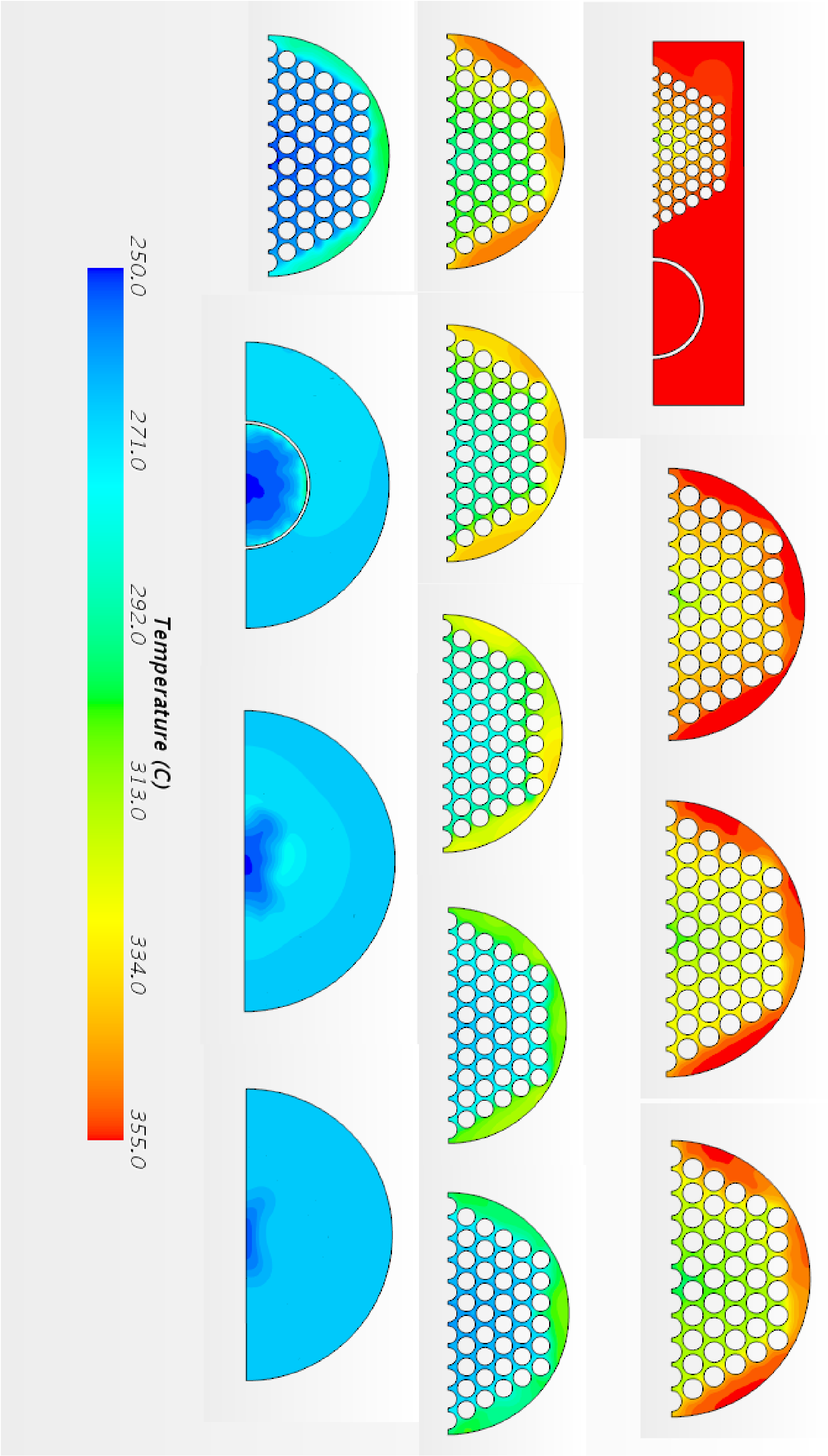

Figure 38:Temperature field at various sections of the HX: the top-left section refers to the separator region, while the bottom right one belongs to the outlet "bulk" region. All other sections are placed intermediately, along the HX column, accordingly to the temperature decrease.

Figure 39 clarifies the spatial distribution of these sections, alongside some streamlines that help to identify recirculation zones and the average direction of the flow.

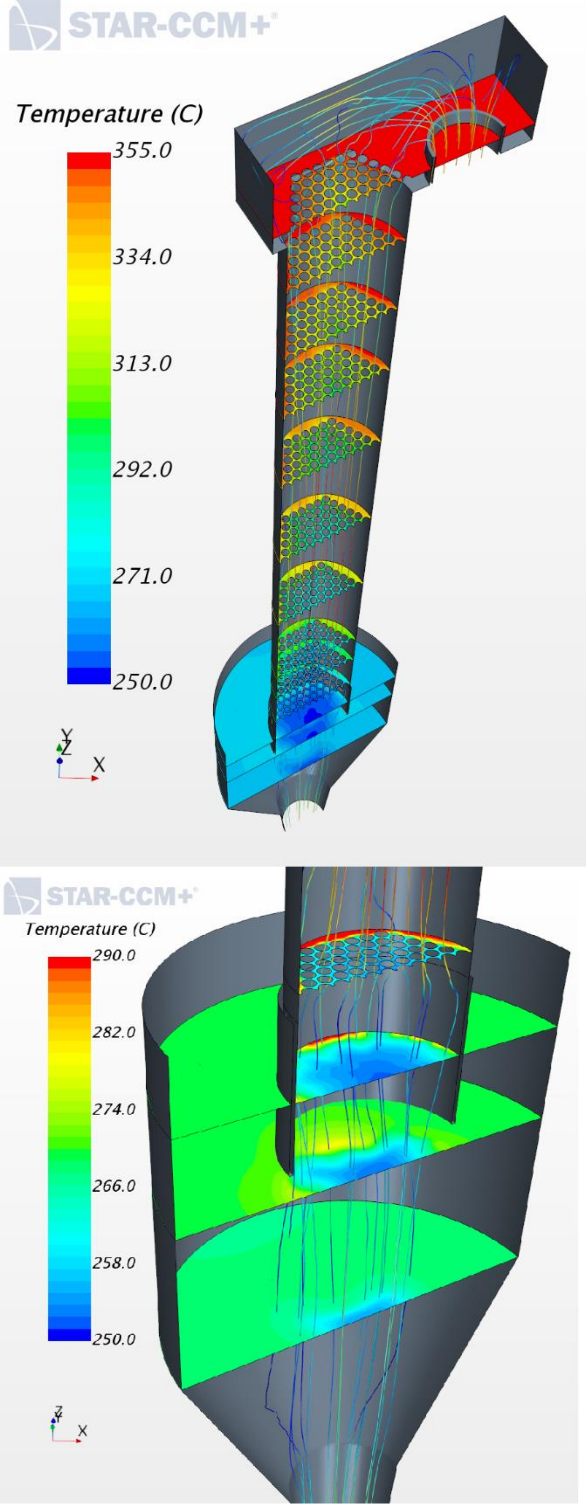

Figure 39:Top: spatial representation of the temperature field on the different sections also depicted in previous Figure 37. Bottom: temperature field on the three bottom sections, depicted with a different scale, in order to highlight the thermal gradients.

It can be easily seen how the LBE inlet temperature varies from the inlet value of 355 °C to an average value around 270 degrees (this will be discussed more precisely later). Also, it is evident that the temperature field in the bottom outlet zone (especially inside the hx skirt) shows some important radial gradients, that can be sources of errors in the temperature measurement, since the HX outlet thermocouples are located in this area (see paragraph 4.3.3.1).The bottom picture in Figure 39 highlights more precisely this radial gradient of temperature by employing a different scale, chosen exclusively for this purpose. It is evident how the temperature ranges from values around 290 °C to a minimum of ~250 °C. (N.B: The color of the streamlines is an indication of the velocity magnitude of the flow.)

4.1.1Natural convection phenomena

Another factor that has been previously theoretically analyzed in paragraph 3.2.1.7 and that plays an important role in the determination of the velocity field of the flow is the natural convection phenomena taking place at the bottom region of the HX, where the temperature inside the tubes reaches its lowest value.

Without discussing again the theoretical aspects that have already been explained before, the following Figure 40 depicts the temperature, density and velocity fields on a section cutting the HX vertically with a 30° angular shift with respect to the symmetry plane. It is evident how strong the effect of the density reduction due to the temperature variation is, and how radically it gets reflected onto the velocity field:

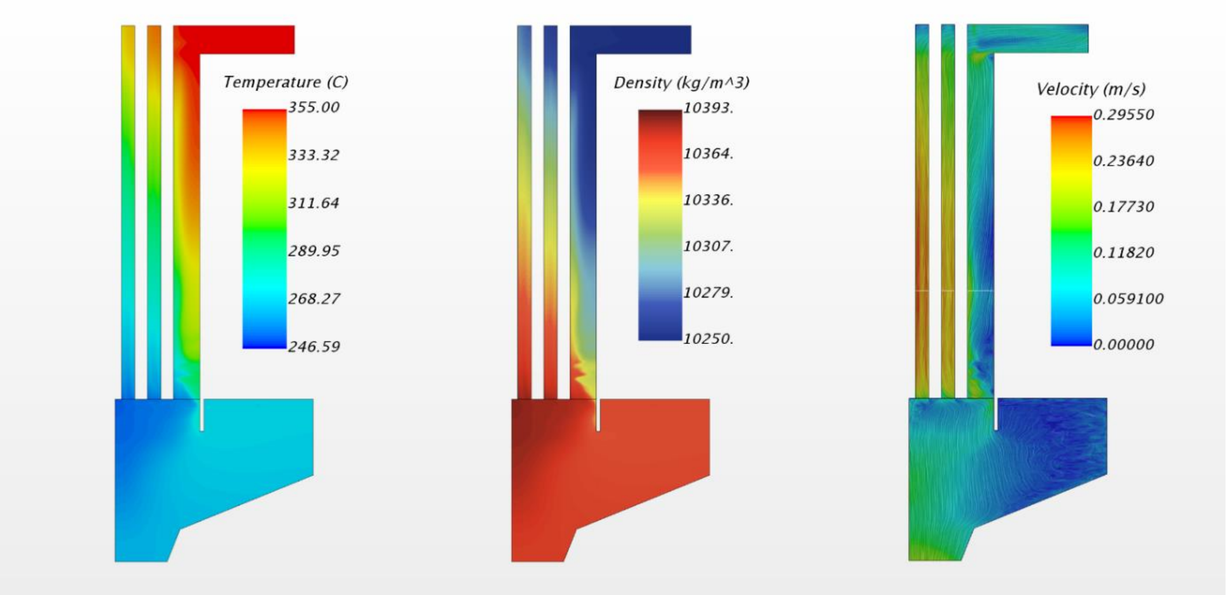

Figure 40:Natural convection phenomena linked to the temperature-varying properties of LBE, analysed on a vertical section of the HX inclined of 30 degrees with respect to the symmetry plane. The previously discussed "pulling” phenomenon takes place near the baffle interface.

4.1.2Heat power removed by various portions of the HX

Going deeper into the HX energetic evaluation, a very important factor to analyze is the behaviour of the HX in terms of heat power removed through its various sections. In order to do this, the HX has been subdivided into eleven separate portions, starting from the baffle interface (bottom grid location) up to the riser exit in the separator, employing 11 vertically equispaced sections (showed inFigure 41).

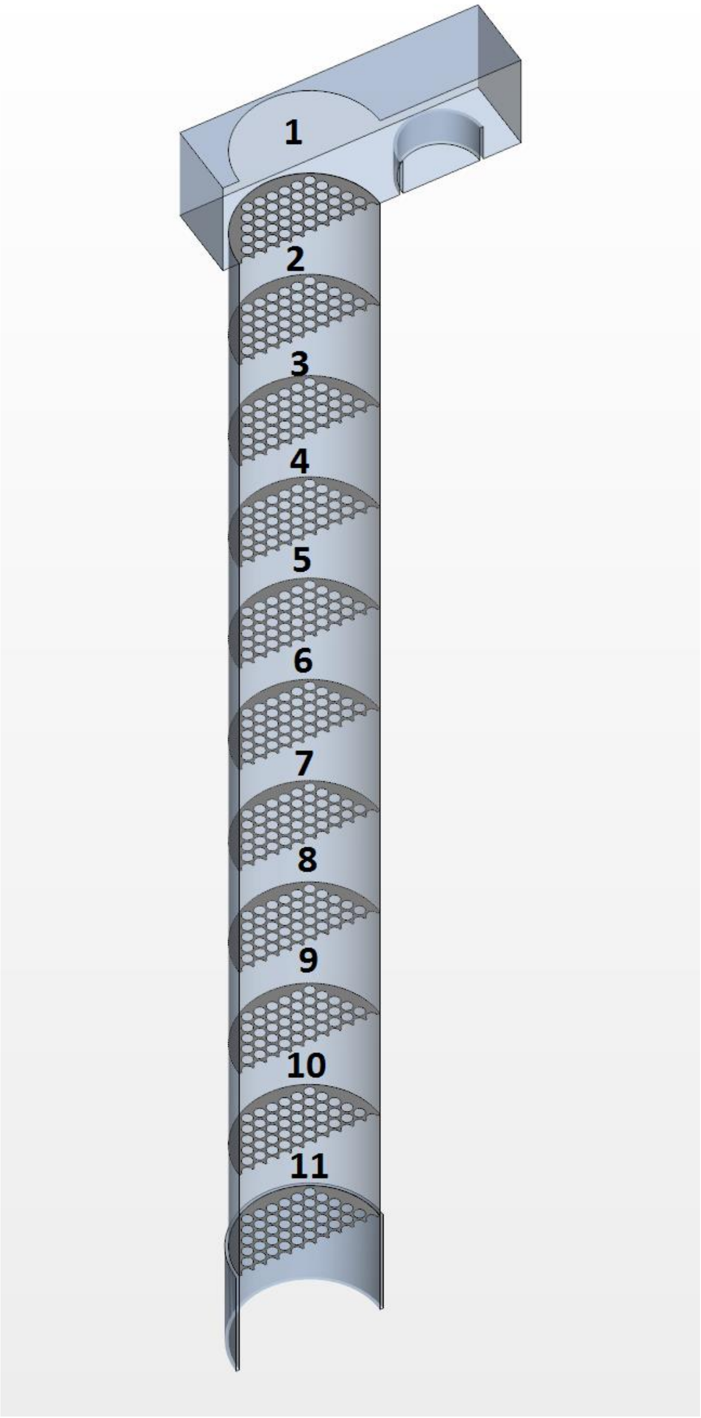

Figure 41:The eleven different portions of the HX.

Portion 1 (top of the HX) coincides with the separator region, while the other 10 regions are distributed along the HX column.

In order to evaluate the heat power removed by the tubes through each single one of these eleven portions of the HX, it has been necessary to evaluate the mass flow averaged value of the specific enthalpy on each section, and then perform eleven energy balances (eqn. (3)) considering each time, as the control volume, a different portion of the HX.

The energy balances yield, for every portion (neglecting the small potential and kinetic contributes):

$$\dot{Q}_{portion} = \dot{m}_{LBE}\left(\bar{h}_{out\ sect.} - \bar{h}_{in\ sect.}\right) \quad (9)$$

The mass flow averaged enthalpies $\bar{h}$ at each section have been evaluated in the form:

$$\bar{h} = \frac{\int_S \rho\vec{u}h\cdot\vec{n}dS}{\int_S \rho\vec{u}\cdot\vec{n}\,dS} \qquad (10)$$

Where S is the the section where specific enthalpy has to be calculated, and $\vec{n}$ the normal vector (in this case always vertical). The LBE mass flow rate $\dot{m}_{LBE}$ considered is 56 kg/s, and thus the found values refer to the whole HX.

These eleven energy balances have been arranged in the following plot (Figure 42), which shows the heat power removed (in absolute value) by the HX through every portion. Notice that the bottom axis is referred to the z coordinate, whose origin lies on the baffle interface of the HX.

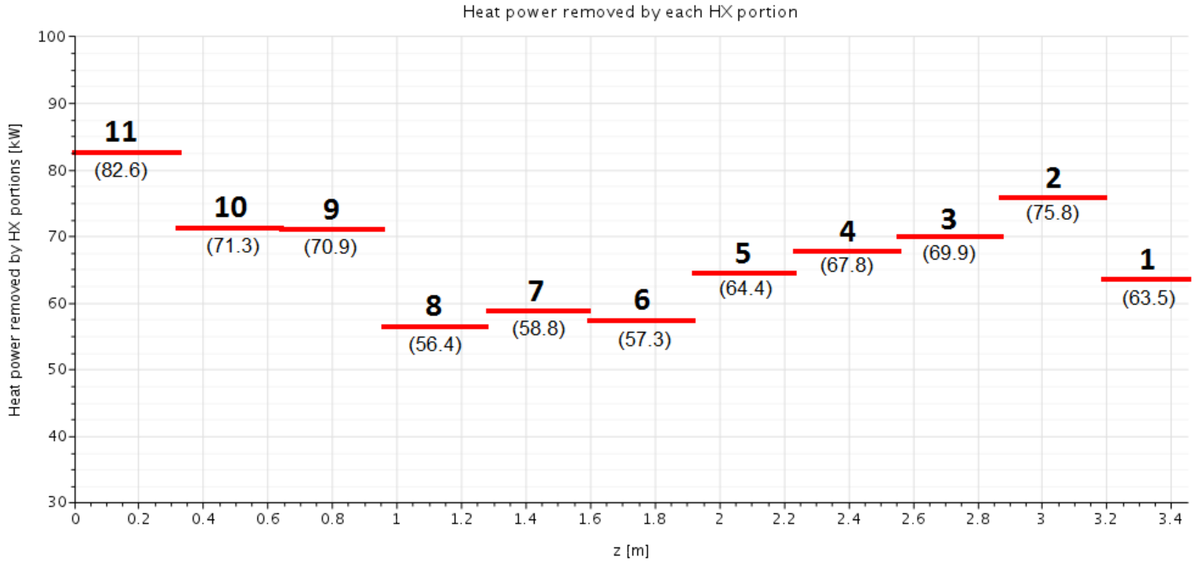

Figure 42:H.PWR removed at each portion of the HX.

As can be easily seen, the average value lies somewhere around ~68 kW per section, with appreciable dispersion (~ ±10 kW), especially on sections 2,6,7,8 and 11. As will later be understood, the determination of these values is of high importance for the analyses on the total heat power removed by the HX, especially when comparing the measured values to the ones determined by employing the actual CIRCE thermocouples.

4.2 Evaluation of the behaviour of the different tubes in comparison to the "medium" theoretical tube behaviour.

Aiming to acquire more precise information on how the heat transfer phenomena are distributed throughout the HX geometry, a necessary step consisted in the evaluation of the behaviour of each single tube in terms of heat power removed. As anticipated in paragraph 3.2.3.9, many reports regarding each single tube inside the HX have been created; the ones that pay a relevant role in this section are:

- Reports on heat power removed by each tube, in absolute value, throughout its whole length.
- Reports on heat power removed by each tube, throughout its whole length, with reference to the heat power removed by the "medium tube".

The "medium tube" heat power was evaluated considering the total heat power removed by the 91 tubes of the HX, in the following way:

$$\dot{Q}_{med.tube} = \frac{\dot{Q}_{HX}}{n.\ of\ tubes} \qquad (11)$$

The total heat power removed by the HX, $\dot{Q}_{HX}$, has been evaluated applying eqn. (6) integrating on the union of the interface surfaces between all the tubes and the LBE fluid region (here called Ω). Since only half of the tubes are represented due to simmetries, the value of the integral had obviously to be doubled:

$$\dot{Q}_{HX} = 2\dot{Q}_{halfHX} = 2\int_{\Omega} \vec{q}\cdot\vec{n}\, d\Omega \cong 736\ kW \qquad (12)$$

Considering this, the heat power removed by the "medium tube" of the HX can be evaluated as:

$$\dot{Q}_{med.tube} = \frac{\dot{Q}_{HX}}{n.\ of\ tubes} = \frac{2\int_{\Omega} \vec{q}\cdot\vec{n}\, d\Omega}{91} \cong 8.09\ kW \qquad (13)$$

Having created the reports that evaluate the heat power removed by each single tube in absolute value ($\dot{Q}_{i/j}$, for a generic tube of the hexagonal matrix, from eqn. (6) integrated on each tube internal surface), the heat power removed by each single tube normalized as percentage of the $\dot{Q}_{med.tube}$ has been calculated as (for a generic tube i/j):

$$\dot{Q}_{i/j,\%} = \frac{\dot{Q}_{i/j}}{\dot{Q}_{med.tube}} \cdot 100 \qquad (14)$$

The values of $\dot{Q}_{i/j,\%}$ have been computed for each i/j-th tube of the matrix (paying attention to adequately correct the values of the tubes cut by the simmetry plane), and their values have been rearranged in the following map:

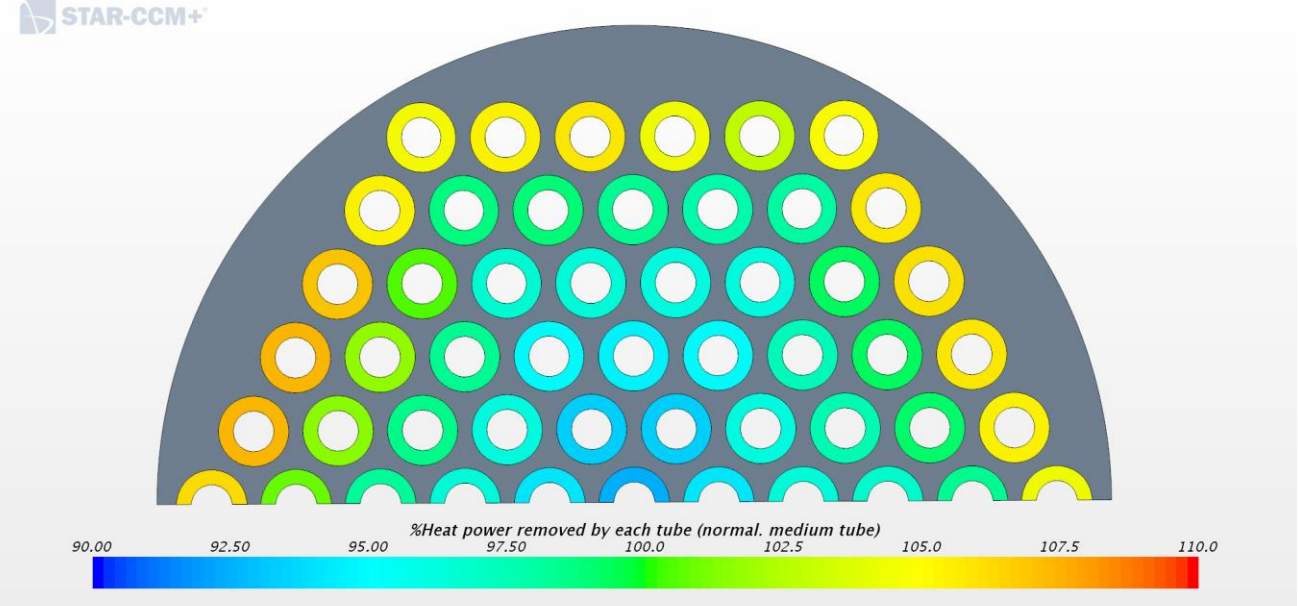

Figure 43: Percentage of H.PWR removed by each tube with respect to the "medium" tube behaviour.

The previous map in Figure 43 highlights a radial gradient of heat power removed by the tubes. It is in fact evident that the tubes belonging to the center of the hexagonal matrix (RING I, II and III) tend to exchange less than the “medium” value of 8.09 kW (100%, center of the scale), reaching a minimum value of ~92.5% for tube 1/6. On the other hand, the tubes belonging to RING V generally exchange more heat power than the one of the “medium tube”, reaching a maximum of ~107.3% of $\dot{Q}_{med.tube}$ for tubes 2/1 and 3/1. This maximum might be an indication of how important the inlet effects caused by the separator geometry (described in the previous paragraph) could be: in fact it is important to remember that a consistent flow of LBE enters the HX column after going through some recirculation effects that take place in the upper-left zone of the separator (as depicted inFigure 29).

The tubes belonging to RING IV exchange approximately 100% of $\dot{Q}_{med.tube}$, thus being in line with the behaviour of the medium tube.

4.3 Evaluation of the total heat power removed by the HX and comparison to the actual values measured at the CIRCE facility (simulation of the real thermocouples).

The focus of this paragraph is on the analysis of the energetic behaviour of the HX in its wholeness, with particular attention to the total heat power removed, calculated with different methods and compared to the one measured by using the thermocouples actually employed in the CIRCE facility.

4.3.1 Evaluating the total heat power removed by the HX

The determination of the total heat power removed by the HX can appear, at a first glimpse, as simple and unambiguous. As could be understood after some time, the search for a coherent result for this value is highly affected by the employed approach, and even more by the choice of averaged input parameters used to pursue it.

In the previous HX slice model, the heat power removed was evaluated by employing a very simple energy balance based on eqn. (3) considering the mass flow averaged enthalpies at the inlet and outlet sections of the domain (see paragraph 3.2.1.10). This value was only used to evaluate the coherence of the model, and has thus been considered only in an approximate way to signal possible macroscopic errors: in fact, an energy balance returning an exaggeratedly high (or low) value for the heat power removed would signal a strong error in the construction of the model.

In this last HX half model, conversely, the evaluation of the heat power has a more relevant role, in that it aims to reach a superior level of precision and give some accurate information about the actual heat exchange phenomena. Hence, the heat power is not an instrument to verify the general coherence of the model anymore, but is focused on giving a concrete evaluation of the heat transfer, in both a qualitative and quantitative way.

4.3.2 The different methods to evaluate the heat exchange in the HX

At this stage of the modeling process, many reports have been created, in order to monitor the heat exchange between various portions of the HX, employing different methods depending on the information needed.

The three main methods used to calculate the heat power removed by the HX through its different portions have been the following:

1) Energy balance, based on CFD calculated mass flow averaged specific enthalpies at inlet and outlet sections of the considered control volume.
2) Energy balance, based on CFD calculated mass flow averaged temperatures at inlet and outlet sections of the considered control volume.
3) Direct integration of the normal component of the heat flux over a chosen surface, following eqn. (6).

These methods will be briefly discussed in the following paragraphs.

4.3.2.1 1) Energy balances employing mass flow averaged enthalpies

This procedure has essentially already been exposed in paragraph 4.1.2 , and in fact the values of the heat powers subtracted in the various portions of the HX have been calculated employing this method.

In general, remembering the eqn. (3) (first principle of thermodynamics for open systems), applying it to a very simple control volume (CV) with only one inlet and one outlet, and with the hypotheses of:

- stationary case
- no mechanical, electrical or chemical power transiting through the boundaries of the control volume
- negligible variation of kinetic energy between inlet and outlet of CV

the heat power transiting through the boundary of the control volume can thus be expressed as:

$$\dot{Q}_{CV} = \dot{m}_{LBE}[(\bar{h}_{out\ CV} - \bar{h}_{in\ CV}) + g(z_{out\ CV} - z_{in\ CV})] \qquad (15)$$

Where $\bar{h}$ is the mass flow averaged specific enthalpy calculated accordingly to eqn. (5) at the desired section (inlet or outlet) of CV.

A particular note has to be made about the specific potential energy variation $g(z_{out\ CV} - z_{in\ CV})$: in fact, this term has been neglected in the calculations about the heat power removed by each portion of the HX, because of its very low magnitude. Since the energy balances that will be calculated from now on involve rather extensive portions of the HX (especially in the z coordinate) it felt inappropriate to neglect it from the beginning without estimating it in the first place.

Even with an approximate calculation, though, it is clear that this term is still negligible, in fact, considering its total contribute to the heat power removed, with an exemplificative height variation of 3 m, and considering the actual mass flow rate of 56 kg/s:

$$\dot{m}_{LBE}\ g(\Delta z) = 56 \cdot 9.81 \cdot 3 \cong 1650\ W = 1.65\ kW \qquad (16)$$

since that the estimated heat power removed by the whole HX, from eqn (12) is of ~736 kW, the relative eror committed in neglecting the contribute of the potential energy variation within the whole balance is ~0.2 %, and is thus totally negligible.

The energy balance then simply becomes:

$$\dot{Q}_{CV} = \dot{m}_{LBE}\left(\bar{h}_{out\ CV} - \bar{h}_{in\ CV}\right) \qquad (17)$$

Henceforth, the heat powers calculated with this procedure will be referred to as $\dot{Q}^{\bar{h}}$, where the superscript $\bar{h}$ refers to the fact that they are calculated employing mass flow averaged enthalpies.

4.3.2.2 2) Energy balances employing mass flow averaged temperatures

As referred to in the official CIRCE documents [1.] and [3.], all the evaluations of the heat power removed by the HX are made with reference to certain particular values of temperature, measured at different sections of the HX employing adequate sets of thermocouples.

In order to be able to reconstruct these measurements while adding the real thermocouples to the model, it was necessary to elaborate a correct procedure to calculate the heat power removed with temperature values rather than enthalpies.

Considering that LBE is at liquid state, it can be said that, with good approximation:

$$dh \cong c_p dT \qquad (18)$$

Thus, for a generic finite variation of enthalpy:

$$\Delta h_{21} \cong \int_1^2 c_p dT \qquad (19)$$

And, considering eqn. (17):

$$\dot{Q}_{CV} = \dot{m}_{LBE}\left(\bar{h}_{out\ CV} - \bar{h}_{in\ CV}\right) \cong \dot{m}_{LBE} \int_{in\ CV}^{out\ CV} c_p dT \qquad (20)$$

Remembering that the expression of $c_p(T)$ has been modeled as a polynomial, with reference to Table 1:

$$c_P = 164.8 - 3.94 \times 10^{-2} T + 1.25 \times 10^{-5} T^2 - 4.56 \times 10^{5} T^{-2}$$

Hence, the integral is:

$$\int_{in\ CV}^{out\ CV} c_p dT = \left[164.8T - 3.94 \cdot 10^{-2}\left(\frac{T^2}{2}\right) + 1.25 \cdot 10^{-5}\left(\frac{T^3}{3}\right) + 4.56 \cdot 10^5 T^{-1}\right]_{in\ CV}^{out\ CV} \qquad (21)$$

Anyway, the value of T in the previous equation (20) should be an adequately averaged value of temperature at the inlet and outlet sections. Hence, the average temperature at these sections has been calculated as a mass flow averaged value, coherently with the following expression:

$$\bar{T} = \frac{\int_S T\, d\dot{m}}{\dot{m}} = \frac{\left(\int_S \rho \vec{u} T \cdot \vec{n} dS\right)}{\int_S \rho \vec{u} \cdot \vec{n} dS} \qquad (22)$$

Where S is the surface upon which the integral is calculated (for $\overline{T}_{in}$, the surface S coincides with the inlet surface of the CV, while for $\overline{T}_{out}$ with the outlet surface, obviously).

When the energy balance will be calculated to simulate the real CIRCE measurements, obviously $\overline{T}_{in}$ and $\overline{T}_{out}$ will respectively be the average values of temperature measured by the thermocoulpes at the inlet and outlet sections.

Henceforth, heat powers calculated with this procedure will be referred to with as $\dot{Q}^{\overline{T}}$, where the superscript $\overline{T}$ refers to the fact that they are calculated employing mass flow averaged temperatures.

4.3.2.3 3) Direct integration of the normal component of the heat flux over a chosen surface

This procedure essentially consists in applying equation (6) integrating over the desired surface, as explained various times. In fact, the heat power removed by the whole HX has been calculated using this procedure already in paragraph 3.2.3.9, integrating on the interfaces between all the tubes and the fluid LBE region, and returning the absolute value of ~736 kW.

Essentially, this is the only calculation where the heat power has been evaluated with this procedure; anyway, it is generally considered the most accurate, as it directly operates on the heat flux.

Henceforth, whenever referring to the heat power removed by the whole HX calculated in this way, the nomenclature will be:

$$\dot{Q}^{\int} \quad \cong 736\ kW$$

Where the superscript refers that this is a value calculated with a surface integral.

4.3.3 Calculating the heat powers and discussing the obtained results.

The previously explained methods have then been used to estimate, in absolute value, the heat power removed by the HX between different sections. In the next paragraph, much emphasis will be posed on the role of the real thermocouples at the inlet and outlet zones of the HX; it is thus of primary importance to specify their position within the HX geometry.

4.3.3.1 Location of the HX thermocouples:

The temperature at the inlet and outlet sections of the HX is monitored by employing a certain number of thermocouples. The spatial distribution of these thermocouples within each section has been chosen with the aim to extract a correct value for the average temperature, which will be used later on to compute some energy balances.

The thermocouples, henceforth referred to as TCs, are distributed as follows:

INLET TCs:

- Location of the inlet section: section of the HX column, perpendicular to Z axis, 30 mm below the separator bottom
- 3 TCs (TC-SG-01,02 e 03), disposed in a 120° pattern, already included in the HX shell.

OUTLET TCs

- Location of the outlet section: section of the HX column, perpendicular to Z axis, 100 mm above the bottom of the skirt
- 6 TCs (TC-SG-13,14,15,16,17 and 18). The distribution of these TCs is more complex than the one of the inlet TCs, in fact they can be divided into two separate groups:
    1. (TC-SG-14,15 and 17): radial length of 53 mm from the internal surface of the HX skirt, disposed in a symmetric 120° pattern.
    2. (TC-SG-13,16, and 18): radial length of 115 mm from the internal surface of the HX skirt, disposed in a symmetric 120° pattern, shifted by 60° with respect to the pattern of TC-SG-14,15 and 17).

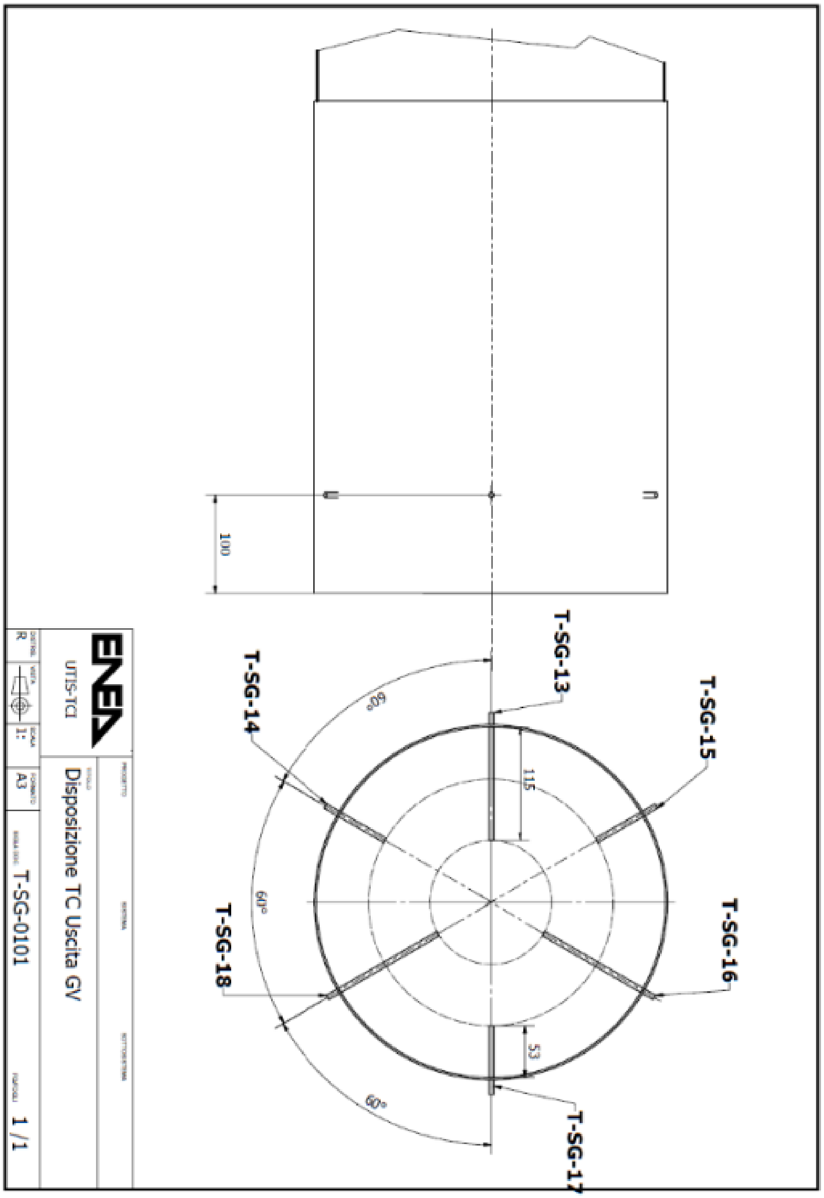

Figure 44:: Official spatial distribution of the 6 outlet TCs.

All these TCs have been represented within the HX half model as probe points, in order to be later able to replicate their measurements. Furthermore, since only one symmetric half of the HX is considered in this model, all the TCs belonging to the “other” half of the HX have also been modeled by “mirroring” their actual positions with respect to the symmetry plane. In this way, the accurate estimation of the temperature measured by all the TCs could be obtained, both at the inlet and outlet surfaces. The representation of the resulting TCs distribution along the CFD domain of the HX half is represented in Figure 45, where both the inlet and outlet TCs sections are highlighted, together with the probe points representing the inlet (red) and outlet (blue) TCs themselves.

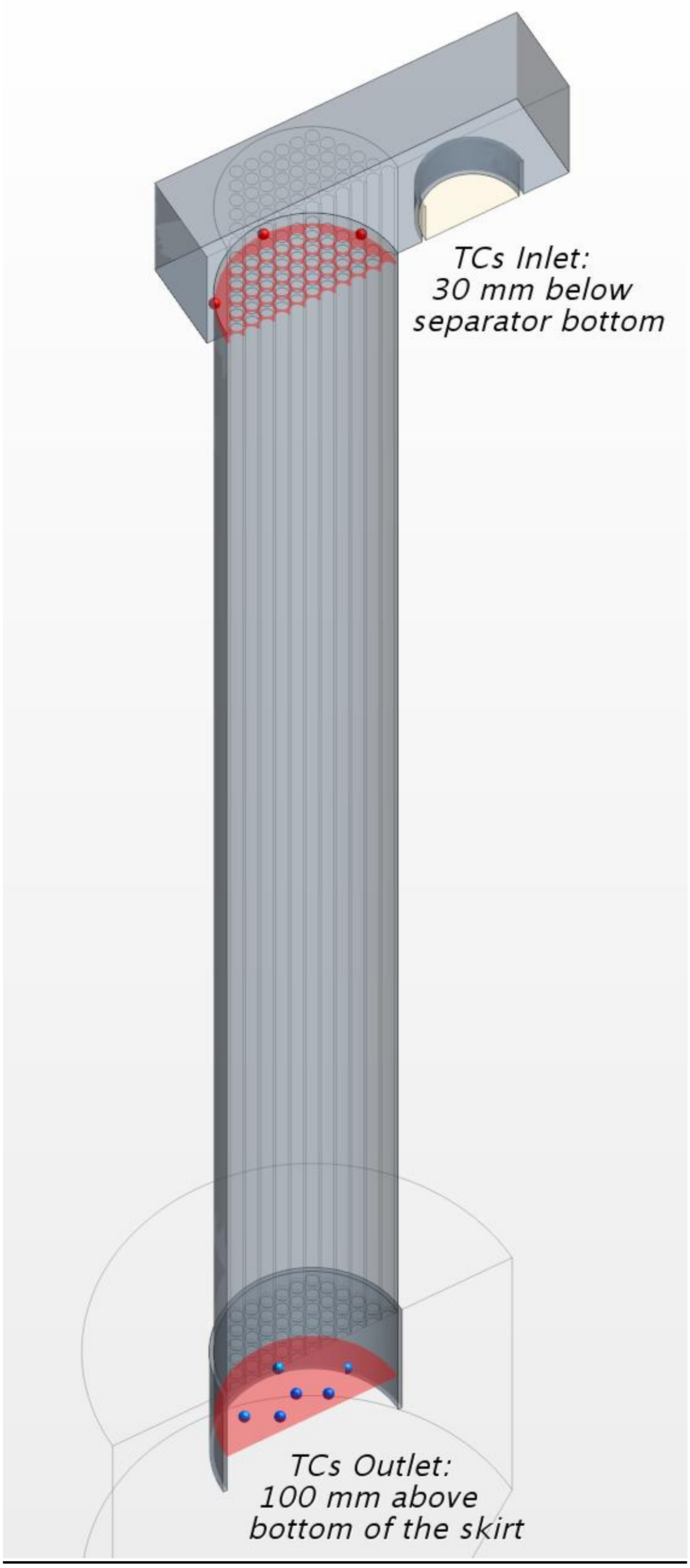

Figure 45:Spatial distribution of the HX inlet (red) and outlet (blue) thermocouples. The inlet and outlet sections are also highlighted in red.

4.3.3.2 Evaluation of the temperature values measured by the TCs:

TCs INLET:

All the temperature values at the inlet TCs locations have been measured with appropriate reports, monitored during the simulation run and their average value could be calculated.

The results are shown in the following plot (Figure 46), showing the temperature values converging adequately after a large number of iterations (the black dashed line represents the average inlet temperature value measured by the TCs):

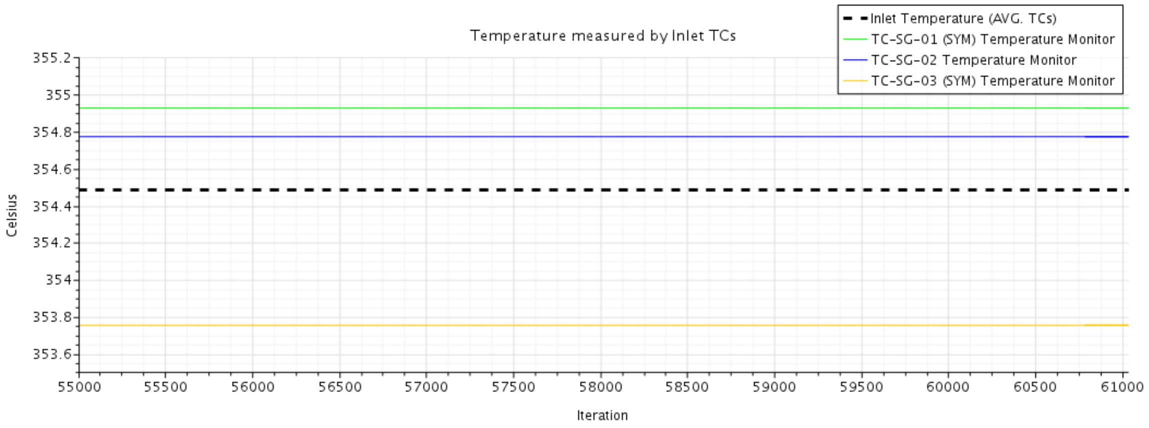

Figure 46:Temeprature values measured by the three Inlet TCs.

The following Figure 47 depicts the temperature field on the inlet TCs section 30 mm below the separator bottom, together with the 3 TCs located there (TC-SG-01,02 and 03), represented as black probe points. Notice that the two TCs that have been "mirrored" due to the previously mentioned symmetry considerations have been marked as "(SYM.)". As can be clearly seen, the TCs are placed in a position that does not actually take into account the coldest region of the section, located at the centre of the hexagonal tubes pattern (Ring I and II of the tubes regions).

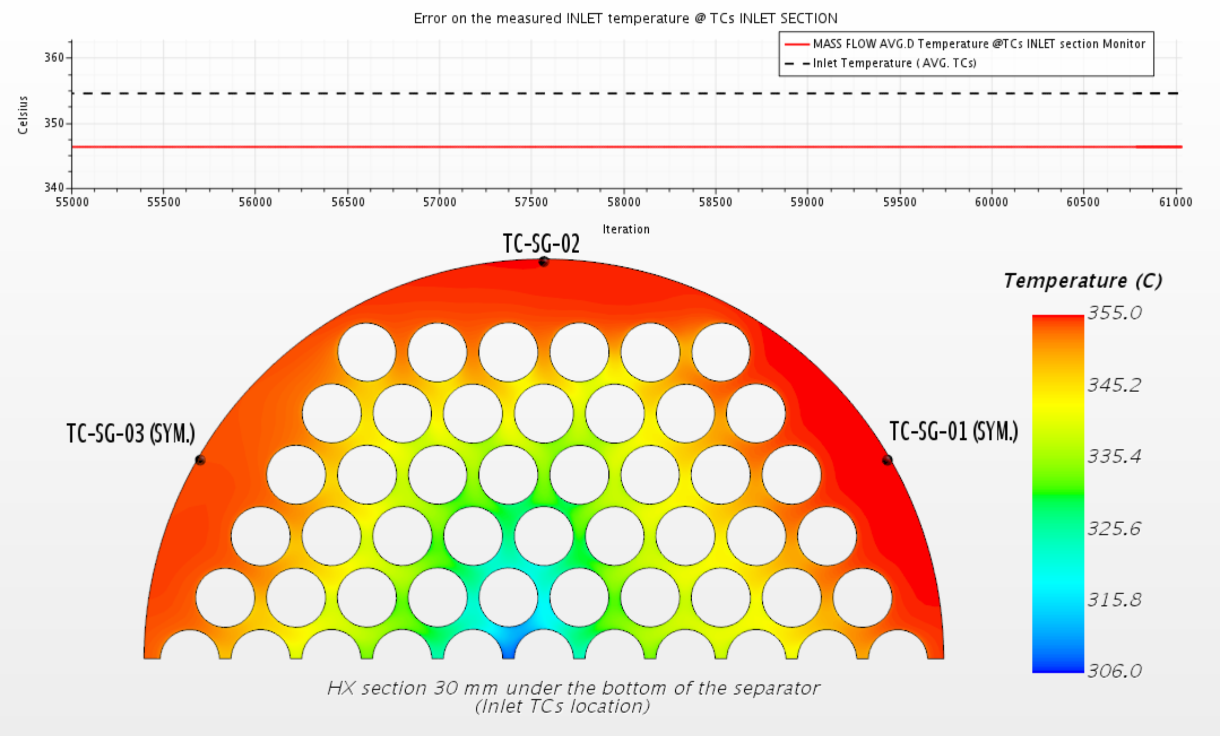

Figure 47:Temperature field at the TCs inlet section, and TCs measured values.

This inevitably leads to errors in the evaluation of the temperature, that will now be discussed.

In the previous Figure 47, the plot above the section reports two values:

- Black dashed line: value of the average temperature measured by the thermocouples (same as reported in Figure 46), referred to as $T_{\substack{avg.inlet\\TCs}}$
- Red line: this is the value of the mass flow averaged temperature $\bar{T}_{\substack{TCs\,inlet\\section}}$ (calculated with reference to eqn. (22)) calculated by integrating on the whole section where the inlet TCs are placed.

The same plot is reported with more detail here below (Figure 49):

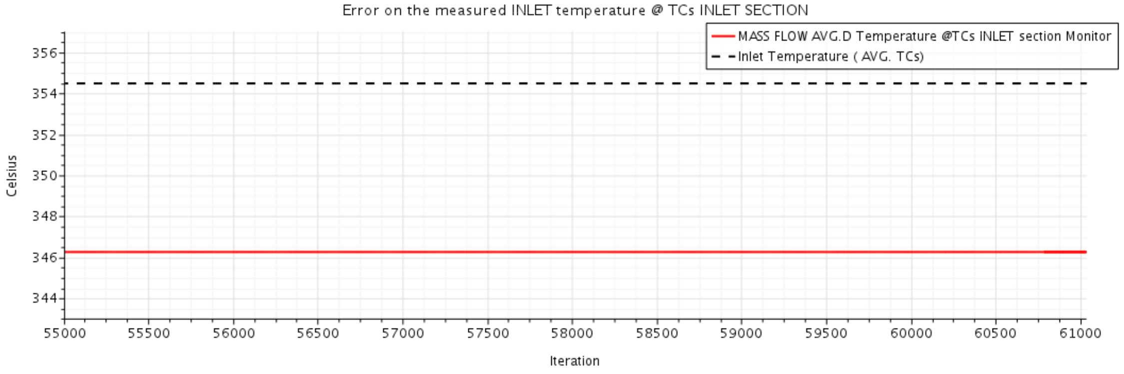

Figure 48: Difference between the avg. value of temperature measured by the inlet TCs and the mass flow averaged value measured at the same section.

The reported temperatures are:

- Average inlet TCs temperature $T_{\substack{avg.inlet\\TCs}} \cong\ 354.5\ ^{\circ}C$
- Mass flow averaged temperature at inlet TCs section $\bar{T}_{\substack{TCs\ inlet\\section}}\ \cong\ 346.3\ ^{\circ}C$

Hence, the three thermocouples TC-SG-01,02,03 appear to measure an average temperature at the inlet section of the HX column that is ~8 °C higher than the mass flow averaged one on the same surface.

TCs OUTLET:

Accordingly to what has been done for the inlet TCs, the same procedure has been applied to the outlet section (100 mm above the bottom of the HX skirt) where the six outlet TCs are located (TC-SG-13,14,15,16,17,18).

The temperature values measured by the TCs show a more irregular behaviour, especially for the TCs measuring the highest values; anyway, since the maximum oscillation for TC-SG-15 is around ~3 °C (~1%, relatively to the average value of ~261.5 °C), the values are acceptable, and showed in the following plot (Figure 49):

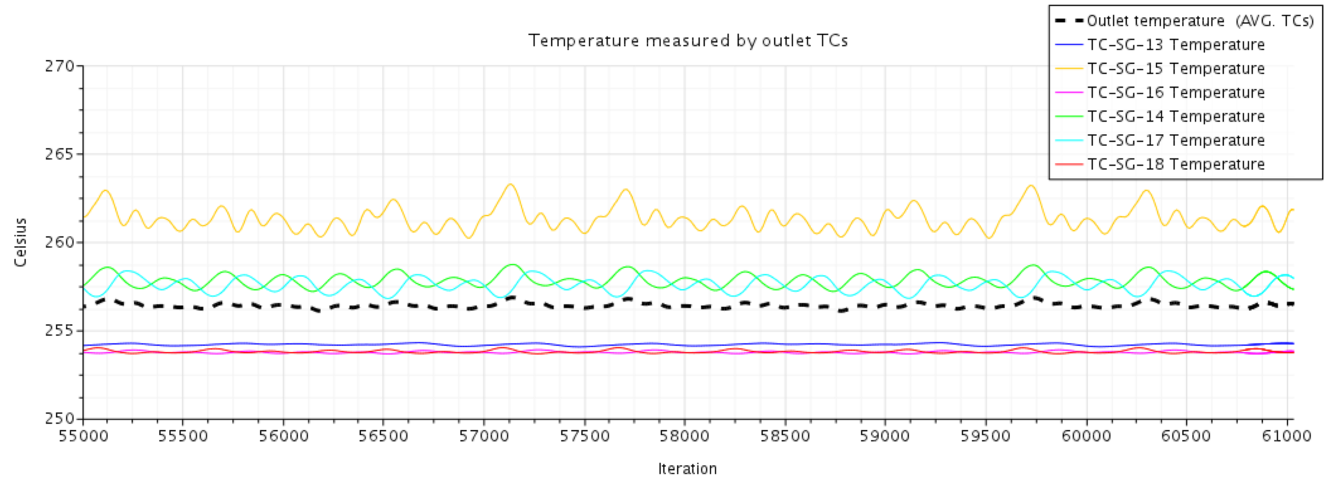

Figure 49: Temperature values measured by the outlet TCs

This is essentially due to the noticeable radial temperature gradient already discussed in paragraph 4.1. This is evident also by directly observing the temperature field in the outlet section where the TCs are placed, as shown in Figure 50.

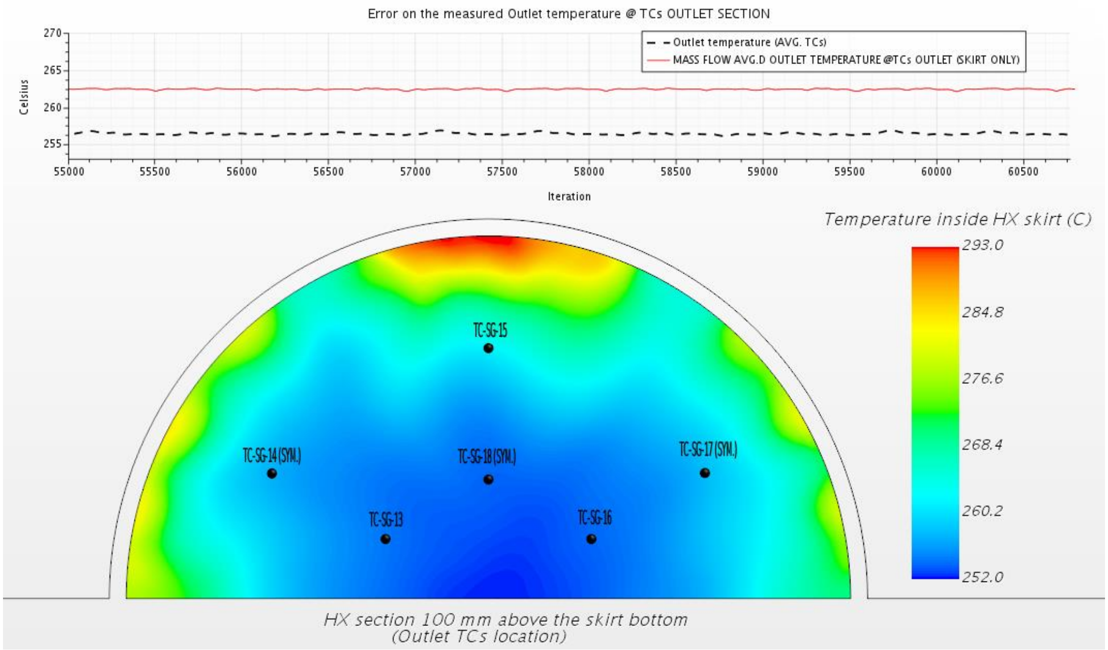

Figure 50:Temperature field at the TCs outlet section, and TCs measured values

The six outlet TCs are displayed as black probe points, and the ones that have been “mirrored” from the other half of the HX are marked as “(SYM.)”.It can be noticed that the flow in the region below the bottom of the tubes (inside the HX skirt) still has “memory” of the geometry of the tubes, due to the presence of three hot “spots”, aligned with the sides of the hexagonal tubes pattern. The six outlet TCs are disposed in a centered position that seems not to take into account these hotter parts of the flow, concentrated near the internal surface of the skirt. Because of this, the outlet TCs measure an average temperature that is lower than the mass flow averaged one on the section where they are placed; in order to estimate this error, one can observe the plot in the previous Figure 50, which is reported here below with more detail (the black dashed line is always referring to the TCs average measured value, while the red one to the mass flow averaged one):

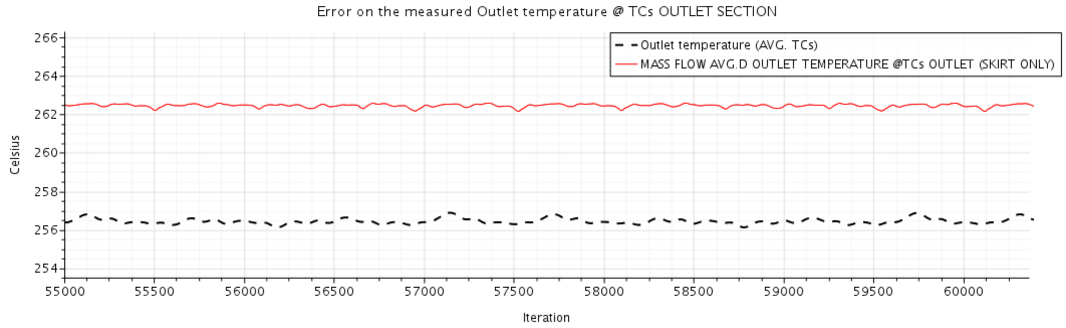

Figure 51:: Difference between the avg. value of temperature measured by the outlet TCs and the mass flow averaged value measured at the same section.

In this case, the measured temperatures are:

- Average outlet TCs temperature $T_{\substack{avg.outlet\\ TCs}} \cong \; 256.5\,°C$
- Mass flow averaged temperature at outlet TCs section $\bar{T}_{\substack{TCs\ inlet\\ section}} \cong 262.3\,°C$

In conclusion, the six thermocouples TC-SG-13,14,15,16,17,18 appear to measure an average temperature at the outlet section of the HX column that is ~6°C lower than the mass flow averaged one on the same surface.

Both the considerations on the inlet and outlet measured temperatures will have an important impact on the calculation of the energy balances, as will be explained in the next paragraph

4.3.4Calculation of the heat power removed by the HX through different portions:

The aim of this paragraph is to describe, with reference to the theoretical issues discussed in paragraph 4.3.2, what are the actual results of the estimation of the heat power removed by the HX through its various parts.In general, three different control volumes have been identified within the HX; the following Figure 52 meant to highlight them by specifying their inlet (red) and outlet (blue) boundary surfaces:

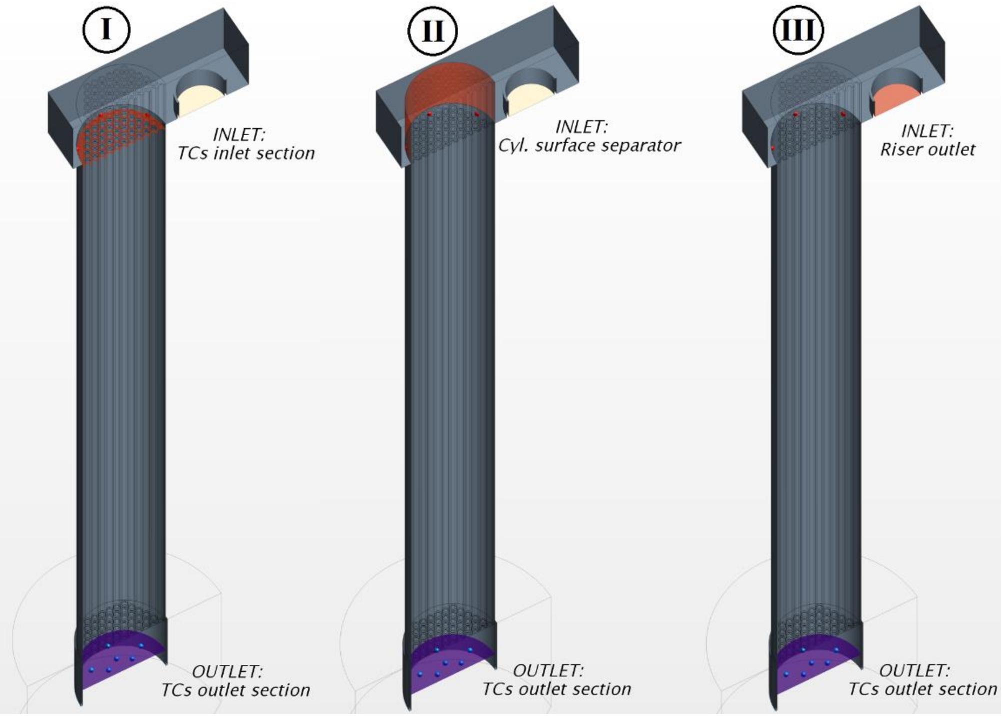

Figure 52: The three different control volumes that have been analysed. Red section: inlet – Blue section: outlet.

N.B.: even if only a symmetric half of the HX is depicted, the energy balances consider the total mass flow rate of $\dot{m}_{LBE} = 56\ kg/s$, and are thus referred to HX in its wholeness.

The results will now be reported for each one of these control volumes.

4.3.4.1 Control volume I: Heat power removed between the TCs inlet and outlet sections

Most of the data that could be found in the CIRCE official documents (about the heat power removed by the HX), refers to this particular control volume. With reference to document [3.], it is clearly precised that the heat power is calculated with an energy balance between these sections, thus not including the heat power removed through the upper, separator zone.

With reference to the theoretical considerations explained in paragraph 4.3.2, and with clear meaning of the symbols, the obtained results for the absolute value of the heat power removed between the TCs inlet and outlet sections are:

Control volume I

$\dot{Q}^{\bar{h}} \cong 673\ kW$ (Energy balance/mass flow avg.d enthalpies)

$\dot{Q}^{\bar{T}} \cong 681\ kW$ (Energy balance/mass flow avg.d temperatures)

$\dot{Q}^{\bar{T}}_{TCs} \cong 796\ kW$ (Energy balance/TCs avg. Measured temperature value)

$\dot{Q}^{\int} \cong 736\ kW$ (Correct total heat power removed by the HX)

A plot showing the abovementioned heat powers as calculated with STAR-CCM+ is reported below (with corresponding legend colors) (Figure 53):

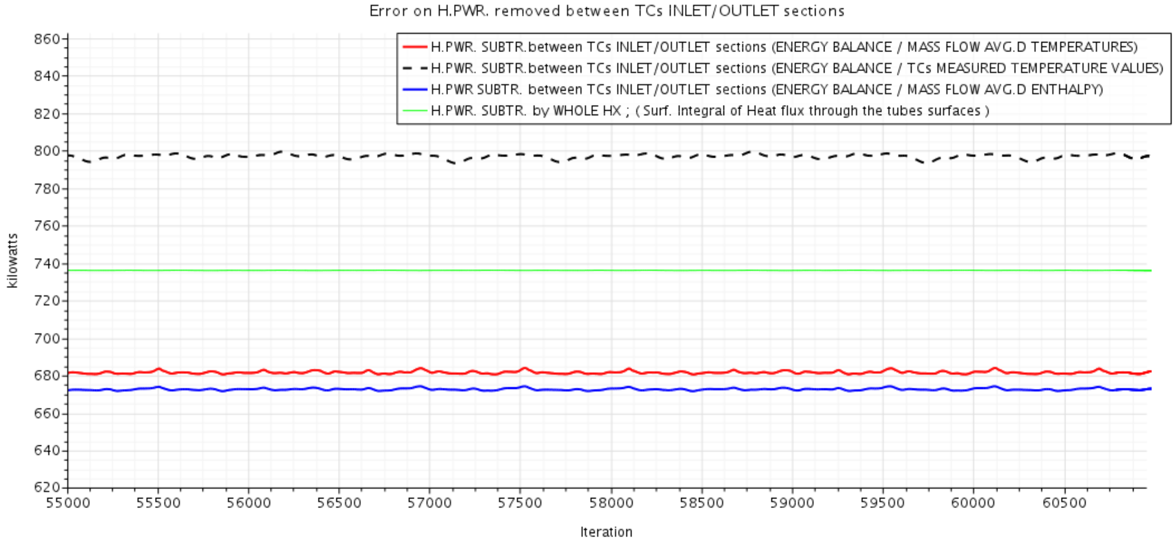

Figure 53:Evaluation of H.PWR removed through CV I with different methods.

(N.B: Please notice that the value of $\dot{Q}^{\int} \cong 736\ kW$ refers to the HX in its wholeness, and not only to the CV I; it has been added here only as a reference for the further analyses)

A first important observation has to be made regarding the two different approaches at calculating the energy balance, namely $\dot{Q}^{\bar{h}}$ and $\dot{Q}^{\bar{T}}$. These two energy balances refer to mass flow averaged enthalpies and temperatures calculated directly from the CFD domain; it is easily noticeable how the two calculated values differ of ~8 kW and, considering an average value between the two of 677 kW, the relative error is ~1%, hence totally acceptable. This evaluation of the relative error between the two methods has been pursued in orer to validate the method by which $\dot{Q}^{\bar{T}}$ has been calculated, because the same procedure has been followed to calculate $\dot{Q}^{\bar{T}}_{TCs}$, from the TCs measured temperatures.

Furthermore, the heat power removed by the whole HX ($\dot{Q}^{\int} \cong 736\ kW$) should differ from $\dot{Q}^{\bar{h}}$ and $\dot{Q}^{\bar{T}}$ only by the amount of heat power removed through the upper region of the separator.

Calculating $\dot{Q}^{\int} - \dot{Q}^{\bar{h}} \cong 63\ kW$, and comparing it to the value of the heat power removed through region 1 (separator) in Figure 42, equal to ~63.5 kW, reassures that the energy balances calculated up to now are coherent with the physics of the model. The slight difference of 0.5 kW (~0.8% of the total 63 kW) is totally referable to interpolation and approximation errors. The value of $\dot{Q}^{\bar{T}}_{TCs}$ is instead very high if compared to both the $\dot{Q}^{\bar{T}}$ and the $\dot{Q}^{\bar{h}}$, but also ~60 kW higher than the total heat power removed $\dot{Q}^{\int}$: this macroscopic difference is surely related to the errors on the temperature measured by the TCs, discussed before in paragraph 4.3.3.2.

In fact, the differences of +6 °C on the inlet temperature and -8°C on the outlet temperature (with respect to the mass flow averaged ones measured from the CFD domain), highly affect the energy balance, and cause this discrepancy. Also, the temperature of~354.5 °C measured by the inlet TCs is more significative if compared to the inlet LBE temperature (355 °C), and so, the value of $\dot{Q}^{\bar{T}}_{TCs}$ should be referred to a global heat power evaluation and not to one over the CV I.

Concluding, in this model the heat power $\dot{Q}^{\bar{T}}_{TCs}$ not only overestimates the one removed between the thermocouples inlet and outlet sections $\dot{Q}^{\bar{h}}$, but also the total one $\dot{Q}^{\int}$, essentially beacause of the particular choice of spatial distribution of the thermocouples.

The value of $\dot{Q}^{\bar{T}}_{TCs}$ for the experiment reported in the official CIRCE document [3.] (upon which this model has been built) is illustrated in the plot in Figure 54, over a total time of 8000 s, alongside with the values of the electrical power supplying the FPS, and an energy balance of the heat section. The value shows important oscillations over time, and even if it seems to reach an average value not very distant from the calculated one of $\dot{Q}^{\bar{T}}_{TCs} \cong 796\ kW$ (~for the first hour) it later decreases, and it is not actually clear if a stable and stationary value will be eventually reached.

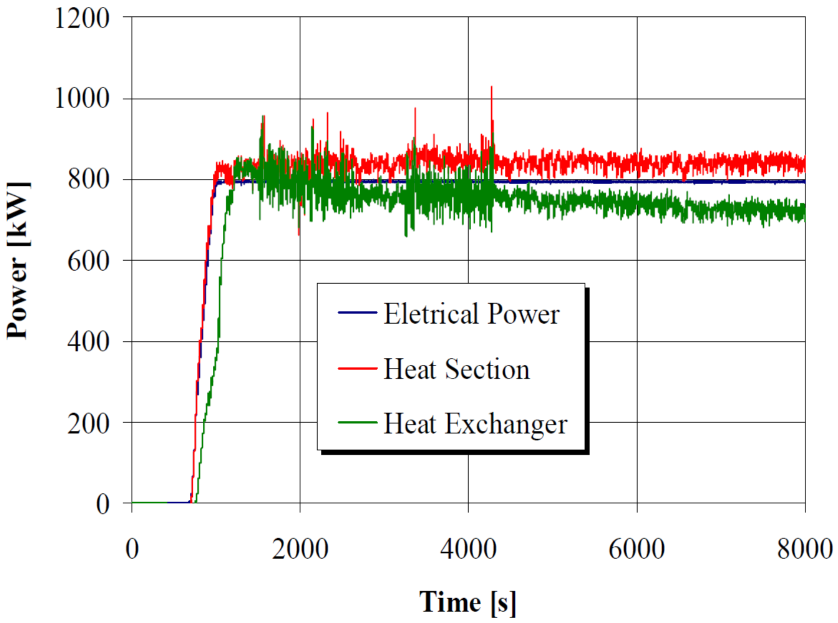

Figure 54:Energy balances for different regions of the CIRCE-ICE facility [3.].

4.3.4.2 Control volume II: Heat power removed between the outlet of the separator (Cylindrical Surface) and the Outlet TCs section

The estimation of the heat power removed through CV II (with reference to Figure 52), has been performed essentially to compare the heat power removed by the whole HX calculated as surface integral of the heat flux over the tubes surfaces ($\dot{Q}^{\int} \quad \cong 736\ kW$), to the value of the heat power removed between the separator outlet (considering the cylindrical surface highlighted in Figure 52) and the outlet TCs section, by means of an energy balance based on mass flow averaged enthalpies calculated over these surfaces ($\dot{Q}^{\bar{h}}$). The following plot in Figure 55 shows the results at convergence:

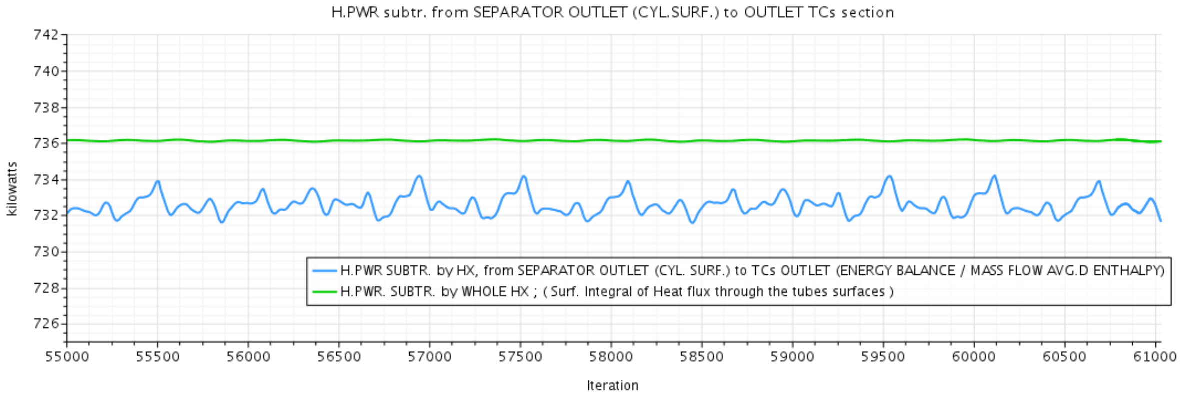

Figure 55:Evaluation of H.PWR removed through CV II with different methods.

The reported values for the abovementioned heat powers are:

Control volume II

$\dot{Q}^{\int} \quad \cong 736\ kW$

$\dot{Q}^{\bar{h}} \cong 733\ kW$ (average value, with small oscillations of ~1 kW of magnitude)

The two values are really close, confirming the adequateness of the $\dot{Q}^{\bar{h}}$ energy balance. The 3 kW difference corresponds to a relative error of ~0.4% of the total $\dot{Q}^{\int} \quad \cong 736\ kW$, which is lower than 1% and thus acceptable.

4.3.4.3 Control volume III: Heat power removed through the whole HX, comprehending the separator region

The energy balance referred to CV III is meant to evaluate the total heat power removed by the HX, comparing the $\dot{Q}^{\int} \cong 736\ kW$ and the one calculated with an energy balance employing mass flow averaged enthalpies calculated at the Riser exit and at the outlet TCs section ($\dot{Q}^{\bar{h}}$). This value almost coincides with the one removed through CV II, due to the fact that no tube is present in the differential volume region between the two control volumes. Anyway, calculating this “total” energy balance gave further reassurance on the coherence of the evaluations.

The results at convergence are shown in the plot below (Figure 56), compared to the value of the heat power removed as measured employing the thermocouples measured temperature values (with reference to CV I), namely $\dot{Q}^{\bar{T}}_{TCs} \cong 796\ kW$:

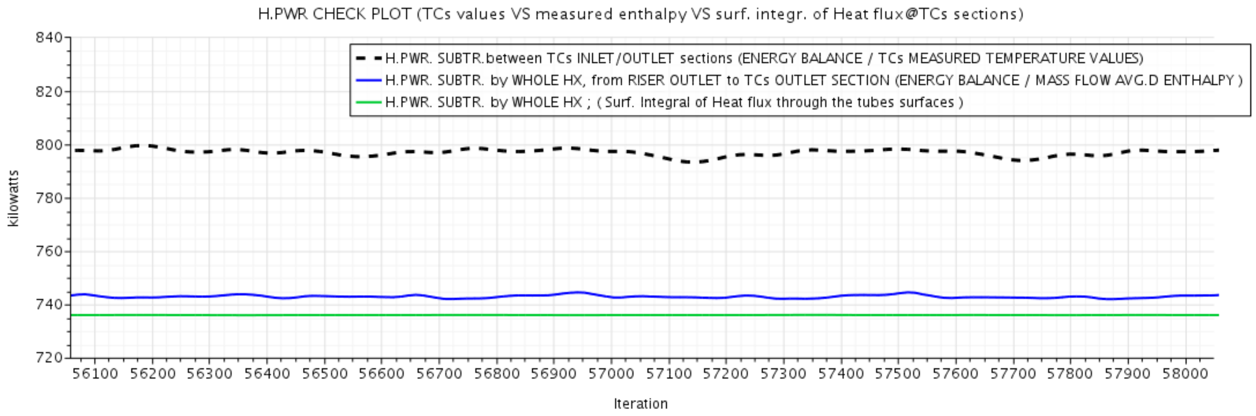

Figure 56:Evaluation of H.PWR removed through CV III with different methods.

Hence:

__Control volume III__

$$\dot{Q}^{\int} \cong 736\ kW$$

$$\dot{Q}^{\bar{h}} \cong 742\ kW$$

$$\dot{Q}^{\bar{T}}_{TCs} \cong 796\ kW$$

The two values of $\dot{Q}^{\bar{h}}$ and $\dot{Q}^{\int}$ differ of ~6 kW, equivalent to ~0.8% of the total correct value of 736 Kw. As previously said and discussed in paragraph 4.3.4.1, the $\dot{Q}^{\bar{T}}_{TCs}$, overestimates the total heat power by ~60 Kw (compared to the $\dot{Q}^{\int} \cong 736\ kW$.

4.3.4.4 General behaviour of the flow in the whole CFD domain:

The figures in the following pages are meant to illustrate the global behaviour of the flow through the whole HX, in terms of temperature, density and velocity magnitude fields (Figure 57, Figure 58 and Figure 59 respectively), together with Figure 60, depicting the temperature on the internal surface of the HX shell.

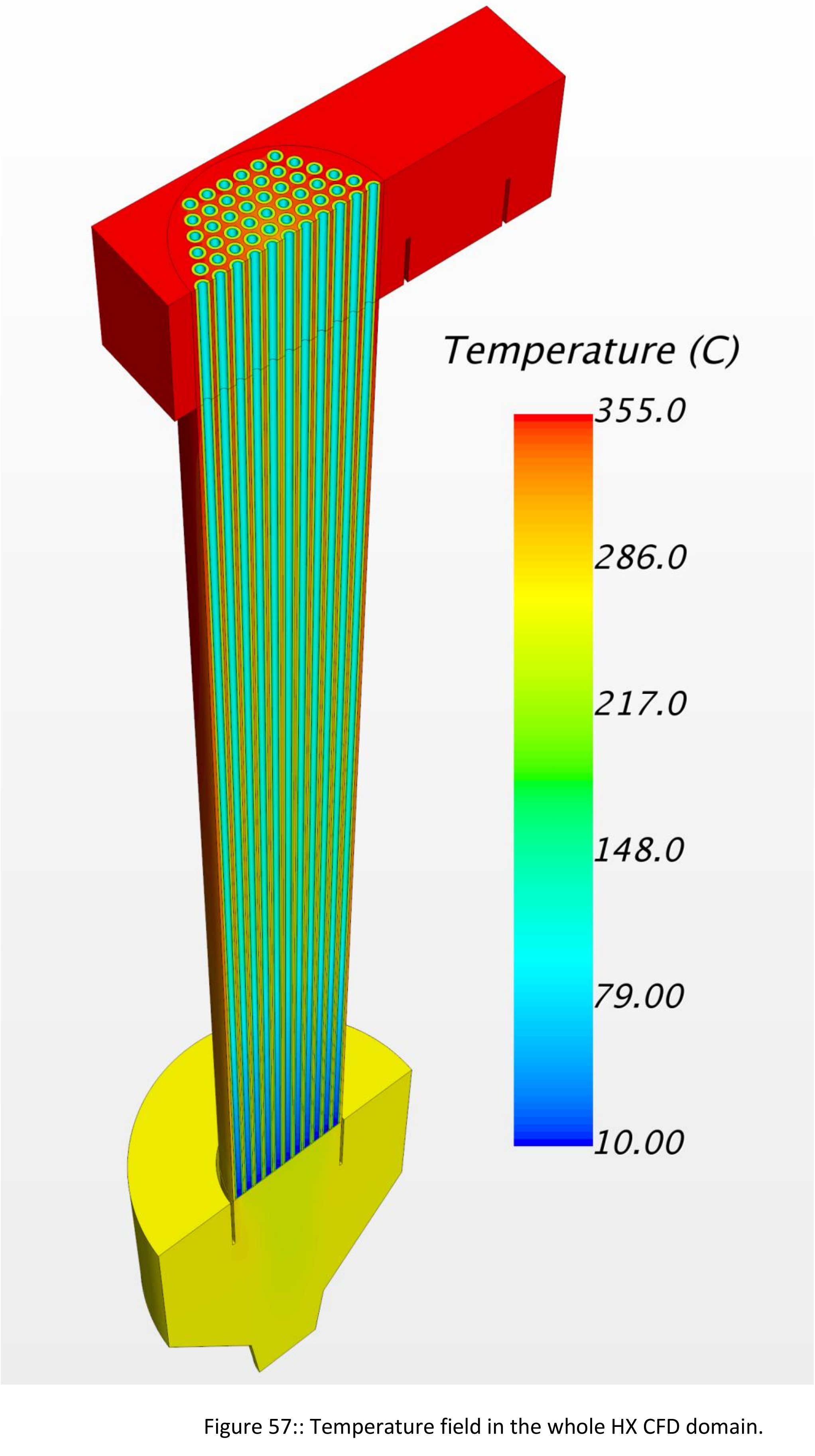

Figure 57:: Temperature field in the whole HX CFD domain.

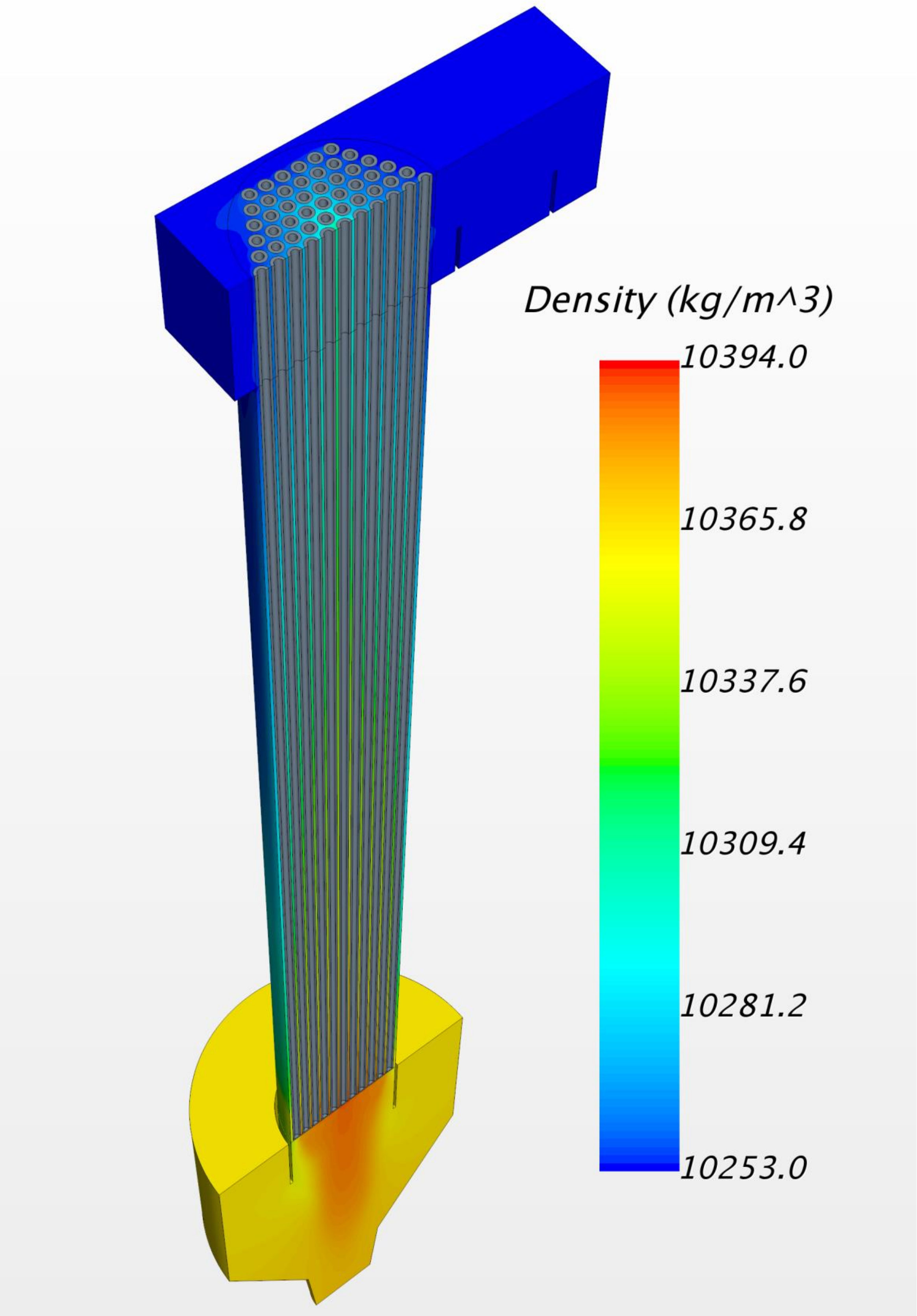

Figure 58:Density field in the whole HX CFD domain.

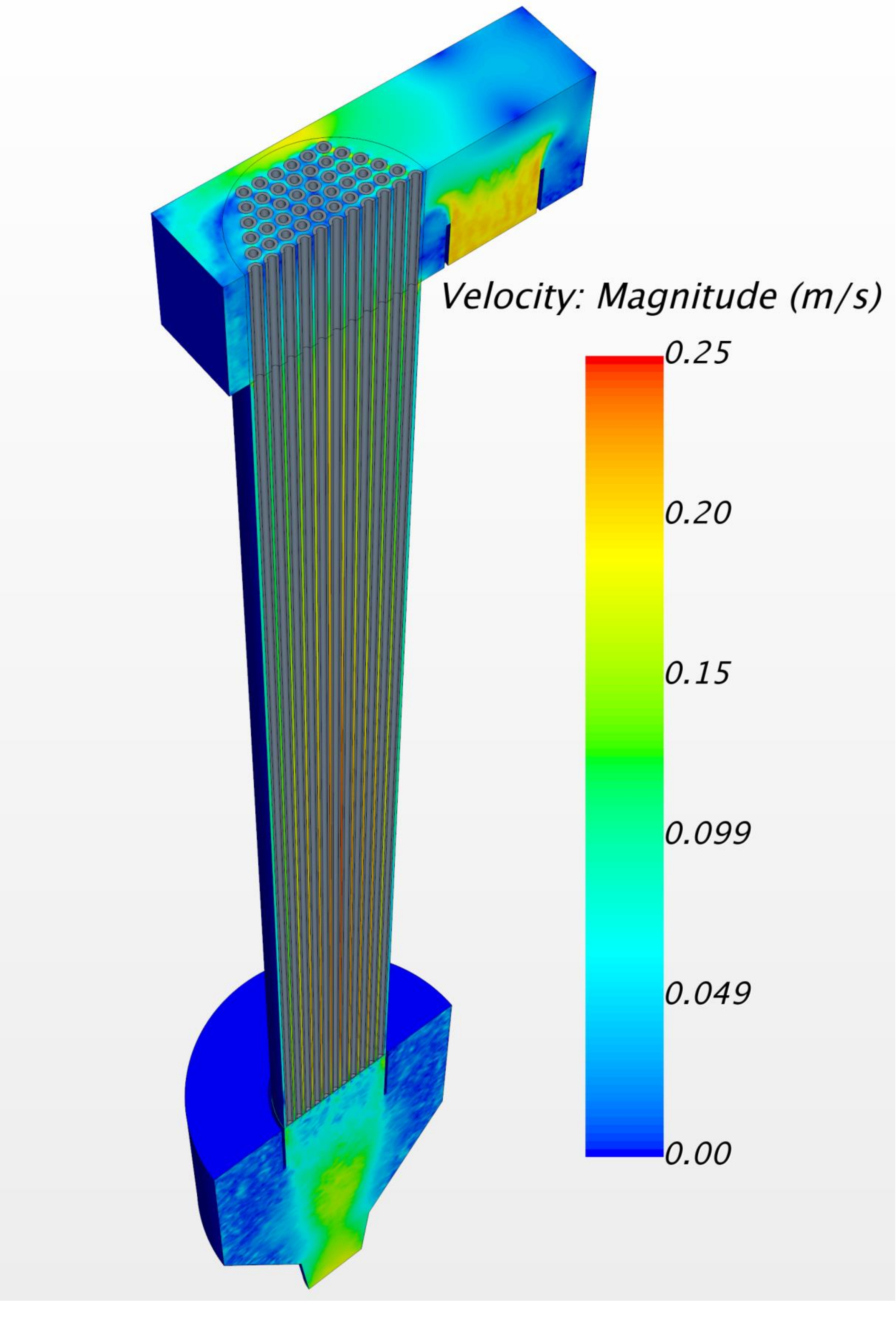

Figure 59;Velocity magnitude field in the whole HX CFD domain.

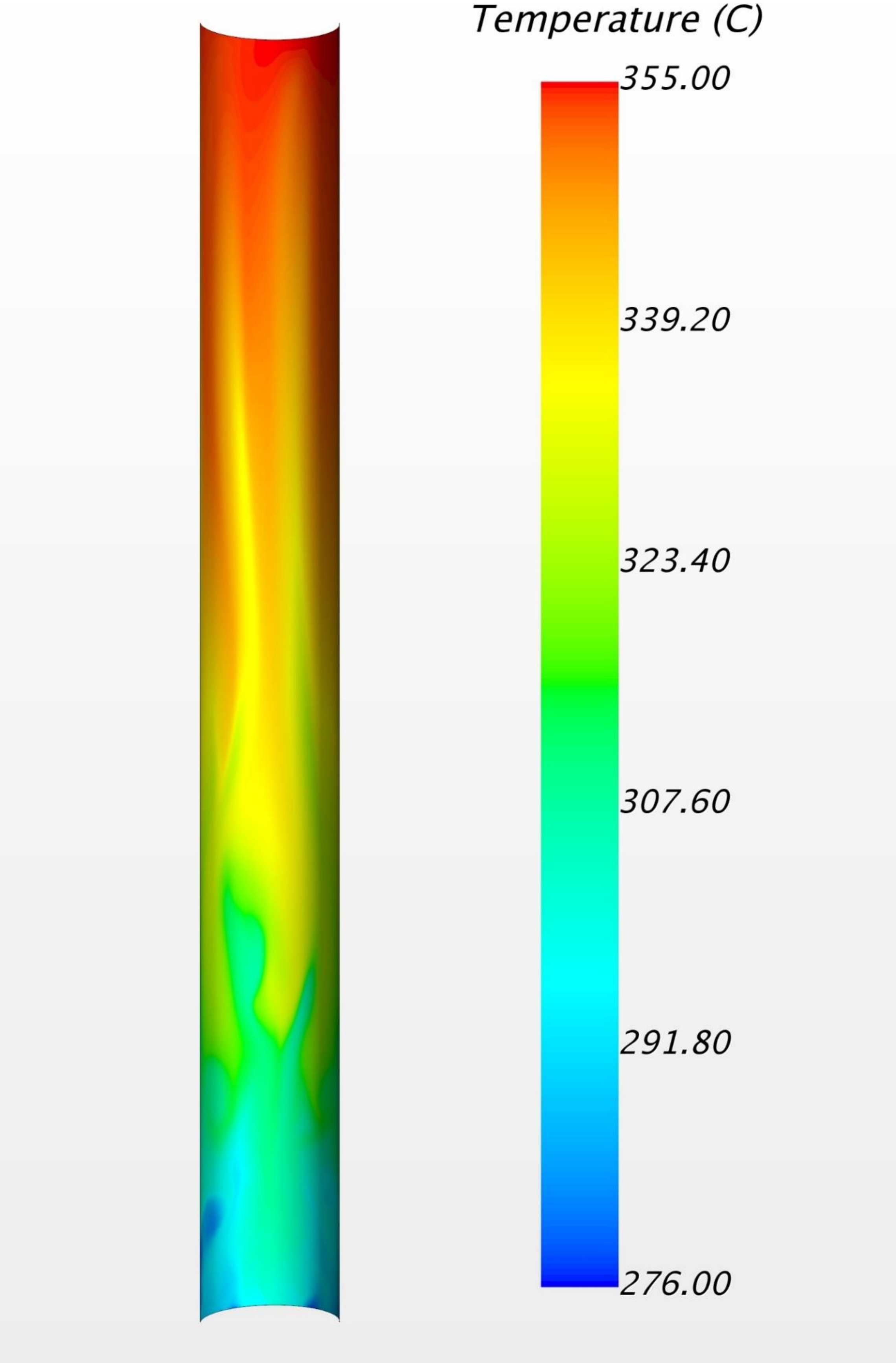

Figure 60:Temperature field on the internal surface of the HX shell.

5. Conclusions

5.1 Technical observations

In the end, after all the different modeling attempts reported in the previous chapters, it has been possible to reach a deeper understanding of the HX global performance and to evaluate with satisfying accuracy its behaviour from the energetic point of view. This knowledge is not meant to stay enclosed in this model, but will be of paramount importance during the next part of the work, dealing with the "bigger picture" of the global CIRCE-ICE experiment and its CFD modeling.

Moreover, some of the issues encountered in the various CIRCE-ICE experiments might be somehow related to inaccurate evaluations of the HX energetic performance.

Most importantly, with reference to the previous chapter 4, the measurement of the total heat power removed by the HX at steady state conditions appears to be heavily influenced by the chosen spatial distribution of the inlet and outlet thermocouples, which tend to measure temperature values rather different from the mass flow averaged ones in the respective inlet and outlet sections; this leads to an overestimated value of the total heat power removed by the HX, as explained throughout paragraphs 4.3.3 and 4.3.4.

Overestimating this value might have an important effect on the energy balance of the whole CIRCE primary loop, since the HX would appear to fictitiously remove more heat power than it actually does, only formally being equal in absolute value to the one supplied by the FPS.

Such imbalance on the heat powers transiting the control volume could cause a gradual increase of the average total energy of the LBE contained in the whole loop over time ($\frac{dE_t}{dt} > 0$, with reference to eqn. (3)). Considering that the total energy E_t is equal to:

$$E_t = E_i + E_m$$

, and knowing that the LBE mechanical energy variation in the whole loop volume ($\frac{dE_m}{dt}$) is negligible, this would translate into a situation where essentially $\frac{dE_i}{dt} > 0$; this would mean that the average temperature of the LBE enclosed into the CIRCE main vessel would tend to increase over time, and the experiment would not reach stable steady state conditions.

In any case, the only way to have further proof of the coherence of these assumptions is to consider the CIRCE-ICE primary loop in its wholeness, and to create a valid CFD model to evaluate its behaviour, not only in the stationary case, but also in transient conditions.

The last HX half model will thus be the starting point for the next master thesis stage.

Due to the expected high computational cost of the whole CIRCE primary loop CFD simulations, it will be compulsory to construct an "equivalent" model of the HX (characterized by a much lower number of volume mesh cells), essentially based on the use of adequate porous media to simulate the tubes, and heat "sink" terms to model the heat subtraction.

5.2 Observations on the whole internship

One of the most crucial objectives of curricular internships in general is to allow students to have a glimpse at the whole atmosphere surrounding the working world. Usually, most students have little (if any) experience in this environment, so stages play a very important educative role in this sense. This internship has then been an occasion to merge the two distant worlds of work and university and, most importantly, it allowed to concretely familiarize with the routines and practices of the research world, thus generating fundamental experience that will be strongly needed in the future.

6. Figure index

7. Bibliography

[1.] D. Martelli, M. Tarantino, P. Agostini, “CIRCE reference document”, issued by ENEA, 2015.

[2.] M. Tarantino, I. Di Piazza, P. Gaggini, G. Bandini, L. Cinotti, “Innovative Heat Exchanger and Steam Generator Designs for Fast Reactors”, issued by ENEA, 2011.

[3.] M. Tarantino, “Integral Circulation Experiment: Thermal-Hydraulic Simulator of a LFR Primary System, issued by ENEA, 2010.

[4.] B. Niceno, A. Badillo, “Summary for the recommended physical properties for the main fluid and liquid materials used for the MELILOO-stand and TALL-3D freezing experiments.”, Paul Scherrer Institute, 2016.

[5.] L. J. Weber, M. P. Cherian, M. E. Allen, M. Muste, “Headloss characteristics for perforated plates and flat bar screens”,2000.

[6.] M. Holger, “Heat Exchangers”, pp. 24-27, 1992.